# Parallel Probe Readout

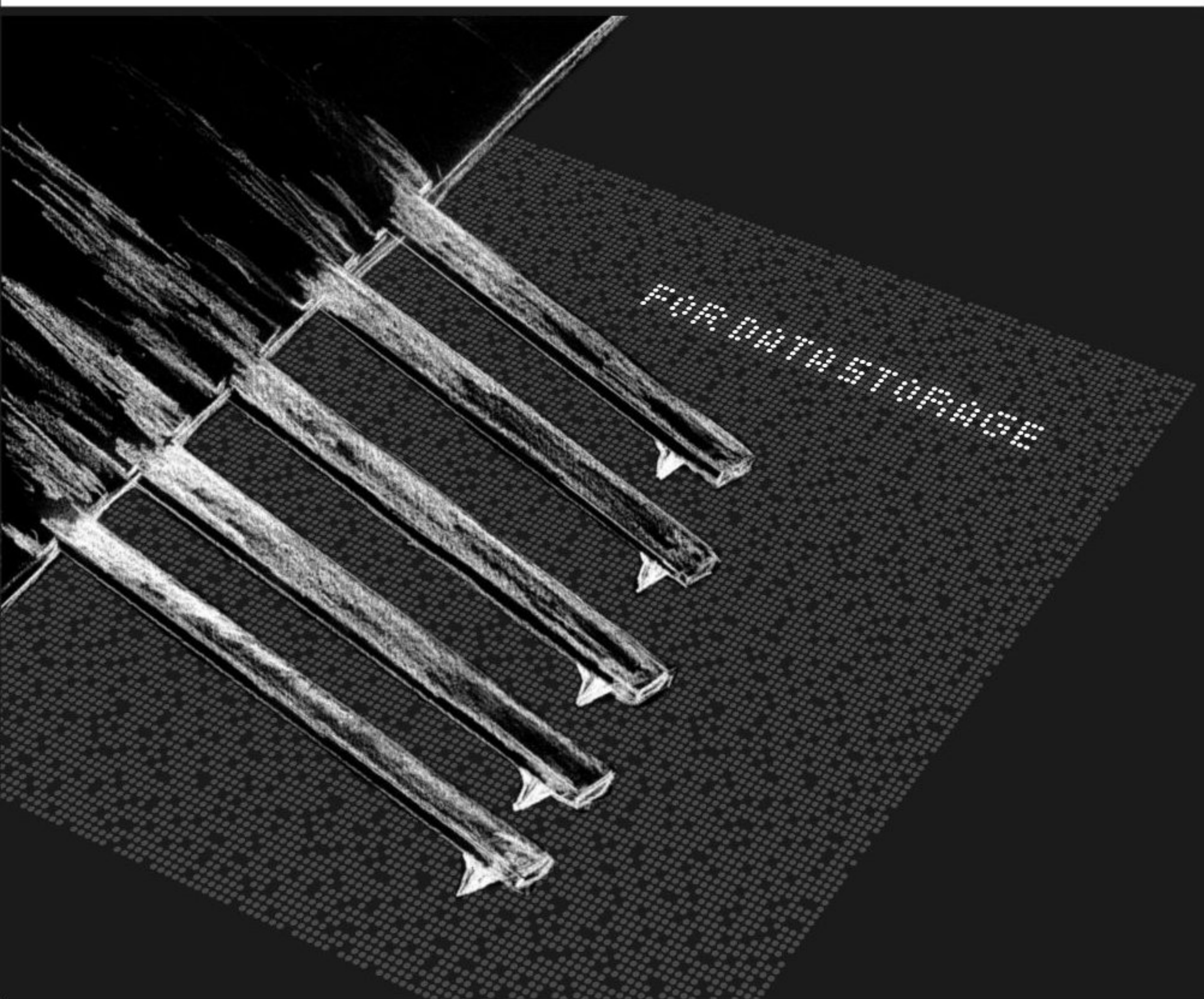


Wabe W. Koelmans

**Graduation committee**

| | |
|---|---|
| Prof. dr. ir. Ton J. Mouthaan | University of Twente (chairman and secretary) |
| Prof. dr. Miko C. Elwenspoek | University of Twente (promotor) |
| Dr. ir. Leon Abelmann | University of Twente (assistant promotor) |
| Prof. dr. C. David Wright | University of Exeter, United Kingdom |
| Prof. dr. Urs Staufer | Delft University of Technology |
| Dr. Peter Vettiger | EPFL Neuchâtel, Switzerland |
| Dr. Abu Sebastian | IBM Zürich Research Laboratory, Switzerland |
| Prof. dr. ir. Harold J. W. Zandvliet | University of Twente |
| Dr. ir. Anne-Johan Annema | University of Twente |

**Paranymphs**

Dr. ir. Johan B. C. Engelen
Ir. Jeroen de Vries

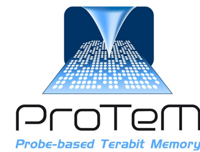


UNIVERSITY OF TWENTE.

The research described in this dissertation was carried out at the Transducers Science and Technology group, part of the MESA$^+$ Institute for Nanotechnology at the University of Twente, Enschede, the Netherlands. The work is supported by the European Research Council within the FP6 project 'Probe-based Terabit Memory'. The work is supported in part by the Dutch Technology Foundation STW, which is the applied science division of NWO, and the Technology Programme of the Ministry of Economic Affairs.

*Cover design by Ellen Koelmans-Holthof*

Printed by Gildeprint Drukkerijen, Enschede, the Netherlands.
© W. W. Koelmans, Enschede, the Netherlands, 2011.
Electronic mail address: w.w.koelmans@alumnus.utwente.nl
ISBN 978-90-365-3192-4
DOI 10.3990/1.9789036531924

# PARALLEL PROBE READOUT
## FOR DATA STORAGE

DISSERTATION

to obtain
the degree of doctor at the University of Twente,
on the authority of the rector magnificus,
prof. dr. H. Brinksma,
on account of the decision of the graduation committee,
to be publicly defended
on Friday, 17 June 2011 at 14:45

by

Wabe Watze Koelmans

born on 14 October 1981,
in Leeuwarden, the Netherlands

This dissertation is approved by

| | |
|---|---|
| Prof. dr. Miko C. Elwenspoek | University of Twente (promotor) |
| Dr. ir. Leon Abelmann | University of Twente (assistant promotor) |

*Make your choice, adventurous Stranger;*
*Strike the bell and bide the danger,*
*Or wonder, till it drives you mad,*
*What would have followed if you had.*

— C. S. Lewis

# Abstract

In this thesis techniques are developed to read out nanoscale probes and arrays of probes. The main targeted application area is probe-based data storage. The work also contributes to other areas, such as metrology, biological sensing, materials research and nano-electro-mechanical switches.

First, an exhaustive literature review of the accomplishments within probe storage is presented. It is found that optical readout techniques are used extensively in applications using probes; however, the very demanding application probe storage is not amongst them. Optical readout of probes offers reliability, high-speed, low noise and low complexity. It has to be extended to operation on arrays of probes for successful implementation in probe storage.

The first technique that is developed in this work is parallel frequency readout of an array of cantilever probes, demonstrated using optical beam deflection with a single laser-diode pair. Multi-frequency addressing makes the individual nanomechanical response of each cantilever distinguishable within the received signal. Addressing is accomplished by exciting the array with the sum of all cantilever resonant frequencies. This technique requires considerably less hardware compared to other parallel optical readout techniques. Readout is demonstrated in beam deflection mode and interference mode. Many cantilevers can be readout in parallel, limited by the oscillators' quality factor and available bandwidth. The proposed technique facilitates parallelism in applications at the nanoscale, including probe-based data storage and biological sensing.

A second technique to perform parallel optical readout of probes makes use of diffraction patterns that result if a laser spot is incident on an array of probes. The cantilevers form an optical grating and the state of deflection of each cantilever within the array determines the diffraction pattern, which is captured by a 1-dimensional array of photodiodes. Each cantilever can be regarded as a slit in a traditional multiple-slit diffraction experiment. In our situation the phase of the reflected light is a function of the amount of deflection of the cantilever, in contrast to a slit diffraction experiment, where the slits are assumed to contain light sources of equal phase. The developed technique is straightforward applicable when two discrete levels are permitted in cantilever bending.

A novel fabrication process is developed to produce probe arrays with sharp tips that are self-aligned on the cantilever. The focus is on achieving an array that gives rise to a highly uniform tip-medium distance. In order to accomplish this we make

use of a silicon-on-insulator (SOI) wafer and define the tips by a highly uniform wet chemical etch. The fabricated micro-cantilever arrays are characterized and shown to have a high uniformity. For an array of 10 cantilevers spanning 430 μm a standard error of 11 nm is demonstrated. Furthermore, we show that it is possible to fabricate both cantilevers and tips using a single mask.

The final part of this work is about scanning probe microscopy employing conductive probes, which is a powerful tool for the investigation and modification of electrical properties at the nanoscale. Application areas include semiconductor metrology, probe-based data storage and materials research. Conductive probes can also be used to emulate nanoscale electrical contacts. Unreliable electrical contact and tip wear have, however, severely hampered the wide-spread usage of conductive probes. In this work we introduce a force modulation technique for enhanced nanoscale electrical sensing using conductive probes. This technique results in lower friction, reduced tip wear and enhanced electrical contact quality. Experimental results using phase-change material stacks and platinum silicide conductive probes clearly demonstrate the efficacy of this technique. Furthermore, conductive-mode imaging experiments on specially prepared platinum/carbon samples are presented to demonstrate the widespread applicability of this technique.

# Contents

**Abstract** **iii**

**Contents** **v**

**1 Introduction** **1**
1.1 Probe storage . . . . . . . . . . . . . . . . . . . . . . . . . . . . 1
1.2 The ProTeM project . . . . . . . . . . . . . . . . . . . . . . . . . 4
1.3 Outline of the thesis . . . . . . . . . . . . . . . . . . . . . . . . 5

**2 Concepts of probe-based data storage** **7**
2.1 Probe and medium technologies . . . . . . . . . . . . . . . . . . . 8
2.1.1 Thermomechanical storage . . . . . . . . . . . . . . . . . 8
2.1.2 Phase-change storage on GST media . . . . . . . . . . . . 13
2.1.3 Ferroelectric storage . . . . . . . . . . . . . . . . . . . . 16
2.1.4 Atomic and molecular storage . . . . . . . . . . . . . . . 19
2.2 Probe arrays and parallel readout . . . . . . . . . . . . . . . . . . 20
2.2.1 Probe technology and arrays . . . . . . . . . . . . . . . . 20
2.2.2 Parallel readout . . . . . . . . . . . . . . . . . . . . . . . 22
2.3 Optical readout of probe arrays . . . . . . . . . . . . . . . . . . . 25
2.3.1 Optical beam deflection . . . . . . . . . . . . . . . . . . 25
2.3.2 Interferometric readout . . . . . . . . . . . . . . . . . . 28
2.3.3 Optical readout in probe storage . . . . . . . . . . . . . . 29
2.4 Conclusion . . . . . . . . . . . . . . . . . . . . . . . . . . . . . . 29

**3 Parallel optical readout of a probe array in dynamic mode** **31**
3.1 Introduction . . . . . . . . . . . . . . . . . . . . . . . . . . . . . 31
3.2 Experimental details . . . . . . . . . . . . . . . . . . . . . . . . 32
3.3 Results . . . . . . . . . . . . . . . . . . . . . . . . . . . . . . . . 34
3.3.1 Beam deflection . . . . . . . . . . . . . . . . . . . . . . . 34
3.3.2 Interferometric readout . . . . . . . . . . . . . . . . . . 34
3.3.3 Comparison . . . . . . . . . . . . . . . . . . . . . . . . . 37
3.4 Noise and bandwidth . . . . . . . . . . . . . . . . . . . . . . . . . 37
3.5 Conclusion . . . . . . . . . . . . . . . . . . . . . . . . . . . . . . 40

**4 Parallel optical readout of a probe array in static mode** **41**
4.1 Readout of a probe array using diffraction patterns . . . . . . . . . 42
4.1.1 Theory . . . . . . . . . . . . . . . . . . . . . . . . . . . 43
4.1.2 Experimental details . . . . . . . . . . . . . . . . . . . . 47
4.1.3 Results and discussion . . . . . . . . . . . . . . . . . . . 48
4.1.4 Improving the detection signal . . . . . . . . . . . . . . . 52
4.1.5 Discussion . . . . . . . . . . . . . . . . . . . . . . . . . 54
4.1.6 Conclusion . . . . . . . . . . . . . . . . . . . . . . . . . 55
4.2 Fabrication of probe arrays . . . . . . . . . . . . . . . . . . . . . 56
4.2.1 Fabrication . . . . . . . . . . . . . . . . . . . . . . . . . 56
4.2.2 Measurement results . . . . . . . . . . . . . . . . . . . . 59
4.2.3 Conclusion . . . . . . . . . . . . . . . . . . . . . . . . . 62

**5 Force modulation for conductive probes** **63**
5.1 Introduction . . . . . . . . . . . . . . . . . . . . . . . . . . . . 63
5.2 Experimental details . . . . . . . . . . . . . . . . . . . . . . . . 65
5.3 Experimental results . . . . . . . . . . . . . . . . . . . . . . . . 67
5.3.1 Formation of electrical contact . . . . . . . . . . . . . . . . 67
5.3.2 Conductive-mode imaging . . . . . . . . . . . . . . . . . . 68
5.3.3 Long-term imaging . . . . . . . . . . . . . . . . . . . . . 70
5.3.4 Imaging of heterogeneous samples . . . . . . . . . . . . . . 72
5.3.5 Tip motion during imaging . . . . . . . . . . . . . . . . . 75
5.4 Discussion . . . . . . . . . . . . . . . . . . . . . . . . . . . . . 76
5.5 Conclusion . . . . . . . . . . . . . . . . . . . . . . . . . . . . . 76

**6 Summary and conclusions** **79**
6.1 Summary . . . . . . . . . . . . . . . . . . . . . . . . . . . . . . 79
6.1.1 Probe storage . . . . . . . . . . . . . . . . . . . . . . . . 79
6.1.2 Optical readout . . . . . . . . . . . . . . . . . . . . . . . 80
6.1.3 Optical readout of probe arrays in dynamic mode . . . . . 80
6.1.4 Optical readout of probe arrays in static mode . . . . . . . 81
6.1.5 Fabrication of probe arrays . . . . . . . . . . . . . . . . . 81
6.1.6 Force modulation for conductive probes . . . . . . . . . . 82
6.2 Conclusions . . . . . . . . . . . . . . . . . . . . . . . . . . . . . 83
6.3 Future work . . . . . . . . . . . . . . . . . . . . . . . . . . . . . 83

**Appendices** **85**

**A Noise of cantilever arrays** **87**
A.1 Introduction . . . . . . . . . . . . . . . . . . . . . . . . . . . . . 87
A.2 Thermal noise . . . . . . . . . . . . . . . . . . . . . . . . . . . . 87
A.3 Shot noise . . . . . . . . . . . . . . . . . . . . . . . . . . . . . . 90
A.4 Noise comparison . . . . . . . . . . . . . . . . . . . . . . . . . . 91
A.4.1 Laser spot size . . . . . . . . . . . . . . . . . . . . . . . 92
A.5 Total noise . . . . . . . . . . . . . . . . . . . . . . . . . . . . . . 92

**B Tortoise – a multi-probe SPM** **95**
B.1 Tortoise system . . . . . . . . . . . . . . . . . . . . . . . . . . . . 95
B.2 Parallel imaging with thermomechanical probes . . . . . . . . . . 99
B.3 Long-range positioning . . . . . . . . . . . . . . . . . . . . . . . . 99

**C Cantilever array process flow** **101**

**Bibliography** **112**

**Samenvatting** **126**

**Woord van dank** **128**

**Publications** **132**

**About the author** **134**

# Chapter 1

# Introduction

How much data can mankind store? We all recognize the desire to store our data; family photos, writings, gained knowledge, poetry, music and much more information that we deem too important to let perish. There is nothing new under the sun. Already thousands of years ago expression was given to the same desire:

> "Oh that my words were now written!
> Oh that they were inscribed in a book!
> That with an iron pen and lead,
> they were engraved in the rock forever!"
>
> Job 19:23-24 ASV

Since then, the amount of information that mankind is capable of storing by technological means has dramatically increased. A study by Hilbert and López, which was recently published in Science, estimates the world's total technological storage capacity. We can store $2.9 \times 10^{20}$ bytes or 290 exabyte of optimally compressed data. Such a number defies all imagination. It is more than 300 times the number of grains of sand in the world[*]. It is the result of many years of hard work to advance our technologies. Hand writing, the printing press, photography, many digital storage technologies; there is a long list of beautiful accomplishments.

## 1.1 Probe storage

The search for digital storage technologies that offer ever increasing data densities, has been ongoing since the introduction of the punch card in 1725. This search has been extremely successful and has led over the past 60 years to a staggering 250 million times increase in data density. In the last two decades the working principle of the old punch card has again attracted a lot of attention. This time for storage on the nanometre scale, with a technology termed probe-based data storage.

[*] www.physorg.com

The invention of the Scanning Tunneling Microscope (STM) by Binnig, Rohrer, Gerber and Weibel in 1982 laid the basis for this probe-based technology at the nanoscale. With the STM it became possible to image atoms and a few years later manipulation at the atomic scale is demonstrated by Eigler and Schweizer (1990). Probe storage has, however, more resemblance to the Atomic Force Microscope (AFM), which was invented by Binnig, Quate and Gerber in 1986. The AFM uses cantilevers with tips and can also image and manipulate non-conductive surfaces, where the STM relies on tunneling to a conductive surface in order to function. The first cantilevers for AFM were ingeniously made of gold foil with a diamond tip glued onto the foil. Binnig et al. used the STM to monitor the deflection of the cantilever; two microscopes were used to image one surface. Their work was not yet ready to be employed for cantilever-tip based storage, commonly referred to as probe storage. The construction of the probes was not easily reproducible, could not be made smaller and fabrication was not accurately controlled. Already in 1982 another development had started that proved to provide the solution. Petersen recognized the potential of silicon as a mechanical material by making the following statement:

> "In the same way that silicon has already revolutionized the way we think about electronics, this versatile material is now in the process of altering conventional perceptions of miniature mechanical devices and components."
>
> Petersen, 1982

Soon after the invention of the AFM, cantilever styli were created from silicon nitride (Albrecht et al., 1990) and silicon (Brugger et al., 1992). The readout of these cantilever-based probes could not be done by STM anymore and a much more practical solution was introduced by Meyer and Amer. They used a very simple, but effective way to detect cantilever motion by shining laser light at the back of the cantilever and recording the motion of the reflected beam.

Nowadays, the optical lever method is widely applied in atomic force microscopes; however, it is not present in any of the reported concepts for probe storage. The main difference between an AFM and a probe storage device is the number of probes that is used. Probe storage uses many probes in parallel and the optical lever method has to be extended in order to perform parallel readout of many probes. This extension is one of the main topics of this thesis.

A second topic of this thesis is the robustness of the probes while they are in read operation. Already in a very early demonstration of probe storage the problem of tip wear arose. Iwamura et al. used silicon micro-technology in 1981 to create a rotating silicon disk memory with a tungsten-carbide probe to read and write data. Their tips wore down to diameters larger than 10 μm, corresponding to data densities a hundred times lower than those of compact discs. In this work we show that tip wear can be considerably reduced by minute tip vibrations, even in the case were electrical contact between tip and medium is required.

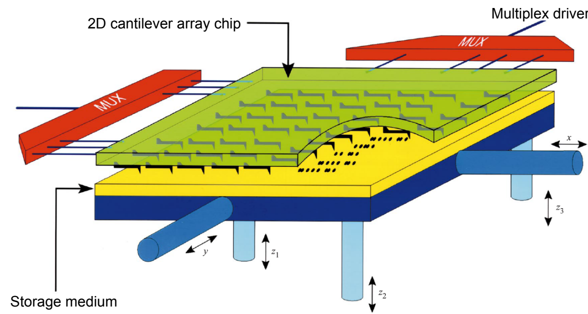


FIGURE 1.1 – *Overview of a probe based recording system (Vettiger et al., 2000).*

Over the past years many more implementations of probe storage are presented and many initial experiments are shown. A few implementations have been matured further and, in case of thermomechanical storage, this has led to a first prototype in 2005 (Millipede, 2005) with, certainly for that time, revolutionary areal densities around 1 Tb in$^{-2}$. Since then, demonstrations of much higher densities have been published, outperforming any other storage technology.

Probe storage is attractive because the bit size is not determined by the maximum resolution of lithographical processes that become increasingly costly. Probes can be chemically etched and have the potential to be atomically sharp without any expensive manufacturing step.

Challenges in probe storage are made more insightful when one considers that a single probe under laboratory conditions needs to be scaled up to large probe arrays working at high speeds in consumer products. When increasing the number of probes, the positioning accuracy has to be maintained, also under externally applied shocks. Deviations between the probes in the array due to fabrication have to be minimized in order to ensure that all probes function correctly and remain working throughout device life-time. Media and tips have to endure many read-write cycles.

A schematic of an architecture that makes a storage device based on probe technology is shown in Figure 1.1. Such kind of architecture was first proposed by IBM (Lutwyche et al., 1999). The core of the storage device is an array of probes with a moving medium on the opposite side. Each probe can locally alter a property of the medium to write a bit. Reading is accomplished by the same probe that wrote the bit.

A variation on the architecture shown in Figure 1.1 uses a spinning disk, like in hard disk drives, to position the medium. Such a design offers high, constant positioning speeds. Spinning disks are researched mostly in combination with ferroelectric probe storage (Hiranaga et al., 2009; Zhao et al., 2008).

## 1.2 The ProTeM project

Probe storage offers a large flexibility due to its high number of probes and scalability, and its application is not necessarily limited to mobile storage devices. For further exploration of the potential of probe storage, a European FP6 project called Probe-based Terabit Memory (ProTeM) has been issued. The ProTeM project is specifically looking into the added value that probe storage has to offer in the archival market. Data archival brings up a whole new set of challenges compared to portable storage devices. The data should be stored for a period of 50 years and the archival system has to have an extremely high capacity of 200 TB to 1000 TB. Within ProTeM two alternative routes are followed to achieve these goals: phase-change and thermomechanical probe storage. Phase-change storage holds the potential of a low write energy per bit and high data rates per probe. Thermomechanical storage has already proven its strength in a working prototype targeting mobile storage (Millipede, 2005).

The contribution of this work to the EU ProTeM project is to investigate a storage drive-concept using optical readout, and to study wear in phase-change probe storage. Both topics intend to prolong the period in which the data can be successfully read back. In other types of archival storage, long-term reliability is achieved by a very robust medium, e.g. a tape or an optical medium (CD, DVD, holographic). The data is read by a drive system that could very well break down in a 50 year timespan, but can easily be replaced. The main-concern is the reliability of the medium and this is quite well controlled. The bit stability can be measured by experiment and implemented accordingly. To prevent external damage, the medium can be stored in a controlled environment. Current probe storage concepts, as reviewed in Chapter 2, do not offer this flexibility. The sensor that measures the data, when the probe is scanned over the bits, is integrated in the probe design. The sensors are hard-wired to the rest of the storage channel and failure of any part of the system leads to data-loss. A period of 50 years poses a severe chance of malfunctioning of a part of the system.

Within ProTeM we propose to make use of two types of redundancy to significantly increase the chance of successful data retrieval after 50 years. The first type can be compared to what is called Redundant Arrays of Inexpensive Disks (RAID) in hard disk storage. The data is distributed over a number of storage modules within the archival device. Redundancy is added, such that loss of a limited number of modules does not lead to data-loss. Even break-down of probes, sensors or read electronics is tolerated up to a certain threshold without any loss of data. A second type is termed cold redundancy and can be compared to the replacement of a DVD player when the internal optics or electronics break down. A unit that is not employed in initial device operation, or that is in stand-by, is activated when needed. In order to use cold redundancy for a probe-based archival system we propose a removable cartridge and drive concept. Removing the medium from the probes is, however, hardly feasible with sub-nanometre positioning tolerances. Though, the integrated sensing of the probes could be replaced by external readout. This reasoning leads us to an architecture in which the medium with the probes can be

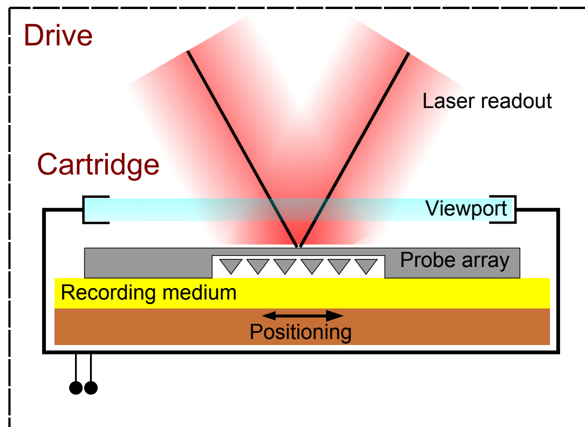


Figure 1.2 – *The storage drive concept with optical readout of the stored data.*

removed, both being within the cartridge, schematically shown in Figure 1.2. Laser light is used to read the data from inside the storage cartridge through a viewport. Photodetectors collect the reflected light, which contains the desired information.

## 1.3 Outline of the thesis

This thesis continues with an overview of the main concepts that are proposed and demonstrated in probe-based data storage. An exhaustive literature study of the accomplishments within each concept is presented in Chapter 2. A new optical readout method for probe arrays is presented in Chapter 3. The optical readout technique is suitable for arrays operating in dynamic mode and requires a minimum amount of hardware. This technique targets the non-contact readout of phase-change media with resonating probes. Non-contact readout offers tip-wear free operation, but the implementation of non-contact methods in probe storage is challenging due to the stringent tolerance requirements in the fabrication of large probe arrays. Fabrication of probe arrays leading to sufficient uniformity in tip-sample spacing remains daunting. However, a promising attempt is shown in the second part of Chapter 4. The first part of Chapter 4 dives further into optical readout techniques for arrays, by studying arrays that are operating in static mode. It is investigated whether arrays of cantilevers with tips that detect topographical changes, as is the case in thermomechanical storage, can be read out by a single laser beam. Chapter 5 is devoted to the readout of conductive probes scanning across phase-change media. In this scenario the probes operate in contact with the medium to sense changes in medium resistivity. Force modulation for conductive probes is introduced and the quality of electrical contact between tip and medium is compared to that of normal operation. Also, wear rates are studied by long-term experiments. The final chapter houses a summary, the conclusions and an outlook.

# Chapter 2

# Concepts of probe-based data storage

To review concepts of probe storage one has to recognize the significant difference in maturity of the different types of probe storage. Some concepts are only very briefly studied, where others have led to large scale read/write demonstrations at high to ultra-high densities. Three types of probe storage can be identified as most mature: phase-change, thermomechanical and ferroelectric probe storage. These are selected for this review. Although less mature, atomic and molecular probe storage is added to the discussion. Atomic and molecular concepts have potential for future work on probe storage because of the extremely high data densities that can be achieved.

There are many challenges that have to be faced for a successful, competitive storage system using probes. First of all, very high data densities have to be achieved, because high density is one of the key advantages of probe storage. Ultimately, probes have shown to be capable of storing data in a single atom (Bennewitz et al., 2002). Data rates for both writing and reading have to be competitive and this leads in many of the probe based system designs to a high degree of parallelization. Furthermore, the endurance of the storage system should be such that it leads to years of care-free operation. The described challenges are listed in Table 2.1 and for each of the three most mature types of probe storage the achieved specifications are shown. Each of them will be discussed in more detail in the relevant sections. There are more demands that are posed on a storage system, such as a fast access time, a low power consumption and an appropriate form factor. These demands are more related to the implementation of the storage concept and are therefore not included in the discussion.

In the following section a detailed overview of the three most mature types of probe storage is given . In each of the subsections the type of storage is introduced, followed by a discussion of how data is written in this particular type of storage. Next, data read-back and the recording medium are discussed, special attention is

This chapter contains an updated version of parts of the book chapter: M. Gemelli, L. Abelmann, J. B. C. Engelen, M. G. Khatib, W. W. Koelmans, and O. Zaboronski, "Probe storage", *Memory Mass Storage*, ISBN 978-3-642-14751-7, Springer Verlag, 2011.

paid to endurance. Endurance is currently a very active topic of research, because it still remains a key issue in further maturing probe technologies. The following section discusses the use and development of arrays in probe storage. In view of the topic of this thesis, a section on optical readout of probe arrays is presented thereafter. A discussion is given on their applicability to probe storage. Finally, the conclusions are summarized.

TABLE 2.1 – *Achievements of most mature probe storage concepts.*

| | phase-change | Thermomechanical | Ferroelectric |
|---|---|---|---|
| Density | 3.3 Tb in$^{-2}$ [a] | 4 Tb in$^{-2}$ [b] | 4 Tb in$^{-2}$ [c] |
| Estimated max. density | ≈10 Tb in$^{-2}$ [d] | ≈10 Tb in$^{-2}$ [b] | >10 Tb in$^{-2}$ [e] |
| Read speed per probe | 50 Mb s$^{-1}$ [a] | 40 kb s$^{-1}$ [f] | 2 Mb s$^{-1}$ [g] |
| Write speed per probe | 50 Mb s$^{-1}$ [a] | 1 Mb s$^{-1}$ [h] | 50 kb s$^{-1}$ [i] |
| Travel per probe | 2.5 m [j] | 750 m [k] | 5000 m [l] |

[a] Hamann et al. (2006)
[b] Wiesmann et al. (2009)
[c] Tanaka and Cho (2010)
[d] Wright et al. (2006)
[e] Cho et al. (2005)
[f] Sebastian et al. (2009)
[g] Hiranaga et al. (2009)
[h] Cannara et al. (2008)
[i] Cho et al. (2006)
[j] Bhaskaran et al. (2009*b*)
[k] Lantz et al. (2009)
[l] Tayebi et al. (2010*b*)

## 2.1 Probe and medium technologies

In this section we discuss the different principles of storing and reading data. We can distinguish a number of categories, each with their own physical parameter that is locally modified to store data; (1) topographic storage, uses a topographical change, (2) phase-change storage in GST (compositions of germanium, antimony and tellurium, e.g. $Ge_2Sb_2Te_5$), uses the difference in conductivity or density of the amorphous and crystalline phases of the GST material, (3) ferroelectric storage, uses electrical polarization and (4) atomic and molecular storage, uses relative orientation of atoms. Amongst topographic storage, thermomechanical storage has attracted the most attention by far and therefore the relevant subsection is termed likewise.

### 2.1.1 Thermomechanical storage

Thermomechanical storage is mainly developed by IBM within a project named 'Millipede' (Vettiger et al., 2000). In thermomechanical storage topographical

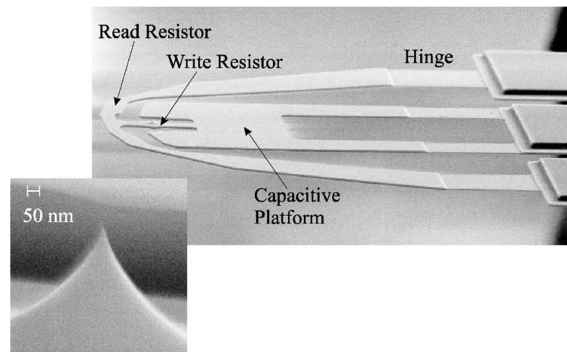


FIGURE 2.1 – *SEM image of the three-terminal thermo-mechanical probe which was used to perform the read/write demonstration at* 641 Gb in$^{-2}$. *During read operation the read resistor is heated to approximately* 250 °C, *during write operation the write resistor is heated to approximately* 400 °C. *The inset shows an enlarged view of the sharp silicon tip which is located on the write resistor (Pozidis et al., 2004).*

change in a polymer medium is created. The change is, in the most straight-forward implementation, an indentation that represents a 1. The absence of the indentation is used both as a spacer between neighboring 1s, as well as for a 0.

### Data writing

Writing is accomplished by heating the tip of the probe and applying an electrostatic force to the body of the cantilever, thereby pulling the tip into the medium. The heating of the tip is, in turn, caused by a localized heater at the base of the tip, see Figure 2.1. The heater consists of a low-doped resistive region of silicon that acts as a heating element. This writing process has been demonstrated to be capable of megahertz writing speeds at densities above 1 Tb in$^{-2}$ (Cannara et al., 2008).

The development of this thermomechanical write process in polymers started with the early work of Mamin and Rugar (1992). They made use of an external laser to supply the heat to the cantilever stylus. Heating times of 0.3 µs and data rates of 100 kb s$^{-1}$ were achieved. The integration of the heater in the cantilever initially led to an increase of the heating time to 2.0 µs. A later design by King et al. resulted in a decrease in heating time down to 0.2 µs (King et al., 2001). This design was realized using a mix of conventional and e-beam lithography (Drechsler et al., 2003). The cantilevers in this design are 50 µm long and only 100 nm thick, yielding extremely low spring constants of 0.01 N m$^{-1}$. The size of the heater platform was reduced to 180 nm, resulting in time constants on the order of 10.0 µs. The writing energy was less than 10 nJ per bit, mainly caused by parasitic effects and an inappropriate measurement setup, so there is potential for improvement. The storage density is limited by the medium properties, but more importantly by the probe tip dimen-

sions. Lantz et al. tried to achieve higher densities by applying multi-walled CNT tips with a tip radius down to 9 nm. The advantage of the carbon nanotube tips is that the tip radius does not increase by wear, instead the tip just shortens. Densities up to 250 Gb in$^{-2}$ were reached (Lantz et al., 2003), which was disappointing because at that time densities up to 1 Tb in$^{-2}$ were already attained with ultra sharp silicon tips. However, power efficiency was improved due to better heat transfer through the nanotube. Data could be written at heater temperatures of 100 K lower than comparable silicon tips.

### Data reading

In order to read back the data a second resistor is present in one of the side-arms of the three-legged cantilever design shown in Figure 2.1. This resistor acts as a temperature dependent resistor, where an increasing temperature causes a higher resistance. The read resistor is heated and the amount of cooling is accelerated by proximity of the medium. When the tip reaches an indentation, the medium is closer to the read resistor and the current that flows through the resistor will increase. The data is read back by monitoring this current. The platform is heated to about 300 °C, well below the temperature needed for writing, and a sensitivity of $1 \times 10^{-5}$ nm$^{-1}$ is obtained (Dürig et al., 2000).

The thermal readout was investigated in more detail by King et al., who showed that the fraction of heat transferred through the tip-medium interface is very small and most of the heat flow passes across the cantilever-sample air gap (King et al., 2002). This observation opened the possibility to heat a section of the cantilever, and avoid reading with heated tips, which causes unwanted erasure and increased medium wear. Simulations were performed to optimize the probe design. A shorter tip increased the sensitivity to $4 \times 10^{-4}$ nm$^{-1}$ (King et al., 2001).

In order to guide and speed up the design of more sensitive probes and assist in the readout data analysis, Dürig developed a closed form analytical calculation for the response of the height sensor (Dürig, 2005). An operator model of thermal readout was developed by Sebastian and Wiesmann (2008), which enabled the experimental identification of the sensing characteristics based on electrical measurements.An optimized design by Rothuizen et al. led to a bandwidth of several tens of kHz at powers on the order of 1 mW (Rothuizen et al., 2009). Later, by the use of feedback, the read speed of the optimized design could be increased from 19 kHz to 73 kHz (Sebastian et al., 2009).

### Recording medium

Polymers are the prime candidate for recording media in thermomechanical storage. The highest achieved density of 4 Tb in$^{-2}$ by Wiesmann et al. (2009) is on a polymer recording medium. The first polymer media used for thermomechanical storage were simply 1.2 mm thick PMMA (perspex) disks (Mamin and Rugar, 1992). Using a single cantilever heated by a laser through the PMMA disc, Mamin and Rugar were able to write bits with a radius below 100 nm and a depth of 10 nm,

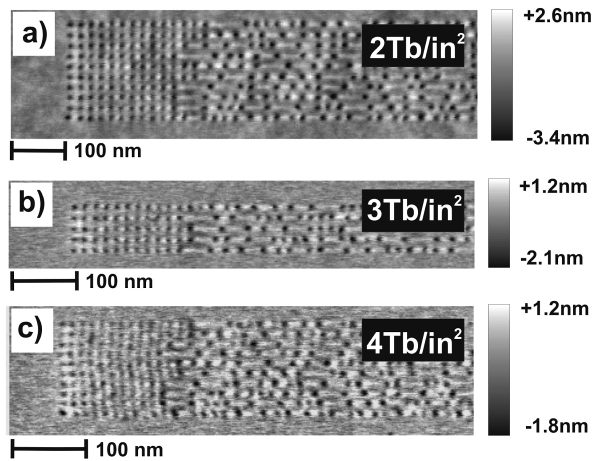


FIGURE 2.2 – *AFM images of a random pattern of indentations recorded in a PAEK polymer. A density of* 2 Tb in$^{-2}$ *was obtained on a normal spin-coated sample. Densities up to* 4 Tb in$^{-2}$ *were achieved on a templated sample. Experimental data by IBM (Wiesmann et al., 2009).*

allowing for data densities up to 30 Gb in$^{-2}$. In following work, the bulk PMMA or polycarbonate (compact disk material) disks were replaced by silicon wafers on top of which a 40 nm PMMA recording layer on top of a 70 nm cross-linked hard baked photoresist was deposited (Binnig et al., 1999). This allowed for small bit dimensions down to 40 nm, and data densities up to 400 Gb in$^{-2}$ were shown. Next to PMMA, other polymers were studied, such as polystyrene and polysulfone (Vettiger et al., 2002). The method of trial and error was taken out of the research by the development of a write model by Dürig (Vettiger et al., 2002). He discovered that a balance needs to be found been between stability and wear resistance of the medium on one side, requiring highly cross-linked polymers (Gotsmann et al., 2006*b*), and wear of the tip on the other side, for which a soft medium is necessary. Based on this knowledge, a so called Diels-Adler (DA) polymer has been introduced (Gotsmann et al., 2006*a*). These DA polymers are in a highly cross-linked, high molecular weight state at low temperature, but dissociate at high temperature into short strains of low-molecular weight. This reaction is thermally reversible: rather than a glass-transition temperature, these polymers have a dissociation temperature. Below the transition temperature, the polymer is thermally stable and has a high wear resistance, above the transition temperature the polymer becomes easily deformable and is gentle on the tip. Using the new DA polymer, densities up to 1.1 Tb in$^{-2}$ were demonstrated.

The work was continued with a polyaryletherketone (PAEK) polymer, which incorporates diresorcinol units in the backbone for control of the glass transition temperature and phenyl-ethynyl groups in the backbone and as endgroups for

cross-linking functionality (Wiesmann et al., 2009). As with the DA polymer, this polymer is highly crosslinked to suppress media wear during reading and to enable repeated erasing. In contrast to the DA polymer, it has a conventional, but very low, glass transition temperature of less than 160 °C in the cross-linked state, enabling indentation on a microsecond time scale using heater temperatures of less than 500 °C. It exhibits exceptional thermal stability up to 450 °C, which is crucial for minimizing thermal degradation during indentation with a hot tip. Using this polymer densities up to 4 Tb in$^{-2}$ have been achieved, onto ultra-flat polymers which were made by templating the polymer on a clieved mica surface (Pires et al., 2009), see Figure 2.2. Modeling shows that in this type of polymer media the density is limited to 9 Tb in$^{-2}$ (Wiesmann et al., 2009). Further improvements could be made by evaporating material rather than indenting, but then rewriteability is sacrificed.

Apart from the IBM work, others have been investigating polymer media as well. Kim et al. from LG demonstrated bit diameters of 40 nm diameter (Kim et al., 2005) in PMMA films. Bao and Li of the Chinese academy of sciences investigated friction of tips with varying diameters on PMMA, and concluded that blunt tips can be used to determine the glass-transition temperature, where as 30 nm diameter tips can be used to detect local ($\beta$) transitions (Bao and Li, 2008).

**Endurance**

Endurance poses one of the largest problems for a probe storage system; however, recently much work has been done to overcome tip wear, which is the main issue in order to obtain a reasonable device life-time. To get a feel for the extent of the problem of tip wear a description of the wear issue in thermo-mechanical storage is taken from (Lantz et al., 2009). Consider a system operating at 1 Tb in$^{-2}$ and a data-rate of 100 kb s$^{-1}$ per probe. With the data storage industry life-time standard of 10 years and continuous operation of the device each probe slides a distance of 10 to 100 km. This translates to a maximum tolerable wear rate on the order of one atom per 10 m sliding distance in order to maintain the 1 Tb in$^{-2}$ density. When operated in normal contact mode on a polymer medium, a silicon tip loaded at 5 nN wears down in 750 m, sliding to a bluntness that corresponds to data densities of 100 Gb in$^{-2}$.

A first estimate of the tip-sample force threshold at which wear starts to become an issue is reported by Mamin et al. (1995). A load force of 100 nN is mentioned to maintain reliable operation for the relatively large sized indentations (100 nm) described in this early work. Such a force is detrimental for any reported probe-medium combination when densities above 1 Tb in$^{-2}$ are targeted. In a more exhaustive study on wear by Mamin et al. (1999) a bit diameters of 200 nm is shown to be maintained throughout a tip travel length of 16 km. Although the tip travel length is sufficient for a probe storage device, the bit diameter is far from competitive. Several strategies to reduce tip wear have been proposed and demonstrated, they include hardening of the tip, softening of the medium and modulation of the tip-sample forces. One of the first attempts to reduce tip wear is the inclusion of a

photo resist layer of 70 nm in between the silicon substrate and the storage medium (PMMA) (Binnig et al., 1999). Several more measures to reduce tip wear from the medium side have been taken, see §2.1.1 for details. Another approach to reduce tip wear is hardening of the probe. Coating the tip with a hard material or molding a tip leads generally to larger tip radii. For thermo-mechanical storage silicon is therefore preferred (Lantz et al., 2009).

A third way of reducing the tip wear is by actuation of the tip with a periodic force at frequencies at or above the natural resonant frequency of the cantilever. It is known from AFM that the intermittent-contact mode of operation reduces tip wear and this is one of the foremost reasons that intermittent-contact is preferred over contact mode in many microscopy environments. Application of intermittent-contact mode is not very straight-forward for probe storage. There are many requirements on the probes, some of which are conflicting with the requirements for intermittent-contact. A high stiffness cantilever required for intermittent-contact AFM conflicts for instance with the feeble cantilever used in thermo-mechanical storage to allow easy electrostatic actuation. The speed of intermittent-contact modes is also reported to be insufficient for probe storage (Lantz et al., 2009). In Sahoo et al. (2008) a solution is presented that uses amplitude modulation of the cantilever through electrostatic actuation, despite of high non-linearity in the cantilever response. The authors show successful read and write operation at 1 Tb in$^{-2}$ densities after having scanned 140 m. A second solution is to slightly modulate the force on the tip-sample contact. Lantz et al. (2009) showed that by application of a 500 kHz-sinusoidal voltage between the cantilever and the sample substrate, tip wear over a sliding distance of 750 m is reduced to below the detection limit of the used setup. Knoll et al. (2010) use a similar actuation voltage between sample and tip to achieve a so-called dithering mode that is shown to effectively prevent ripples on a soft polymer medium. The authors attribute the absence of, otherwise present, ripples to the elimination of shear type forces due to dithering at high frequencies.

### 2.1.2 Phase-change storage on GST media

phase-change storage is well-known from optical disks, for which laser light is adapted to modify phase-change materials such as $Ge_2Sb_2Te_5$ to store information. Storage is performed by locally changing an amorphous region to a crystalline region and vice versa. This transition is not only accompanied by an increase in reflectivity, also by a decrease in resistivity by several orders of magnitude. Major work has been done on probe recording on phase-change media at Matsushita (Kado and Tohda, 1997; Tohda and Kado, 1995), Hokkaido University (Gotoh et al., 2004), CEA Grenoble and the University of Exeter (Aziz and Wright, 2005; Gidon et al., 2004; Wright et al., 2003, 2006, 2008, 2010) and Hewlett-Packard (Naberhuis, 2002).

#### Data writing

phase-change recording in probe storage uses an electrical current instead of laser light. A conductive probe locally transforms the phase of the medium by passing a

current through the storage medium. The current locally heats the medium and at sufficiently high temperatures, a transition from the amorphous to the crystalline phase is induced. This write process is self-focusing, resulting in bit densities greater than 1 Tb in$^{-2}$ (Gidon et al., 2004). The power consumption for the writing process is low with respect to other technologies (smaller than 100 pJ per written bit (Satoh et al., 2006)). This is because only the bit volume, as opposed to the entire tip volume, is heated. There are alternative strategies in which the tip itself is heated. Lee et al. (2002) use a resistive heater to increase the tip temperature and write crystalline bits. Hamann et al. (2006) achieve an impressive density of 3.3 Tb in$^{-2}$ by heating the AFM probe with a pulsed laser diode, see Figure 2.3 for an example of a bit pattern. Write speeds of 50 Mb s$^{-1}$ for one probe are anticipated with the use of a spinning disk to position the medium (like in hard disk drives) and a nano-heater instead of the laser diode. Rewriteability is demonstrated by erasing part of the written data using a focused laser diode. The dynamics of the AFM tip is too slow to realize the fast heating needed for amorphization. In general, re-amorphizing a bit is very challenging with a probe (Bhaskaran et al., 2009*d*). phase-change storage offers the possibility for more advanced write strategies such as multi-level recording (Burr et al., 2010) and mark length encoding (Wright et al., 2010). The latter holds promises to increase user densities with at least 50% and potentially up to 100%.

### Data reading

The most common method of data read back is measuring the conductance of the medium by applying a low potential on the probe and monitoring the current. The probe is in direct contact with the medium, one essentially performs conductive-mode AFM (Bichet et al., 2004). Also non-contact modes exist that operate by changes in field emitter currents (Naberhuis, 2002) or tip-sample capacitance by Kelvin probe force microscopy (Nishimura et al., 2002), which measures the work function of the surface. The difference in density between the amorphous and crystalline phase can also be exploited. The crystalline phase has a higher density causing a written bit in an amorphous background to appear as a valley of several angstroms deep (Bichet et al., 2004; Gidon et al., 2004). The topographic map of the surface can be obtained by standard tapping mode AFM (Hamann et al., 2006) as is shown in Figure 2.3. In the same work, the read speed is increased with a nano-heater to an estimated 50 Mb s$^{-1}$ per probe.

### Recording medium

GST recording medium is an active topic of research for nonvolatile memory applications, which are not limited to probe storage. A nice overview of the status of solid state phase-change memory is given in (Burr et al., 2010). phase-change recording media are attractive because they are intrinsically overwriteable, the maximum achievable density is estimated at approximately 10 Tb in$^{-2}$ (Wright et al., 2006).

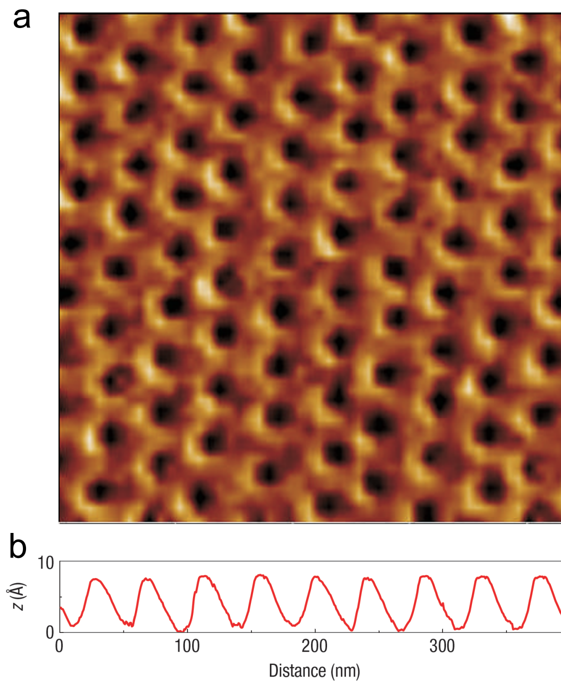


Figure 2.3 – *Thermal recording of ultra-high density phase-change bit patterns, with (a) a standard tapping-mode AFM image of the crystalline bit pattern written with a heated AFM tip in an amorphous GST film at a density of* 400 Gb in$^{-2}$ *and (b) a line profile of the recorded bits corresponding to the dotted line in the AFM image (Hamann et al., 2006).*

### Endurance

Tip wear is a quite severe issue because not only the tip sharpness has to be maintained, also the tip's ability to conduct. Tips for phase-change recording have been successfully made more wear-resistant by changing the fabrication material. The deposition of platinum on a silicon tip and subsequent annealing, creates a hard layer of platinum silicide (Bhaskaran et al., 2009*a*). An ingenious second measure to strengthen the tip is encapsulation of the conductive platinum silicide tip with a relatively large layer of silicon oxide. See Figure 2.4 for an example of such an encapsulated platinum silicide tip. The pressure on the tip apex is now decreased due to the increase of the tip area. The resolution of storage is still determined by the small conductive core (Bhaskaran et al., 2009*b*,*c*). Such a design does lead to more stringent demands on the medium side, because the larger tip apex will typically generate larger forces at the tip-sample interface, thereby potentially wearing down

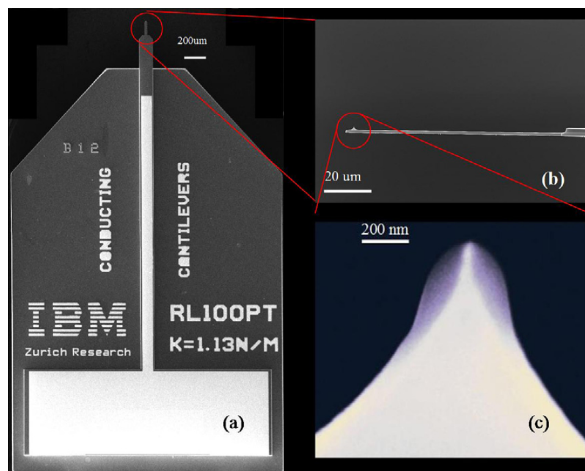


Figure 2.4 – *Images of an encapsulated platinum silicide tip, with (a) the complete chip, (b) a side view of the cantilever and tip stylus by SEM and (c) a zoom by SEM on the tip, where the conductive core is recognizable in the image (Bhaskaran et al., 2009b).*

the medium.

### 2.1.3 Ferroelectric storage

The electrical counterpart of magnetic recording, ferroelectric storage, has been investigated for decades. In ferroelectric media, the domain walls are extremely thin, indicating a very high anisotropy. A promising piezoelectric material such as PZT has a typical coercive electric field of 10-30 $\mathrm{MV\,m^{-1}}$ (Pertsev et al., 2003) and a polarization of 0.5 $\mathrm{C\,m^{-2}}$ (Zybill et al., 2000). The energy densities therefore appear to be in the order of 5-15 $\mathrm{MJ\,m^{-3}}$, which is a factor of two above the highest ever reported energy densities for magnetic materials. More important is the fact that the write head field is not material limited, as is the case with the yoke in the magnetic recording head.

#### Data writing

Domain reversal is achieved by a conductive cantilever that is in contact with or in close proximity of the medium. It is reported that a voltage pulse as short as 500 ps can successfully switch domains (Cho et al., 2006). Actual data rates of 50 $\mathrm{kb\,s^{-1}}$ per probe are realized due to the low speed of the piezoelectric scanner that is used.

Franke et al. (1994) at IFW Dresden were the first to demonstrate the modification of ferroelectric domains by conductive AFM probes. In their case the probe was in contact with the surface. Writing was achieved simply by applying a tip-

sample voltage up to 30 V. Later, Maruyama et al. at Hewlett-Packard in Japan obtained storage densities up to 1 Tb in$^{-2}$ (Hidaka et al., 1996; Maruyama et al., 1998). Rather than using probes, (Zhao et al., 2008) at Seagate realized a read/write head similar to hard-disk heads, where bits are defined at the trailing edge of the head. Using this novel type of head, densities up to 1 Tb in$^{-2}$ were demonstrated.

#### Data reading

It is not entirely clear which method of data readback is currently best performing. A very fast method, offering MHz rates at domain dimensions on the order of 10 nm is demonstrated by Seagate (Forrester et al., 2009). Reading is destructive, like in conventional FeRAM, which adds significant complexity to the storage system. A constant read voltage is applied to a conductive probe, causing reversely polarized domains to switch. When this happens the surface screening charge will change polarity. The required current is supplied and measured by electrical circuitry connected to the probe.

Readout of the polarization state of ferroelectric domains is usually accomplished by Piezo Force microscopy (PFM). PFM monitors the response of the probe to a small AC tip-sample voltage at a frequency below the cantilever resonance (Hidaka et al., 1996). The sample thickness varies with this frequency due to the piezoelectric effect, and with double the frequency due to electrostriction. It should be noted that on application of an electric field, also the permittivity changes, which gives rise to second harmonics as well (Franke et al., 1994).

Readout can also be performed in non-contact mode. In the early nineties, Saurenbach and Terris at IBM Almaden induced and imaged charges in polymer disks, using tungsten probes (Saurenbach and Terris, 1990, 1992). Imaging was done in non-contact mode by measuring the electric field generated by the polarization charges. Saurenbach measured in dynamic mode, monitoring the changes in resonance frequency of the cantilever caused by changes in the force derivative. At Tohoku university, ferroelectric probe storage research started in the same period with experiments on PZT by Lee et al. (2002) and $LiTaO_3$ by Cho et al. (2002). A frequency modulation technique was used for data readout. The method is based on the fact that the storage medium's capacitance changes slightly on reversal of the ferroelectric polarization due to the non-linear terms in the permittivity tensor. This minute change in capacitance causes tiny changes in the resonance conditions, which can for instance be detected by monitoring the cantilever vibration if excited with a fixed AC voltage, preferably using a lock-in technique. Recently, a new method was reported in which the direct piezoelectric effect is exploited to build up charge on the tip as a result of the tip-sample load force (Kim et al., 2009). The resulting current is proportional to the load force, leading to a trade-off with endurance, because tip wear increases with load force.

### Recording medium

The maximum achieved densities are 10.1 Tb in$^{-2}$ and 4.0 Tb in$^{-2}$ on a $LiTaO_3$ single crystal medium (Cho et al., 2005; Tanaka and Cho, 2010) and 3.6 Tb in$^{-2}$ on an atomically smooth PZT medium (Tayebi et al., 2010*b*). The storage areas are 40 nm × 50 nm, 6 mm × 6 mm and 1 μm × 1 μm, respectively.

In 2000, Shin et al. at KAIST experimented with AFM data storage on sol-gel deposited PZT. Dots, with diameters on the order of 60 nm to 100 nm, were written at 14 V. Data was read back by measuring electric forces either in non-contact or contact mode (Shin et al., 2000). Data retention appeared to be a problem, either because free charges accumulated on the medium surface or polarization was lost. Later work, in cooperation with Samsung, revealed that the polycrystalline nature of sol-gel deposited PZT films (Kim et al., 2006*a*) limits the data density, similar to hard-disk storage. The authors conclude that the grain size needs to be decreased.

Experiments at Tohoku university were continued on $LiTaO_3$ (Cho et al., 2003*b*, 2004; Hiranaga et al., 2002, 2003), which has superior stability. Because epitaxial films were used, pinning sites are needed for thermal stability (Cho et al., 2003*a*). By using thin (35 nm) $LiTaO_3$ single crystal films and a background field, arrays of domains could be written at a density of 13 Tb in$^{-2}$ (Tanaka et al., 2008*a*). A realistic data storage demonstration was given at 1.5 Tb in$^{-2}$. A raw bit error rate below $1{\cdot}10^{-4}$ could be achieved at a density of 258 Gb in$^{-2}$ and at data rates of 12 kb s$^{-1}$ for reading and 50 kb s$^{-1}$ for writing (Hiranaga et al., 2007). See Figure 2.5 for an image of bits written in a $LiTaO_3$ film. The data retention was measured by investigating readout signals at elevated temperatures, and an activation energy of 0.8 eV at an attempt frequency of 200 kHz was found, which is sufficient for a data retention of 10 years (Tanaka et al., 2008*a*). An overview of the work at Tohoku University until 2008 can be found in (Tanaka et al., 2008*b*). A spin-off of this activity has started at Pioneer, mainly in the production of probes (Takahashi et al., 2004, 2006*b*, 2007, 2009).

A recent study counters the concern about bit stability when the ferroelectric domains get smaller than 15 nm (Tayebi et al., 2010*a*). The authors fully reverse domains through the entire ferroelectric film thickness and thereby achieve stable domains with diameters down to 4 nm.

### Endurance

Force modulation has also been applied on the readout of ferroelectric data to increase the endurance of the tip. A slide test where a platinum iridium tip slides for 5 km at 5 mm s$^{-1}$ is shown where the authors claim that no loss in both read and write resolution has occurred (Tayebi et al., 2010*b*). The total wear volume is estimated to be $5.6 \times 10^3$ nm$^3$, which is impressively low. The result has been achieved at a load force of 7.5 nN and with the application of force modulation at an amplitude of 11 nN.

Another approach that has been demonstrated, in order to increase the endurance of the tip, makes use of a dielectric-sheathed carbon nanotube probe, resem-

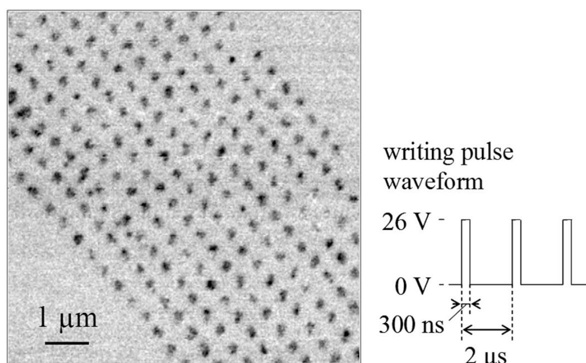


FIGURE 2.5 – *Scanning Nonlinear Dielectric Microscopy images of bits written in a $LiTaO_3$ film at a bit rate of* 1 Mb s$^{-1}$. *The bit spacing is* 206 nm *(Hiranaga et al., 2007).*

bling a 'nanopencil' (Tayebi et al., 2008). These micrometre long tips with constant diameter can sustain significant wear before the read and write resolution they provide, decreases. Domain dots with radii as small as 6.8 nm have been produced.

Tip wear can be effectively prevented by operating in non-contact mode. However, non-contact mode leads to lower data densities (Hiranaga et al., 2009).

### 2.1.4 Atomic and molecular storage

With ever shrinking bit dimensions, it is inevitable that mechanically addressed data storage will become impossible in continuous thin films, whether they are polymer based, ferroelectric, magnetic or phase-change. We will finally end up at the single molecule or atomic level. That this is not mere science fiction is elegantly proven both in molecular and atomic systems.

Cuberes, Schlitter and Gimzewski at IBM Zürich demonstrated as early as 1996 that $C_{60}$ molecules can be manipulated and positioned on single atomic Cu steps with a STM (Cuberes et al., 1996). The experiments were performed at room temperature, and molecules remained stable during imaging. If the binding energy of the molecules is above 1 eV, indeed this method could be used for long-term data storage. Instead of fullerenes, which bind by Van der Waals forces, Nicolau (2004) therefore suggest to use ionic and chelation bonds between the molecules and the metal surface.

Storage of data into single atoms has been beautifully demonstrated by Bennewitz et al. (2002), who deposited silicon atoms from an STM tip onto a 5×2 reconstructed silicon-gold surface (Figure 2.6). Due to the nature of the reconstructed surface, every bit is stored into an area of 20 surface atoms, resulting in a density of 250 Tb in$^{-2}$. The method used by Bennewitz is a write-once technique, but one can also envision deposition of atoms from the gas phase, using for instance hydro-

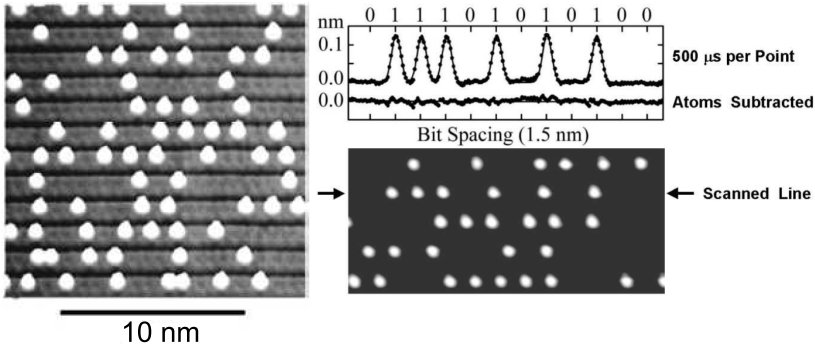


Figure 2.6 – *Atomic storage at room temperature: silicon atoms are positioned on top of a reconstructed silicon surface, leading to a density of* 250 Tb in$^{-2}$ *(Bennewitz et al., 2002).*

gen (H) or chlorine (Cl) (Bauschlicher Jr. and So, 2001; Rosi and Bauschlicher Jr., 2001).

Even higher storage densities can be achieved, if one does not use the position of molecules or atoms, but modifies their state. For molecules one could use conformal changes, or change the charge state of single atoms (Repp et al., 2004). Another option is to store data in the atomic spin (Loth et al., 2010).

## 2.2 Probe arrays and parallel readout

Although the probes used in probe-based data storage are originally derived from standard AFM and STM probes, with time they have become very complex. Not only do the probes require electrical actuation and readout, they also have to be extremely wear resistant and have to fit within a restricted area. Another challenging task is to realize probe arrays with thousands of tips in parallel. Readout of these arrays is far from trivial, especially when the number of probes is increasing.

### 2.2.1 Probe technology and arrays

The most advanced probe arrays have been realized by the IBM Zürich probe-storage team. Already in 1999, Lutwyche et al. realized a 5×5 array of probes with tip heaters and piezoresistive deflection readout. Ultra sharp tips were obtained by oxidation sharpening of isotropically etched tips. The tips are located at the end of cantilevers that are bent towards the medium by purposely introducing stress gradients, in order to clear the lever anchors from the medium. Boron implantation of specific regions of silicon cantilevers was used to define piezoresistors and tip heaters. In order to increase the sensitivity up to a $\Delta R/R$ of $4 \times 10^{-5}$ nm$^{-1}$, constrictions were introduced at the base of the cantilever. These constrictions, however, lead to a higher resistance, increasing the 1/f noise.

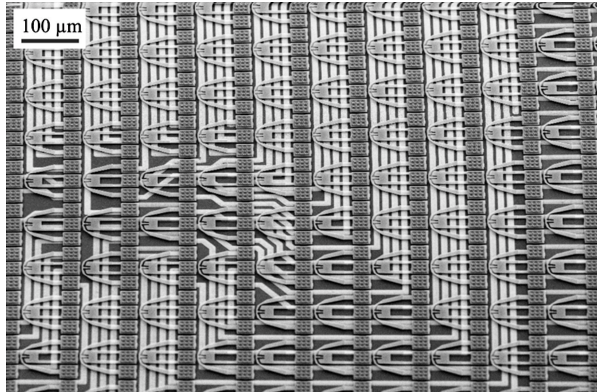


FIGURE 2.7 – *Scanning Electron Microscopy image of part of a 4096 cantilever array, interconnected to a wiring wafer (Despont et al., 2004).*

In the next 32×32 array piezoresistive heating was abandoned (Despont et al., 2000). In this array the cell size was reduced from 1000 µm to 92 µm, while keeping the cantilever spring constant at $1\,\mathrm{N\,m^{-1}}$ with a resonance frequency of 200 kHz. The array size was 3×3 mm, and thermal expansion deteriorating the tip alignment became an issue. Integrated heaters were positioned in the array to keep temperature variations within 1 °C over the chip. The array worked remarkably well, 80% of the cantilevers worked (Lutwyche et al., 2000), and a density of $200\,\mathrm{Gb\,in^{-2}}$ at $1\,\mathrm{Mb\,s^{-1}}$ net data rate was shown (Dürig et al., 2000).

Because tip wear is reduced by applying less force to the tip, the probe design was modified so that the spring constant reduced to $0.05\,\mathrm{N\,m^{-1}}$. As a result, during read actions, the probe applies very little force to the tip. During write actions, this force can be electrostatically increased to 1 µN by means of a capacitive platform at a potential of 20 V. With the new polymer media developed at that time, densities up to $1\,\mathrm{Tb\,in^{-2}}$ could be reached. Using this array a read/write demonstration at $840\,\mathrm{Gb\,in^{-2}}$ was given, following the stringent rules of the hard disk industry (Pantazi et al., 2008). Figure 2.1 displays a SEM image of the thermo-mechanical probe used in the demonstration.

An impressively tight integration of the probe array with CMOS was demonstrated by Despont et al. (2004). In this method only the integrated cantilevers are transferred to the CMOS chip, and the MEMS carrier wafer is first ground and then etched away. On one square millimetre, as many as 300 high electrical copper interconnects of 5 µm were realized. An array of 4096 probes with outer dimensions of 6.4 mm × 6.4 mm was realized (Figure 2.7) and the interconnects had a yield of 99.9%.

The work of IBM triggered the interest of other companies. For heated tip writing on piezoelectric and phase-change media, researchers at LG Electronics in Korea realized a small array of thermal probes (Lee et al., 2002). Heater platforms

were integrated in boron doped silicon by realizing a constriction at the cantilever end and covering the cantilever legs with gold. Conductive tungsten tips were grown by focused ion beam deposition. In the next generation, readout was added by integrating piezoelectric PZT layers on the cantilever legs (Lee et al., 2003). Feature heights of 30 nm could easily be distinguished. The array was extended to a size of 128×128 probes, and sensitivity improved to 20 nm (Nam et al., 2007). A wafer transfer method was developed for a 34×34 array (Kim et al., 2006*b*, 2007), very much along the lines of the IBM process. Rather than silicon, 300 nm thick silicon nitride probes were used with polysilicon integrated heaters. The spring constant was still relatively high ($1\,N\,m^{-1}$). Sharp tips were realized by KOH etching of pits into the silicon wafer and subsequent filling with silicon nitride, enabling bit dimensions of 65 nm.

Researchers at the Shanghai Institute of Microsystems and Information Technology have realized a small cantilever array, with integrated heater tips and piezoelectric deflection detection (Yang et al., 2006). These arrays have been used to characterize wear of polymer recording media as a function of tip temperature and radius (Bao and Li, 2008).

At the Data Storage Institute in Singapore, Chong et al. (2005)realized 20×1 and 15×2 arrays, using a fabrication technique along the lines of the early IBM work. The scanning concept is, however, different, featuring a large stroke actuator in one direction. The total storage area can thus be much larger than the size of the array (Yang et al., 2007). The 90 µm long and 1 µm thick cantilevers of the array had a spring constant of $1\,N\,m^{-1}$ and resonance frequency of 164 kHz. The tip radius was rather large (220 nm), resulting in bit dimensions in the order of 600 nm. An interesting experiment was performed where the temperature of the heater platform was monitored by means of an infrared camera. Cooling times of 2 µs were measured this way.

Researchers at Pioneer and the Tohoku university in Japan investigated arrays of probes with diamond tips and integrated piezoresistive sensors for ferro-electric data storage (Takahashi et al., 2006*a*,*b*), see Figure 2.8. The boron implanted silicon piezoresistive Wheatstone bridge had a high sensitivity of $1 \times 10^{-7}\,nm^{-1}$. In contrast, the diamond probes had relatively poor radius of curvature. Attempts were made to replace the diamond tip by metal versions, and it was demonstrated that ruthenium tips perform relatively well (Takahashi et al., 2007).

### 2.2.2 Parallel readout

The massive parallelism of the probe arrays, which is requisite for obtaining data rates comparable to magnetic hard disk heads, poses a large challenge in probe-based data storage. Several thousands of probes have to be simultaneously addressed. The main functions of each probe are positioning, reading and writing. Positioning is in most cases done by moving the complete array or the storage medium in plane and parallel to the probe array, simplifying the task of each probe.

Scanning the medium has two distinct advantages over scanning the probes (Sebastian et al., 2008). To obtain desired read and write speeds arrays have to

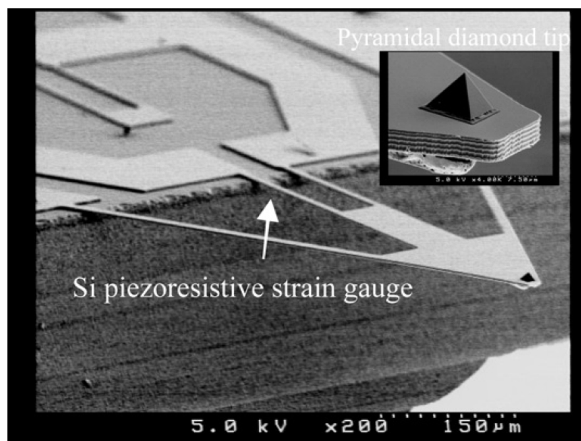


FIGURE 2.8 – *Diamond probe with silicon-based piezoresistive strain gauge (Takahashi et al., 2006a).*

scan at considerable rate, thereby inducing high frequency vibrations, that create unwanted cantilever movement. Preventing the occurrence of these vibrations is a major extra challenge for any control-loop. Secondly, electrical connections to the probes can more easily be realized, because the probes are not moving with respect to the read-channel electronics. Researchers at the Data Storage Institute show a solution where the coarse positioning has a flexible wire to the readout electronics, though also in this design the fine positioning is directly connected to the cantilever array (Yang et al., 2007).

Movement in the $z$ direction, where $z$ is defined as the direction normal to the medium, can be done on a per-array basis instead of a per-probe basis. This hugely simplifies the control required to operate an array of thousands of probes. On the other hand, the fabrication tolerances of the array and medium have to be such that every probe in the array is in the appropriate tip-medium distance range. A too large tip-sample separation results in a failure when an attempt to write or read a bit is done. The other extreme leads to a probe that is pushed into the medium with considerable force (depending on the spring-constant of the cantilever) leading to excessive tip wear. Without independent $z$ motion these demands on the medium and probe array increase tremendously. The technically most mature probe storage system, described in (Pantazi et al., 2008), is based on thermomechanical storage and features a $64 \times 64$ array where 32 levers are active. By determining the electrostatic pull-in voltage for each cantilever the initial tip-sample separation is calculated to have a standard deviation of 180 nm. With a cantilever spring constant of $1\,\mathrm{N\,m^{-1}}$ this would lead to a maximum additional load force of 180 nN.

The read and write operation requires the independent addressing of each probe. Traditionally, AFM probes are monitored by an optical readout system of which the

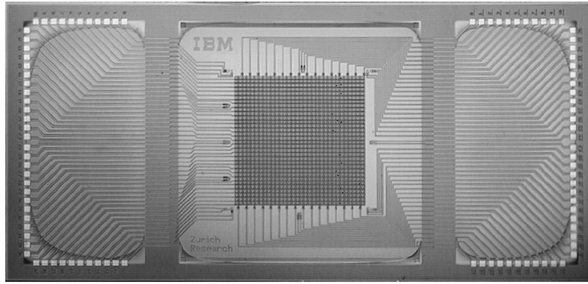


Figure 2.9 – *Photograph of a* 32 × 32 *array* (14 mm × 7 mm)*. The probes are interconnected by a* 32 × 32 *row/column addressing scheme. The* 128 *bondpads provide connection to the outside world (Despont et al., 2000).*

optical beam deflection technique (Meyer and Amer, 1988*a*,*b*) is the most widely used. Although optical readout has been demonstrated for arrays of cantilevers (Alvarez and Tamayo, 2005; Lang et al., 1998; Sulchek et al., 2001) none of the readout schemes has been implemented in probe storage. See for a detailed overview of optical readout schemes of cantilever arrays §2.3. Optical readout alone would however not suffice. The probes have to be actuated for the write operation. Wired schemes are implemented to achieve this. Wireless schemes and passing signals through the storage medium have also been proposed (Abelmann et al., 2003), but are not yet realized.

Wiring solutions are based on a time-multiplexing scheme to address the array row by row (Despont et al., 2000; Kim et al., 2007), similar to DRAM operation. With a growing number of probes the maximum current passed through a row or signal line grows. For higher numbers of probes an electrically stable wiring material, capable of carrying high current densities and also having a low resistivity, must be used. Despont and co-workers have used a 2-level wiring of both gold and nickel in the 32×32 array that is reported in (Despont et al., 2000). Schottky diodes formed by doped silicon/nickel interfaces were introduced to avoid cross-talk between probes. Bondpads are used for connection to the outside world, as shown in Figure 2.7. In the 64×64 array, reported in (Despont et al., 2000), the number of connections has increased to three per probe. In this case a second wafer with the CMOS circuitry is used to which the probes are bonded, as is the case in (Kim et al., 2007). An alternative integration with CMOS is a single wafer process described in (Severi et al., 2009). In this process the CMOS circuitry is first created on top of the last metalization by starting with a chemical mechanical polishing (CMP) step, see Figure 2.10. Next an insulating layer of 400 nm silicon carbide and a sacrificial oxide layer of 3 μm are deposited. A structural silicon germanium layer of 3 μm is later on deposited to allow definition of the cantilevers. Consequently, the cantilevers are etched and the sacrificial oxide is removed to allow cantilever actuation. Others are still working on the integration of the cantilever array with the readout electronics (Nam et al., 2007; Yang et al., 2007).

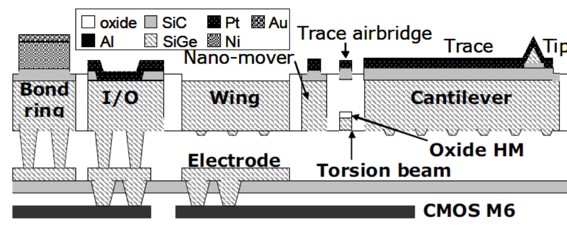


Figure 2.10 – *Schematic drawing of a cross-section showing the integration of a cantilever array with CMOS circuitry based on a one wafer design (Severi et al., 2009).*

## 2.3 Optical readout of probe arrays*

Shortly after the invention of the AFM (Binnig et al., 1986) researchers started to adopt the optical lever method for use in scanning force microscopy. Meyer and Amer (1988*a*,*b*) introduced this simple and reliable method in an AFM. Since then, the optical beam deflection method has become the most widely used technique for sensing cantilever displacements.

The use of cantilevers has far extended the reach of scanning force microscopy nowadays. Cantilevers are used in applications such as nano-lithography, chemical and biochemical sensing (Ilic et al., 2000; Lang et al., 2005), molecular recognition, mass-detection, many other sensing and actuation applications and, as discussed in the previous sections, probe-based data storage. Many of these applications are benefited by the implementation of an array of cantilevers instead of a single cantilever. Higher speed and throughput can be achieved, along with the possibility to tailor each cantilever for a specific task, e.g. coating each cantilever with a different sensing layer for an electronic nose (Baller et al., 2000; Lang et al., 2007).

With the use of cantilever arrays comes the need for reliable and simple readout methods. Optical beam deflection can be modified for application on a cantilever array and several schemes have been presented that are discussed in the following, including the sensing of cantilever array deflections using interferometry.

### 2.3.1 Optical beam deflection

Beam deflection using optical waveguides fabricated on top of cantilevers is reported by Hoffmann et al. (1994). The light escapes the waveguide at the end of the cantilever and the propagation direction of the light is determined by the angle of the cantilever. Across a 2 μm gap a second waveguide is placed in which light is collected. The amount of light power that is coupled into the second waveguide

*This section is not present in Gemelli et al. (2011); it is added to this chapter in view of the topic of this thesis.

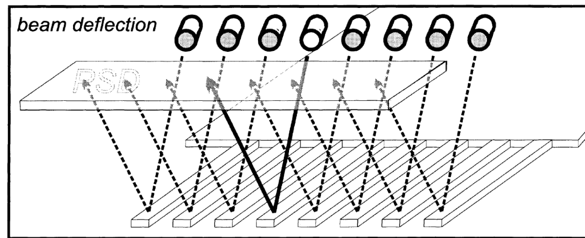


Figure 2.11 – *Beam deflection technique extended to cantilever arrays. The technique uses one laser source per cantilever and by means of time-multiplexing each cantilever is addressed (Lang et al., 1999).*

across the gap can directly be related to the deflection of the cantilever. This optical waveguide deflection technique is easily adapted to arrays by guiding the light with an optical branching structure (cascaded Y-junctions) to multiple cantilevers. The obtained resolution is in in the sub-micron regime and low compared to the sub-nm resolution achieved with standard optical beam deflection on a single lever (Alexander et al., 1989). Another disadvantage is that the implementation of waveguides on cantilevers is a considerable expansion of the fabrication process.

Lang et al. (1998) have shown sequential position readout of micro-cantilever arrays as illustrated in Figure 2.11. Each cantilever has their own light-source and an optical fiber ribbon is used to guide the light to the cantilevers. A time multiplexer switches the eight light sources on and off sequentially to address all of the cantilevers. The reflected light is collected by a position sensitive detector (PSD) and a computer relates the signal on the PSD to the corresponding cantilever. Disadvantages of this technique are the loss of bandwidth, the need for one light source for each cantilever and the timing issues that have to be addressed to avoid overlapping of the reflected beams. Advantages are that the proposed technique does not require any mechanical action to address a different cantilevers and that static bending of the cantilevers can be measured. Static bending can be caused by stress, due to the presence of an extra layer on the cantilever. This principle is used in the artificial nose, also presented by Lang et al. (1999).

Alvarez and Tamayo (2005) have demonstrated a technique that uses only one laser to read out a cantilever array. The setup is illustrated in Figure 2.12. The laser is translated in the $x$ direction to address each cantilever sequentially, so there is no risk of overlapping laser spots. The PSD signal is combined with the position of the scanning laser source to relate the signal to the appropriate cantilever. The technique uses only one laser source and can be extended to monitor the complete bending profile of the cantilevers by translating the laser source in the $y$ direction (Mertens et al., 2005). Readout is, however, slow and uses additional hardware to scan the laser.

Maute et al. (1999) describe the fabrication of a polymer coated cantilever array to serve as a gas sensor. The sensing mechanism causes the resonance frequency of

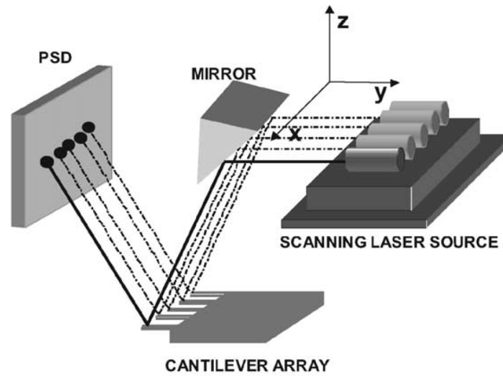


FIGURE 2.12 – *Schematic depection of the beam deflection technique extended to cantilever arrays. The laser translates in x direction to address each cantilever sequentially (Alvarez and Tamayo, 2005).*

the cantilever to change, as is the case in many cantilever based sensors. This resonance frequency change is indicative for the amount of adsorbed gas molecules. The researchers fabricated a cantilever array with a different natural resonant frequency for each cantilever by varying the length of the cantilevers. In 2000 the same group publishes an experiment in which they show a Fast Fourier Transform (FFT) spectrum as a function of time of five cantilevers that have different natural resonance frequencies (Kim et al., 2000). The FFT spectrum changes by mass-loading of the cantilevers. Later, Ghatnekar-Nilsson et al. (2006) also demonstrate the multi-frequency response of an array of cantilevers with different resonance frequencies. A similar demonstration of a frequency response of an array of cantilevers is given. The resonance frequencies are changed by deposition of a layer of gold on top of the cantilevers. A disadvantage of the proposed techniques of determining either the frequency response, or the FFT spectrum of a cantilever array is that it is not very fast. In both examples a frequency is swept, in time, over a certain frequency band to perform a FFT or obtain a frequency response. Thus that means that the frequency shifts of the cantilevers are sequentially read out.

Kim et al. (2003) present another technique to perform optical beam deflection with cantilever arrays. The laser spot is focused on two cantilevers and both reflected spots are recorded on a large CCD area. Due to the distance between the spots, software is able to track the motion of each spot and relate this motion to the deflection of the cantilevers. This technique is truly parallel, because all the laser spots are recorded simultaneously with the CCD. A disadvantage is that the process of image analysis and spot-tracking is slow.

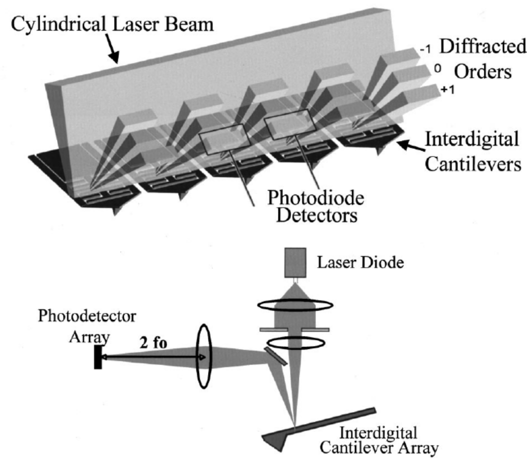


FIGURE 2.13 – *Parallel readout of an array of interdigitated cantilevers. The comb-drive like structures acts as diffraction gratings (Sulchek et al., 2001).*

### 2.3.2 Interferometric readout

The group of C.F. Quate introduced the interdigital cantilever that contains interdigitated fingers (Manalis et al., 1996; Yaralioglu et al., 1998). When the tip end deflects, alternating fingers are displaced with respect to fixed reference fingers. In this way a a phase sensitive diffraction grating is created. The irradiance of the zeroth and first order principal maxima contain the deflection information. The readout scheme opened the way for parallel atomic force microscopy using interferometric detection, which was demonstrated a few years later (Sulchek et al., 2001). See Figure 2.13 for a schematic illustration of the setup. The technique does require a separate photodetector for each cantilever and also needs a strongly modified cantilever design.

Another readout technique that makes use of interdigitated fingers, which form a diffraction grating, is proposed by Thundat et al. (2000). The cantilever has fingers extending on both sides and a frame around the cantilever supports the reference fingers. The authors hint at the possibility of sensing in Fourier space motivated by the opportunities provided by spatial Fourier transform techniques.

Fast Fourier transforms (2D) are employed to readout a 2D array of cantilevers targeting probe storage (Sache et al., 2007). The authors show successful parallel readout of $7 \times 7$ cantilevers using interference between a reference beam and light reflected off the cantilevers. The exact mechanism is not reported. An acquisition rate of 15 fps is reached and 280 fps is envisioned after improvement, but still this speed is far from competitive for data storage applications. A second technique to monitor 2D arrays, for imaging purposes, is presented by Koyama et al. (2007). A CCD image of the diffraction pattern of the complete array is processed to retrieve

cantilever positions. The measurements show detection of a step of 300 nm, it remains unclear which image processing steps are performed, how fast they are and what the detection limit is. A third technique is presented by Favre et al. (2011) and targets applications in cell biology. The technique is based on a Linnik interferometer and results in a rearrangement of the interferometric fringes that appear on each cantilever image. LabVIEW software is used to run an algorithm that detects the rearrangement by image processing. This image processing software mainly limits the bandwidth, which is 10 Hz in the current setup.

### 2.3.3 Optical readout in probe storage

Several optical readout techniques for cantilever arrays have been proposed and demonstrated. Until now, none of them is used for probe storage. One of the reasons for the absence of these optical readout techniques is that industrial research and development projects such as those from HP (Naberhuis, 2002), Nanochip (Severi et al., 2009) and IBM (Vettiger et al., 2002) targeted small form factors; ranging from mobile storage to hard disk drive format. An archival system as targeted within ProTeM does not have this stringent size limitation. In despite, a readily implementable optical readout for an archival system is not available. All techniques that are available thus far, either offer insufficient bandwidth and/or require large amounts of hardware. Sequential readout does not offer competitive data rates for reading. See Table 2.1 for current data rates. Moreover, sequential readout means that many of the probes are sliding across the medium without their motion being detected. Image processing is time-consuming for digital signal processors and can not be employed for data storage.

The use of additional hardware, e.g. one laser-diode pair for each cantilever, leads to a very challenging system design. Despite the challenge, this could be a viable route. Light from one laser can be split-up and micro-lenses can be employed to focus light on each cantilever, photodetectors can be made very small when integrated on a chip. Still, the need for parallel readout remains, because such a system would tremendously benefit from the ability to detect the motion of multiple cantilevers per laser-diode pair. A technique that is capable of doing this is presented in Chapter 3.

## 2.4 Conclusion

Three different concepts of probe storage have been discussed and it is not clear which of the concepts is best. There are some differences between the three technologies, mainly in data rates and endurance. High data rates are shown at phase-change storage, however endurance remains an issue for conductive probes. Data densities are very high for each of the concepts and are demonstrated or expected to reach 10 Tb in$^{-2}$ or higher. Thermomechanical storage is the most mature and has already been demonstrated in a prototype (Millipede, 2005). Despite the significant progress that has been made in the development of a probe-based data

storage device no commercial product is currently available. It is very well possible that probe storage gains new attention in the future, when mechanically addressed storage reaches atomic densities.

Optical readout techniques for arrays of cantilevers are thus far not used in probe storage, most likely due to the form factor of the pursued storage device, the low data rate per probe the readout techniques provide for reading and the added complexity in terms of system design.

# Chapter 3

# Parallel optical readout of a probe array in dynamic mode

Parallel frequency readout of an array of cantilever probes is demonstrated using optical beam deflection with a single laser-diode pair. Multi-frequency addressing makes the individual nano-mechanical response of each cantilever distinguishable within the received signal. Addressing is accomplished by exciting the array with the sum of all cantilever resonant frequencies. This technique requires considerably less hardware compared to other parallel optical readout techniques. Readout is demonstrated in beam deflection mode and interference mode. Many cantilevers can be readout in parallel, limited by the oscillators' quality factor and available bandwidth. The proposed technique facilitates parallelism in applications at the nanoscale, including probe-based data storage and biological sensing.

## 3.1 Introduction

Arrays of micro-cantilevers are fast and highly sensitive sensors having enormous potential in a variety of applications, among which probe-based data storage (Abelmann et al., 2003; Vettiger et al., 2002), biochemical analysis and gas detection (Lang et al., 2005). Optical illumination of cantilever arrays can provide an accurate, reliable and non-invasive readout. Previous work has shown sequential optical readout (Alvarez and Tamayo, 2005; Lang et al., 1998) by illuminating only one cantilever at each instance of time. Parallel readout requiring one detector for each cantilever in the array and a considerably more complex cantilever design has also been demonstrated (Sulchek et al., 2001). Others have detected the multi-frequency response of a cantilever array (Ghatnekar-Nilsson et al., 2006), but neither a selective shift of a cantilever resonance frequency was measured, nor the absence of cross-talk between cantilevers. Here we present a technique for the optical readout

This chapter is based on W. W. Koelmans, J. van Honschoten, J. de Vries, P. Vettiger, L. Abelmann and M. C. Elwenspoek, "Parallel optical readout of cantilever arrays in dynamic mode", *Nanotechnology*, **21**, 395503, 2010.

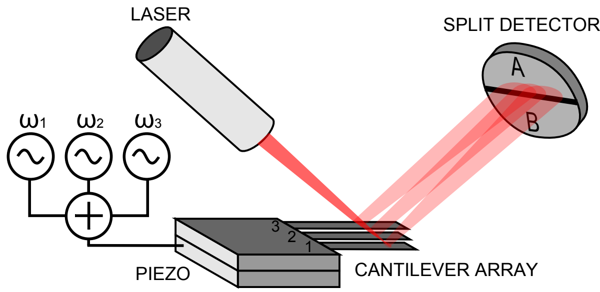


FIGURE 3.1 – *Schematic depiction of the technique for parallel readout of cantilever arrays.*

of resonance frequency shifts of individual cantilevers within an array using a single laser-diode pair, see Figure 3.1 for a schematic overview. The targeted application is the readout of bits stored in phase change media. Electrostatic force microscopy creates cantilever resonance frequency changes for each transition from amorphous to crystalline and vice versa. The readout technique is demonstrated using cantilever torque magnetometry (Stipe et al., 2001) to create resonance frequency shifts.

## 3.2 Experimental details

The cantilever arrays are fabricated from one large cantilever that is about 40 μm in width and 320 μm in length. First, a 600 nm thick magnetic layer (CoNi 80/20) is deposited by e-beam evaporation. The deposition is done on one side of the can-

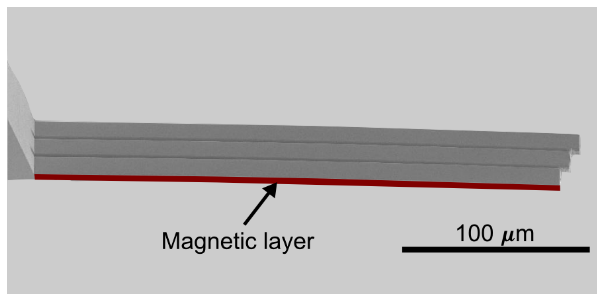


FIGURE 3.2 – *SEM image of a cantilever array consisting of three cantilevers each with a slightly different length. The array is machined by FIB out of a large, single cantilever.*

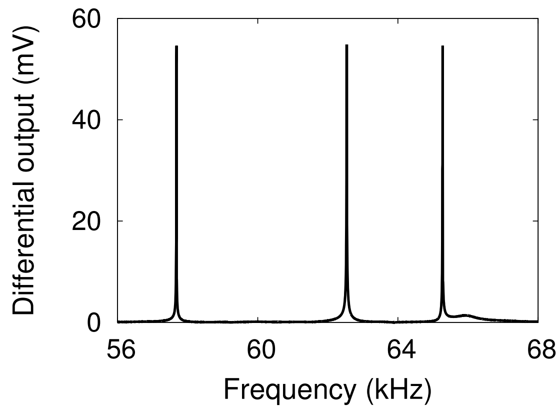


Figure 3.3 – *Frequency spectrum of a cantilever array with three cantilevers of slightly different length. The three peaks are well separated in the frequency domain.*

tilever to create the final array with one magnetic cantilever (see Figure 3.2). Only one cantilever is made magnetic to be able to identify possible mechanical coupling between the cantilevers. Next, we use a focused ion beam (FIB) to machine the cantilever into three cantilevers of slightly different length (roughly 5 µm ). The natural resonance frequency of a cantilever is inversely proportional to the cantilever length squared. The varying length yields a different resonance frequency for each cantilever and allows multi-frequency addressing. The resonance frequency shift of the magnetic cantilever due to an applied field can now be distinguished from the detector signal by locking on the corresponding frequency. The cantilever we use is a CantiClever (Van den Bos et al., 2002) for its rectangular cross-section. The selection of the CantiClever is mainly intended to obtain three cantilevers with the same inertial moment such that the resonance frequency of each cantilever only varies due to the length difference.

The experimental setup is a standard optical lever setup where a laser spot of approximately 60 µm in size is focused on the free ends of all three cantilevers. A HeNe laser (1 mW, $\lambda = 632.8$ nm) is used as illumination source. The reflected light is collected on a split-photodiode (OptoDiode ODD-3W-2). The cantilever array is piezoelectrically actuated, and in order to increase the quality factor it is placed in a vacuum environment ($10^{-2}$ mbar). The frequency response of the cantilever array as measured by a lock-in amplifier is displayed in Figure 3.3. The total duration of the frequency sweep is 31 s. The measurement shows that the resonance of each individual cantilever is well separated from the others.

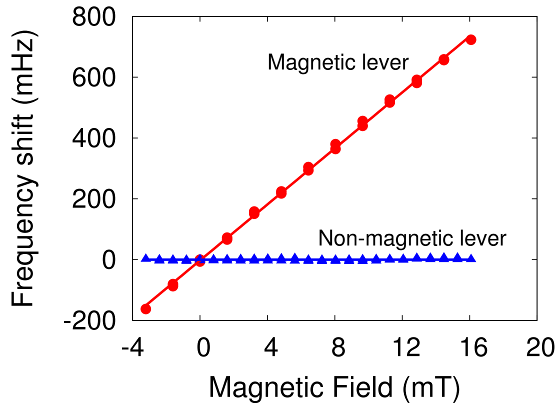


Figure 3.4 – *Measured frequency shift vs the externally applied magnetic field. The magnetic field is increased in steps and subsequently decreased. A linear regression fit is made to our data. The magnetic cantilever shows a sensitivity of* 46 mHz mT$^{-1}$. *The neighboring, non magnetic cantilever has a maximum shift of* 6 mHz *not showing any relation to the applied field.*

## 3.3 Results

### 3.3.1 Beam deflection

Figure 3.4 shows the field dependent measurement of the resonance frequencies of the magnetic cantilever and the non-magnetic neighboring cantilever. The orientation of the field is along the length direction of the cantilever, where the positive direction is from the base to the free end. The strength of the magnetic field is varied in steps and after each step a PID controller acquires the new value for the resonance frequency by keeping the phase difference between the driving voltage and the cantilever oscillation constant. A clear linear response (46 mHz mT$^{-1}$) of the resonant frequency of the magnetic cantilever to the applied field is observed. The resonance of the neighboring cantilever is not affected by the applied field showing a maximum variance of 6 mHz without any relation to the applied field, indicating that mechanical cross-talk is undetectable.

### 3.3.2 Interferometric readout

Next to the beam deflection method used above, we also demonstrated interferometric readout. In our experiment the 12 µm wide cantilevers are closely spaced at an inter-cantilever distance of 1 µm giving rise to a diffraction pattern on the detector side (Figure 3.5). We can therefore use the cantilever array as an optical

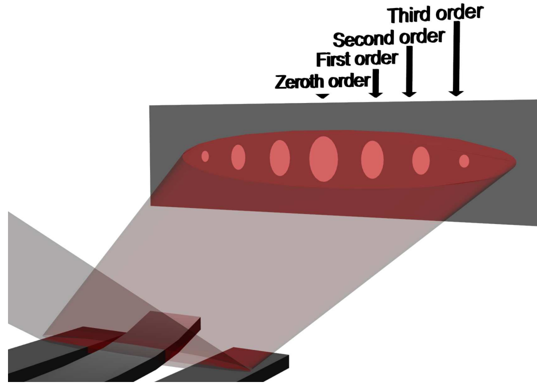


FIGURE 3.5 – *Schematic drawing of coherent laser light reflected off the back of a cantilever array, which functions as a reflection grating, creating a diffraction pattern in the detector plane.*

grating, in contrast with previous demonstrations of interferometric readout where a grating has been fabricated within a single cantilever (Sulchek et al., 2001; Thundat et al., 2000). Since Fresnel numbers are smaller than 1, the diffracted irradiance profile can be adequately described by Fraunhofer diffraction.

The laser spot covers the free ends of the cantilevers completely in the width direction, but in the length direction of the cantilever the spot size ($d$) is smaller than the cantilever length. The cantilever operates in the first vibration mode and for simplicity we make a linear approximation to the cantilever bending profile over the range of the spot. The cantilever angle with the horizontal is $\theta_n$ and we define the downward shift of the cantilever tip end as $\delta_n$, where $n$ represents the $n$-th cantilever in the array, with $n \in \{-1, 0, 1\}$. $I(0,0)$ is the irradiance at $(0,0)$ when no cantilevers are deflected. The irradiance $I(x,y)$ of the reflected light can be described as the sum of the contributions of all three cantilevers

$$I(x,y) = I(0,0)\, sinc^2\left(\frac{qw}{2}\right)\left|\sum_{n=-1}^{1} sinc\left(\frac{d}{2}(m + k\theta_n)\right)e^{-i\phi_n}\right|^2 \tag{3.1}$$

where $w$ is the cantilever width, $q = kx/R$ and $m = ky/R$, with $R$ the distance from the cantilever array to the detector. The phase $\phi_n$ is equal to $(2k\delta_n - nqp)$, with $p$ the cantilever period. The origin of the $(x, y)$ coordinate system is centered on the detector.

The light irradiance $I(x,y)$ as calculated according to Equation (3.1) is shown in Figure 3.6. The left plot shows the irradiance on the detector side when all three cantilevers are in equilibrium position. The right plot is calculated for a $\lambda/6$ deflection of the tip end of the center cantilever, showing the decrease in the zeroth order peak together with an increase in the first order peaks. To illustrate

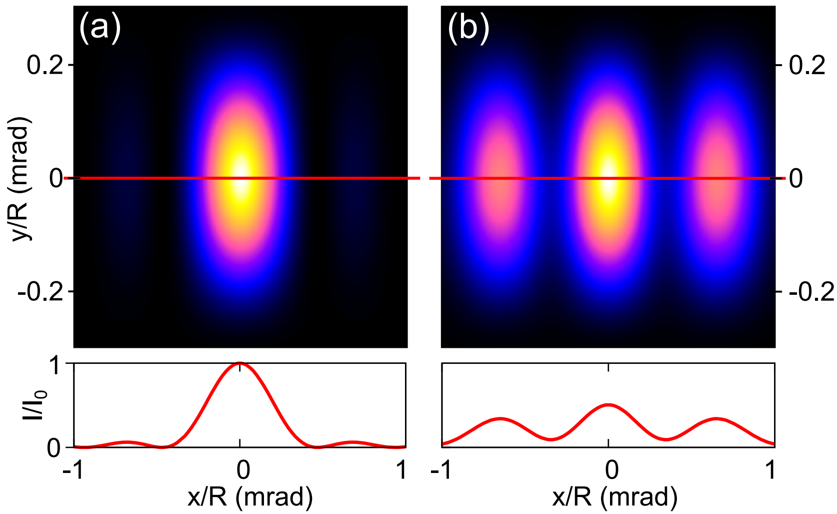


Figure 3.6 – *Calculated irradiance of light reflected from a three-cantilever array. (a) Reflection of the array with all cantilevers in equilibrium position. (b) Irradiance plot when the center cantilever is deflected downwards over $\lambda/6$. The resulting translation in the negative y-direction of the zeroth order irradiance peak is hardly visible on this scale.*

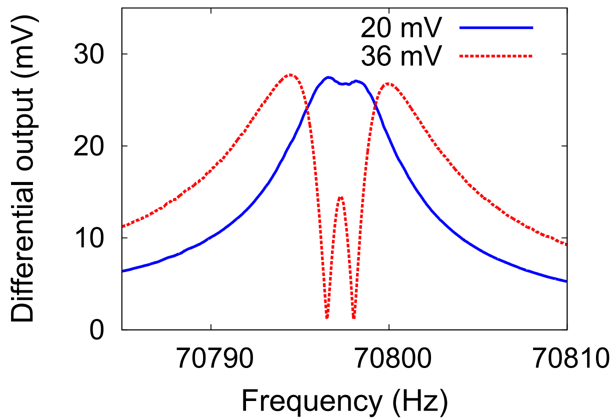


Figure 3.7 – *Measurement of a cantilever resonance curve that starts to show indents due to destructive interference when the deflection amplitude is increased, displayed for two different actuation voltages.*

the consequence of interference we again aimed only the zeroth order mode of the reflected laser light on the split-photodiode, the first order modes fall outside the detector area. Now the vibration amplitude of the center cantilever is increased. Figure 3.7 displays a high-accuracy frequency sweep showing the resonance peak of one cantilever within the array. The array that is used in this experiment is similar to the one shown in Figure 3.2, however the values of the resonance frequencies are slightly different. The measurement is performed using the differential output of the split-photodiode. At increased cantilever amplitude the irradiance decreases, leading to maximum light extinction at $\lambda/4$ deflection. The resulting indented resonance peak of Figure 3.7 follows from the behaviour of a split-photodiode detector, which is sensitive to both translation of the laser spot as well as to a change in the irradiance. The irradiance modulation of the light occurs twice every oscillation period of the cantilever and can thus be measured at twice the cantilever oscillation frequency.

To demonstrate the interferometric readout a similar 3-cantilever array with one magnetic cantilever is used. Instead of subtracting the signals from both diodes now a sum amplifier is used. The inset of Figure 3.8 shows the frequency response of the cantilever array measured at twice the excitation frequency of the array. The frequency band is limited to the resonance peak of the magnetic cantilever. Next, a magnetic field is applied and the resonance frequency shift as a function of applied magnetic field is obtained (Figure 3.8). The single photodiode instead of the split-photodiode measures only the irradiance modulation and no laser spot displacements. Consequently the alignment of the laser spot on the detector is much less demanding than in the case of a split-photodiode.

### 3.3.3 Comparison

The two demonstrated readout techniques require the same hardware and can therefore be interchangeably used. Readout of the beam deflection by a split-photodiode is preferred if a cantilever array has a large pitch such that it can no longer be treated as a grating. We foresee that sizable arrays pose a challenge in the focusing of all reflected laser spots on a split-photodiode. A cylindrical or line shaped laser spot is useful to improve the uniformity of laser light distribution over the complete array. Compared with conventional parallel readout of cantilever arrays where laser sources have to match the periodicity of the cantilever array, the flexibility for deviations in geometry of cantilever arrays is now strongly increased. The interferometric readout method offers the advantage of the usage of a single photodiode, which eases the alignment of the laser spot. Interferometry does require the deflection amplitude of each individual cantilever to stay below $\lambda/4$.

## 3.4 Noise and bandwidth

A parallel optical readout technique is bound to have a higher noise level than a technique that reads out a single cantilever. The thermal noise of each cantilever

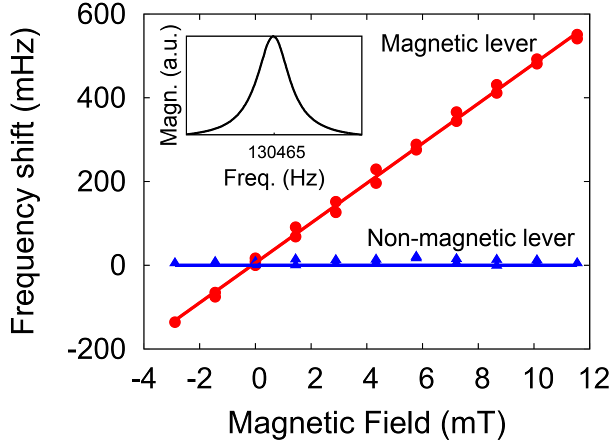


FIGURE 3.8 – *Measurement of the resonance frequency of a magnetic cantilever and its non-magnetic neighbor in an array using the irradiance change in the laser spot. The magnetic cantilever shows a sensitivity of* 48 mHz mT$^{-1}$. *The inset shows a typical frequency sweep of the same cantilever. The FWHM is* 6.5 Hz. *Notice that the measurement frequency (on the x-axis) is exactly twice the oscillation frequency of the cantilever.*

is independent and random and thus, the total increases when adding more cantilevers. When the optical power rises proportional to the number of cantilevers in the array, also the laser irradiance noise and shot noise increases. The total noise can be calculated when the parameters of the optical beam deflection setup are known. A generic example of a beam deflection setup is given in Sarid (1991) and has been used in Appendix A to derive the noise of a cantilever array. The thermal noise and shot noise give the largest contributions and the total noise is expressed as equivalent noise on the position of the cantilever tip end $\delta z$;

$$\sqrt{\langle \delta z^2 \rangle}_{\text{total}} = \sqrt{\langle \delta z^2 \rangle_{\text{thermal}} + \langle \delta z^2 \rangle_{\text{shot}}}$$
$$= \sqrt{B\frac{4k_{\text{B}}TQ}{k\omega_0} + nB\frac{\lambda^2 l^2}{9\pi^2 a^2}\frac{2e}{P\eta}},$$

where

$$\begin{aligned}
B &= \text{bandwidth (Hz)} \\
k_B &= \text{Boltzmann constant} = 1.38 \times 10^{-23}\,\text{J}\,\text{K}^{-1} \\
T &= \text{temperature (K)} \\
Q &= \text{quality factor}(-) \\
k &= \text{spring constant (N}\,\text{m}^{-1}) \\
\omega_0 &= \text{resonance frequency (rad}\,\text{s}^{-1}) \\
n &= \text{number of cantilevers in the array (-)} \\
\lambda &= \text{wavelength (m)} \\
l &= \text{cantilever length (m)} \\
a &= \text{half of laser spot width and height (m)} \\
e &= 1.6 \times 10^{-19}\,\text{C} \\
P &= \text{light power per cantilever (W)} \\
\eta &= \frac{i}{P}\text{diode efficiency (A/W)}
\end{aligned}$$

The main parameters influencing the amount of noise per $\sqrt{Hz}$ are, for thermal noise, the spring constant and quality factor and, for shot noise, the available laser power per cantilever. Thermal noise of each cantilever will arrive at the split-photodiode; however, due to the bandpass filter that is present in the detection electronics, the thermal noise of only one cantilever is present in the output signal. This reduction of thermal noise is a significant advantage of this readout technique. Note that there will be thermal noise contributions of neighboring cantilevers in the frequency band of interest; however, the quality factor is assumed to be high ($Q \geq 100$ is sufficient up to 1000 cantilevers), which makes these contributions negligible. See for more details Appendix A.

When we assume that the light power $P$ per cantilever remains constant, shot noise increases with an increasing number of cantilevers in array. However, when we assume that the light power is allowed to rise, shot noise may decrease. Since shot noise scales with $\sqrt{P}$ and the signal of the split-photodiode scales with $P$, the signal-to-noise ratio increases with $\sqrt{P}$. The parameters shown in Table 3.1 are used for an example calculation. In this case a light power of 150 μW per cantilever results in equal contributions of thermal and shot noise. Under 150 μW per cantilever the shot noise dominates. To make thermal noise dominate, a laser power above 15 mW is required to read out an array of 100 cantilevers. In summary, the influence of shot noise can be reduced by increasing the light power per cantilever.

The bandwidth of the proposed technique depends on the distance between the resonance frequency peaks of the cantilever in the frequency domain. When the bandwidth exceeds half the distance between the resonance peaks, electrical cross-

Table 3.1 – *Specification of the parameters used for calculation.*

| | | |
|---|---|---|
| $n$ | = | 100 (cantilevers) |
| $k$ | = | $1\,\mathrm{N\,m^{-1}}$ |
| $\omega_0$ | = | 500 kHz |
| $T$ | = | 300 K |
| $B$ | = | 100 Hz |
| $Q$ | = | 100 |

talk occurs. This means that high resonance frequencies or operation at higher vibration modes is desirable.

## 3.5 Conclusion

Two optical readout techniques have been developed for the parallel readout of cantilever arrays in dynamic mode. The well-known optical lever technique is extended to arrays without any modification to the detection hardware while maintaining the high throughput. Addressing each cantilever at its own resonance frequency is the key in distinguishing the response of each individual cantilever. The interferometric detection functions likewise, however it requires only a single photodiode instead of a split-photodiode by exploiting the inherent destructive interference effects occurring when light is reflected from closely spaced cantilevers. Both techniques have been demonstrated showing accurate measurements of a single cantilever within the array that changes its resonance frequency. Mechanical coupling effects were not observed within the measurement precision (<10 mHz). The bandpass filter in the detection hardware causes thermal noise not to increase with an increasing number of cantilevers in an array. Shot noise does increase with an increasing number of cantilevers in array when the light power per cantilever remains constant. The influence of shot noise can be reduced by raising the light power per cantilever. The bandwidth of the proposed technique is equal to the spacing between the cantilever resonance peaks in the frequency domain.

## Acknowledgments

The author thanks Martin Siekman for experimental support, Johnny Sanderink for operating the FIB and SmartTip for providing the CantiClevers. This work has been carried out as part of the European FP6 project 'Probe-based Terabit Memory'.

# Chapter 4

# Parallel optical readout of a probe array in static mode

Topographically stored data can be read back by a probe array operating in contact mode while scanning across the bits. The cantilever deflection is determined by the local height of the medium. Such a probe array is said to operate in static mode. A schematic depiction of a probe array detecting indentations in a polymer medium is shown in Figure 4.1. A probe can either be on top of the polymer sample or inside an indentation. This chapter houses two sections, which both relate to this scheme. The first section presents an optical readout method for probe arrays operating in static mode while detecting stored data. The second section gives a detailed description of a fabrication process for cantilever arrays that is specifically designed to reduce fabrication complexity and produce a highly uniform tip-sample distance. Both sections have their own conclusion paragraphs.

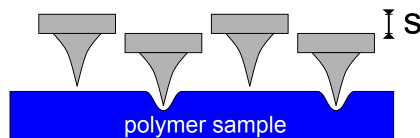


FIGURE 4.1 – *Schematic depiction of a probe array detecting indentations in a polymer medium. The indentations all have an equal depth s.*

This chapter is an extensive elaboration of W. W. Koelmans, T. Peters, L. Abelmann and M. C. Elwenspoek, "Fabrication of cantilever arrays with tips for parallel optical readout", presented at the *21$^{st}$ Micromechanics and Micro systems Europe Workshop (MME 2010)*, Enschede, the Netherlands, 26-29 Sept. 2010. The theoretical analysis of diffraction patterns is based on J. van Honschoten, H. W. de Jong, W. W. Koelmans, T. P. Parnell and O. V. Zaboronski, "Information storage and retrieval for probe storage using optical diffraction patterns", accepted for publication in *Journal of Applied Physics*. A concept-version is available at arxiv.org/abs/1104.0871.

## 4.1 Readout of a probe array using diffraction patterns

Sensing of cantilever deflection with the use of optical diffraction patterns has been introduced by Manalis et al. (1996). By fabricating a cantilever containing interdigitated fingers a diffraction grating is formed. When the cantilever is bent, alternating fingers are deflected while remaining fingers are held fixed. The technique is extended to parallel operation by illuminating multiple interdigital cantilevers and capturing the diffraction pattern from each cantilever on a separate detector (Sulchek et al., 2001). Others have fabricated a similar design where the fixed fingers are attached to a frame surrounding the cantilever, instead of to the cantilever itself. The authors foresee a great potential of sensing in Fourier space (Thundat et al., 2000).

We present a new scheme where the cantilevers itself form an optical grating and the state of deflection of each cantilever within the array determines the diffraction pattern, which is captured by a 1-dimensional (1D) array of photodiodes. Each cantilever can be regarded as a slit in a traditional multiple slit diffraction experiment. In our situation the phase of the reflected light is a function of the amount of deflection of the cantilever, in contrast to a slit diffraction experiment, where the slits are assumed to contain light sources with equal phase. A significant advantage of interferometry at short distances, i.e. the distance between the cantilevers, as opposed to the use of a reference beam, is a high robustness for external shocks and immunity for thermal expansion of the optical path.

We will show that the diffraction patterns obey one-dimensional Fraunhofer diffraction theory, which makes it possibly to very quickly obtain the cantilever positions. Possible detection algorithms and their performance in a recording channel are presented in Van Honschoten et al. (2011). In this chapter we confine our discussion to the theory and experimental validation of the technique, including strategies to increase the read signal when the cantilever deflections become very small.

The presented technique targets applications were two levels of cantilever deflection occur. The most prominent application is probe-based data storage on polymer media (Pantazi et al., 2008), where data is defined by means of indentations of equal depth. Another potential application area is imaging of surfaces that have two levels of depth, e.g. in quality control of lithographical processes.

The organization is as follows. In Section §4.1.1 the theory of the readout technique is discussed. The equation of the irradiance profile that is created by a cantilever array is derived, based on the Fraunhofer approximation. In Section §4.1.2 the experimental verification is introduced by a detailed explanation of the experimental procedure. For these experiments we employ a 2D CCD camera instead of a 1D array of photodiodes, because a larger detection area simplifies alignment procedures. The following section, Section §4.1.3, presents an analysis of the results. Simulations show in Section §4.1.4 that in case of small cantilever deflections the signal strength can be drastically increased. Finally, a discussion of the newly developed technique is given in Section §4.1.5, followed by the conclusions in Section §4.1.6.

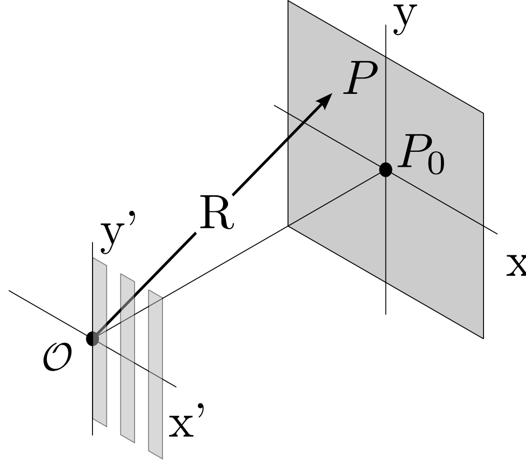


FIGURE 4.2 – *Geometry of the model. The plane of the light source is described by* $(x', y', \mathcal{O})$*, the plane of observation by* $(x, y, P_0)$*. The length of R is assumed to be constant in the Fraunhofer approximation.*

### 4.1.1 Theory

We start by assuming that laser light with wavelength $\lambda$ reflected from a cantilever array obeys Fraunhofer diffraction theory. This assumption can be justified by ensuring that Fresnel numbers are well below 1. The geometry of our model is depicted in Figure 4.2. The Fresnel number is given by $F = a^2\ \lambda^{-1}\ R^{-1}$, where $a$ is the greatest width of the aperture or obstacle.

The cantilevers are illuminated by a laser beam with wave number $k = 2\pi/\lambda$. A portion of the light is reflected, which can be described by $\chi(x')$. This is a source strength per unit area, with unit V m$^{-2}$, and is assumed to be constant per cantilever. The diffraction integral (Hecht, 2002) gives the wave function $\psi(x, y)$ describing the electric field at the projection plane $(x,y)$ as

$$\psi(x, y) = e^{ikR}/R \iint_{\text{array}} \chi(x') e^{-ik(xx')/R} dx' dy'.$$

The length of a cantilever is large compared to its width ($l > 5w$) so we can neglect the dependence of the diffraction pattern on the direction parallel to the cantilever length, $y'$. The integral reduces to a one-dimensional problem. We now write the reflected portion as a source strength per unit length on the cantilevers as $\xi(x')$, resulting in

$$\psi(x) = e^{ikR}/R \int_{\text{array}} \xi(x') e^{-ik(xx')/R} dx'. \tag{4.1}$$

Note that $\psi(x)$ is similar to the Fourier transform of $\xi(x')$. The geometry of the cantilever array is inserted into Equation (4.1). The cantilever index is $n \in \{0, 1, 2, 3, \ldots, N-1\}$, with $N$ is the total number of cantilevers. Momentarily assuming that $\xi(x') = 1$, we obtain

$$\psi(x) = Cw \operatorname{sinc}\left(\frac{qw}{2}\right) \sum_{n=0}^{N-1} e^{-iqnp}, \tag{4.2}$$

where $C$ is a constant, $q = kx/R$ and $p$ the cantilever period. Next, deflection of a set of cantilevers is introduced. If the deflection of a cantilever is $s$, the additional path length of the light of the laser beam is, for small angles, approximated by $2s$. So that the wave function of the light undergoes an additional phase shift $2ks$. We can describe this situation by incorporating the function $\xi(n)$ in Equation (4.2), giving

$$\psi(x) = Cw \operatorname{sinc}\left(\frac{qw}{2}\right) \sum_{n=0}^{N-1} \xi(n) e^{-iqnp}.$$

where

$$\xi(n) = \begin{cases} 1 & \text{for undeflected cantilevers,} \\ e^{-2iks} & \text{for deflected cantilevers.} \end{cases}$$

The irradiance in W m$^{-2}$ is then given by

$$I(x) = \left|\psi(x)\right|^2 = I(0) \operatorname{sinc}^2\left(\frac{qw}{2}\right) \left| \sum_{n=0}^{N-1} \xi(n) e^{-iqnp} \right|^2, \tag{4.3}$$

where $I(0)$ is the irradiance at $P_0$ with no cantilevers deflected. The irradiance profile as a function of $x$ can be obtained by measurement. Because $\psi(x)$ has to be multiplied by its complex conjugate, $I(x) = \psi(x)\overline{\psi(x)}$, to obtain the irradiance, information about the phase of the optical field is lost. It can no longer be guaranteed that the irradiance, as described by Equation (4.3), can be transformed back to $\xi(x')$, because optical fields that only differ in phase of the light at the array of photodiodes will yield the same irradiance profile.

It is shown in Van Honschoten et al. (2011) that this relation can nonetheless be exploited to easily retrieve the state of each cantilever with the use of digital Fourier transforms and low complexity signal processing algorithms.

### Equal irradiance profiles

To determine which situations lead to irradiance profiles that can be caused by more than one $\xi(x')$, we examine all possible configurations of deflections of cantilevers in an array. We define a '0' as representation for an undeflected cantilever and a '1' to represent a cantilever deflected by the amount $s$, as is shown in Figure 4.3. Each cantilever is represented by its cross-section, where a deflected cantilever is lowered by the amount $s$. Cantilever configurations leading to equal irradiance profiles can be obtained by rotating a front-view of the given configuration by 180°,

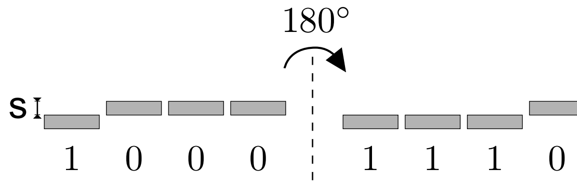


Figure 4.3 – *Schematic front view of two cantilever configurations that result in equal irradiance profiles. The equivalent configuration is obtained by rotating the configuration at the left by* 180°.

as is illustrated in Figure 4.3. We term the configurations of deflected cantilevers that lead to equal irradiance profiles 'equivalent configurations'.

Some configurations are rotated to find exactly the same configuration. This only occurs in arrays with an even number of cantilevers. Therefore these do not have an equivalent configuration.

An array of e.g. $N = 5$ cantilevers has a maximum of $2^N = 32$ configurations, which are represented by all binary numbers with $N = 5$ bits. The potential equivalent configuration can now be found by mirroring and inverting the binary number, which gives the same result as the 180° rotation in Figure 4.3. This transformation is mathematically described by

$$B_n = \overline{C_{N-n-1}}, \tag{4.4}$$

where $B$ and $C$ are equivalent configurations in binary representation.

We derive the total number of unique irradiance profiles. For cantilever arrays with $N$ is odd, each configuration has exactly one unique equivalent configuration. This makes the number $A$ of unique irradiance profiles (or the number of useful configurations) half of the total number. For $N$ is even, the configurations that have no equivalent configuration, can be found by all combinations of half of the number of cantilevers in an array, $N/2$. The state of the other half of the cantilevers is now given by Equation (4.4). This means there are $2^{N/2}$ configurations without an equivalent. Summarizing:

$$A_{\text{unique}} = \begin{cases} 2^{N-1} & \text{if } N \text{ is odd,} \\ 2^{N-1} + \frac{1}{2}2^{N/2} & \text{if } N \text{ is even.} \end{cases} \tag{4.5}$$

### Worst-case configurations

The set of configurations that does not yield equal irradiance profiles can be distinguished after detection. This set will contain configurations leading to profiles that are similar, but not equal. The set contains other configurations that give rise to profiles that differ significantly. In order to quantize the difference between two

irradiance profiles, we define a measure for this difference as $\Delta I_\mathrm{P}$. It can be viewed as the strength of the signal difference between the two profiles. $\Delta I_P$ is calculated by integration over the complete profile, with angle of diffraction $\theta$ as integration variable. $\Delta I_P$ is defined as

$$\Delta I_\mathrm{P} = \sqrt{\int_{\text{profile}} [I_{\mathrm{P}_1}(\theta) - I_{\mathrm{P}_2}(\theta)]^2 d\theta} \, \frac{1}{I_{\mathrm{P1,max}}}, \tag{4.6}$$

where the two profiles are expressed by $I_{\mathrm{P}_1}(\theta)$ and $I_{\mathrm{P}_2}(\theta)$. $I_{\mathrm{P1,max}}$ is the maximum value of $I_{\mathrm{P}_1}$. $I_{\mathrm{P}_1}$ and $I_{\mathrm{P}_2}$ are always chosen with $I_{\mathrm{P1,max}} \geq I_{\mathrm{P2,max}}$. The scaling with this maximum value represents the scaling of the signal to the maximum range of the signal amplifiers (transimpedance amplifier in case of a photodiode) in an experimental situation. Using Equation (4.6) the signal $\Delta I_\mathrm{P}$ can be calculated for all pairs of configurations of a given cantilever array with deflection size $s$. The pairs of two irradiance profiles that are most difficult to distinguish are termed worst-case pairs. If, for a certain array and a certain size of deflection, the worst-case pairs can be distinguished in a measurement, each profile can successfully be traced back to the cantilever configuration. In order to find the worst-case pairs, simulations are performed in MatLab. As an example we look at all pairs of configurations of an array of five cantilevers.

Using Equation (4.5), there are $2^{N-1} = 2^4 = 16$ unique profiles. The total number of pairs is then given by $1/2 \times 16 \times (16-1) = 120$. For the simulation, the deflection is set to $s$=10 nm, the cantilevers have a width $w$=10 μm and a period of $p$=40 μm. The wavelength of the laser light is $\lambda$=640 nm. Figure 4.4 shows the calculated $\Delta I_\mathrm{P}$ for all 120 pairs. The mean $M$ of all $\Delta I_\mathrm{P}$ is $5.11 \times 10^{-3}$. It is seen from this data that there are 10 pairs that are significantly more difficult to distinguish. All 10 worst-case pairs are listed in Table 4.1. In the table the $\Delta I_\mathrm{P}$ of these pairs is shown as a fraction of the mean $M$. There is significantly smaller amount of signal generated by these

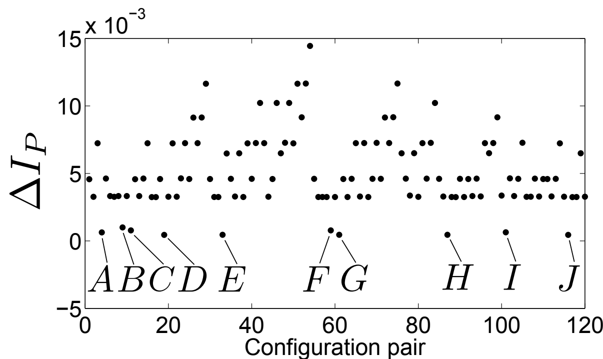


FIGURE 4.4 – *Signal $\Delta I_P$ for all 120 pairs of configurations with five cantilevers using a deflection of* 10 nm. *The 10 worst-case pairs are labeled and specified in Table 4.1.*

Table 4.1 – *Worst-case pairs of configurations.*

| | Configuration 1 | Configuration 2 | $\Delta I_P$ / M |
|---|---|---|---|
| *A* | 00000 | 00100 | 0.12 |
| *B* | 00000 | 01010 | 0.20 |
| *C* | 00000 | 01110 | 0.15 |
| *D* | 00001 | 00101 | 0.09 |
| *E* | 00010 | 00110 | 0.09 |
| *F* | 00100 | 01010 | 0.15 |
| *G* | 00100 | 01110 | 0.09 |
| *H* | 01000 | 01100 | 0.09 |
| *I* | 01010 | 01110 | 0.13 |
| *J* | 10000 | 10100 | 0.09 |

10 pairs. Of the other 110 pairs, the pair giving the lowest signal has $\Delta I_P/M = 0.63$. This can also be recognized in Figure 4.4 by the gap between the 10 worst-case pairs and the other data points. This is an issue which has to be considered when coding user data into bits to be stored on the medium. One could simply avoid worst-case configurations, or allow for more complex coding schemes.

### 4.1.2 Experimental details

The experimental setup is a multi-probe scanning probe microscope (SPM) that can house one-dimensional arrays of probes. The array of probes can be aligned with the sample surface with a slip-stick motor that adjusts the roll-angle of the array. A second slip-stick motor moves the array up and down ($z$-direction) to approach the sample, commonly referred to as coarse approach. The sample is mounted on a commercial piezoelectric scan table with $xyz$ motion capability. See for a detailed description of the setup Appendix B.

The SPM is equipped with an optical setup to readout arrays of cantilevers. A schematic depiction of the optical path is shown in Figure 4.5. The spot from a diode laser with a wavelength of 635 nm and 3 mW power is expanded five times using a beam expander. The beam is sent through a rectangular shaped slit and then focused in one direction by a cylindrical lens with a back focal distance of 200 mm. A prism reflects the beam on the cantilever array. The array is positioned in the back focal plane of the cylindrical lens. The laser spot is now line shaped and illuminates each of the cantilevers in the array. The reflected light from the cantilever array creates a diffraction pattern. The pattern is reflected by a second prism into a second cylindrical lens with a back focal distance of 60 mm. The lens is rotated 90° with respect to the first cylindrical lens. The second lens determines the width of the diffraction pattern on the CCD camera, which is positioned in the back focal plane of the lens. The image plane is now effectively at infinite distance; an ideal construction to produce a Fraunhofer diffraction pattern. The CCD camera has an active area of 2048 pixels × 1536 pixels and a pixel size of 3.2 µm. The camera

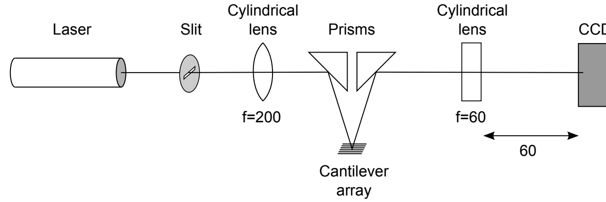


Figure 4.5 – *Schematic depiction of the optical path to read out cantilever arrays. A rectangular laser spot is focused by a cylindrical lens into a line shaped beam, illuminating all cantilevers within the array. A second cylindrical lens (rotated 90° with respect to the first) shapes the diffraction pattern to fit the active CCD area. All measurements are in mm.*

is connected to a computer equipped with software capable of reading the image data. The exposure time is 9.0 ms, making the measurement bandwidth 111 Hz. The CCD images are analyzed by image-analysis scripts written in MatLab software. The procedure is as follows: the irradiance values are extracted from a rectangular area within the image. The long side of the rectangle is aligned with the direction of diffraction ($\theta$). Irradiance values are averaged over the height of the area. The height can be tuned and is usually taken around 250 pixels, minimizing influence of dust and particles. Low-pass filtering is performed to remove high-spatial-frequency noise.

The cantilever arrays are specially prepared for the experimental verification of the optical readout technique. Two types of arrays have been fabricated: (type 1) arrays without tips, and (type 2) arrays with silicon tips. During the experiments shown here type 1 cantilevers are used. For a detailed description of the fabrication process we refer to §4.2, where the fabrication of type 2 arrays is described. Because type 1 is fabricated much along the lines of the fabrication process of type 2; however, with exclusion of the steps that define the tips on the cantilevers, we suffice to report the more elaborate fabrication process of type 2. Type 2 cantilever arrays are scheduled to be used in a later stage of the experimental verification.

### 4.1.3 Results and discussion

#### Fraunhofer diffraction patterns

The first experiments are performed to investigate whether the recorded diffraction patterns are in agreement with Fraunhofer diffraction theory. The second cylindrical lens is removed for this experiment, because the non-ideal lens will cause deviations in the diffraction pattern. An array consisting of five cantilevers, which are 14 µm wide and have a period of 20 µm, is selected and mounted in the setup. The cantilevers are all in undeflected position, because they are not in contact with the sample stage. This situation is described by '00000' in the previously defined binary representation. The diffraction pattern is recorded and an irradiance

profile is extracted and displayed in Figure 4.6. The irradiance is normalized using the height of the zeroth-order principal maximum $I(0)$. In the same figure a theoretical curve calculated according to Equation (4.3) is shown that is in very good agreement with the measurement. The difference between the curves according to Equation (4.6) is $\Delta I_P = 1.8 \times 10^{-3}$. This measurement clearly demonstrates that Fraunhofer theory can be applied to a cantilever array acting as a grating.

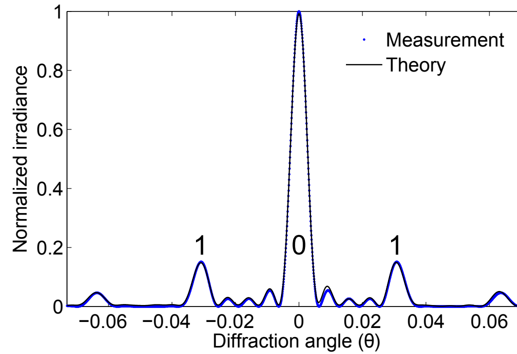


FIGURE 4.6 – *Irradiance profile of the diffraction pattern of a cantilever array consisting of five cantilevers. The measurement fits very well with Fraunhofer diffraction theory:* $\Delta I_P = 1.8 \times 10^{-3}$. *Principal maxima are numbered for zeroth-order and first-order.*

**Introducing cantilever deflections**

In the following set of experiments we introduce deflections in the cantilevers. Deflection of a cantilever by the amount $s$ will create offset in the reflecting surface of this cantilever with respect to the rest of the array. The laser spot is focused on the array to a line width $d$ of approximately 80 µm. The spot is aligned on the cantilever tip end as is illustrated in the schematic top view in Figure 4.7. The same figure also gives a side view of the situation and it is seen that, although a deflection $s$ is realized at the tip end, the deflection $h$ at the position of the laser spot is smaller. It is illustrated that curvature is introduced in the cantilever surface across the width $d$ of the laser spot. This means that the amount of deflection is not constant, but is averaged over the width of the laser spot. Therefore, the measured deflection $h$ is not equal to size of the deflection $s$ of the tip end, but a function of the position of the laser spot.

A series of measurements is performed where the amount of deflection $s$ is varied. The measurements are performed on the same array of three cantilevers of Figure 4.6. The two outer cantilevers are deflected upwards by the same amount. An increasing deflection leads to lowering of the zeroth-order principal maximum,

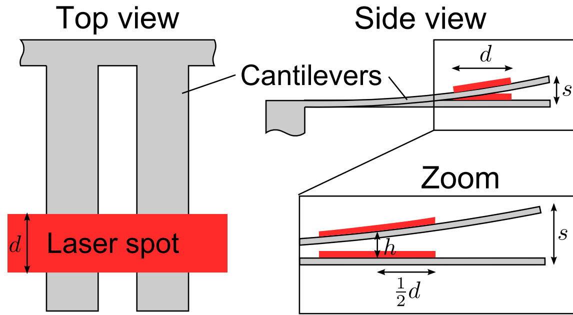


FIGURE 4.7 – *Schematic depiction of a line shaped laser spot focused on a cantilever array, for clarity only two cantilevers are shown. The side view illustrates that deflection of a cantilever leads to curvature of the reflection surface. The amount of deflection h at the centre of the laser spot is shown to be smaller than the deflection s at the tip end.*

whereas the two first first-order maxima grow in amplitude. The ratio between the amplitude of the zeroth-order maximum and the amplitude of the first-order maxima significantly decreases and is thus a good measure to monitor the cantilever deflection. This ratio is presented in Figure 4.8 as a function of deflection $h$. Note the log-scale on the $y$-axis. Each data point is obtained after increasing the deflection $s$ with the $z$-piezo of the scantable by 50 nm. A simulated curve of the ratio is fitted to the measured curve as shown in Figure 4.8. The good fit shows that deflected cantilevers can also be described by one-dimensional Fraunhofer theory. The amount of deflection at the centre position of the spot on the lever is calculated to be 22.5 nm. This is an average value across the width of the laser spot. An error in this calculated deflection of 1 nm would lead to a shift of 20 nm for the data point at maximum deflection. The distance between the measured and simulated curve at maximum deflection is, however, 2.5 nm. This indicates the high sensitivity of the method. Figure 4.8 shows regions of higher and lower sensitivity. At a deflection $h$ of 150 nm to 170 nm there is almost no change in amplitude ratio. In this region, around $h = \lambda/4 = 160$ nm, the signal for will be minimum for small deflections. Around $h = 0$ nm and $h = \lambda/2 = 320$ nm the sensitivity is also very low. At $\lambda/8$ it is at its maximum. In the following this observation will be exploited.

#### Offset in deflections

We illustrate the effect of offset in deflection with an array of four cantilevers having a width of 15 µm and a period of 25 µm. The outer right of the four cantilevers is bent in steps of $s = 50$ nm at the tip. The deflection $h$ at the centre of the laser spot is calculated to be approximately 23 nm per step.

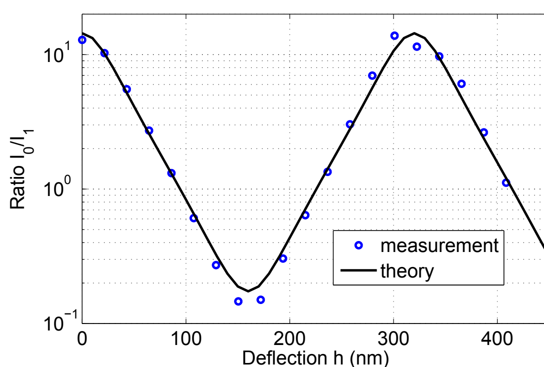


FIGURE 4.8 – *The ratio of the amplitudes of zeroth mode ($I_0$) and first mode ($I_1$) as a function of the deflection h at the centre of the laser spot is plotted. The measurements are in close agreement with the theory.*

For two deflections of $h = 22$ nm and $h = 45$ nm the two measured profiles are shown in Figure 4.9. $\Delta I_P$ is calculated to be $12.6 \times 10^{-3}$. The simulated value is slightly lower at $11.8 \times 10^{-3}$. A second set of measurements is performed at deflections of 136.2 nm and 159.0 nm. The two resulting profiles are plotted in Figure 4.10. $\Delta I_P$ is calculated to be $20.0 \times 10^{-3}$. Simulations give an expected value of $20.9 \times 10^{-3}$. Despite the bent cantilever surface, the simulations are again in good agreement with the measurements. The difference in $\Delta I_P$ for the two pairs of profile in Figure 4.9 and Figure 4.10 is significant. Although the deflections are approx-

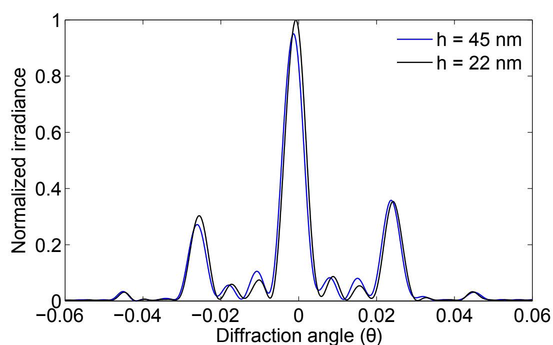


FIGURE 4.9 – *Two irradiance profiles created by an array of four cantilevers that has its outer right cantilever deflected by $h = 22$ nm and $h = 45$ nm. $\Delta I_P = 12.6 \times 10^{-3}$ for this pair of profiles.*

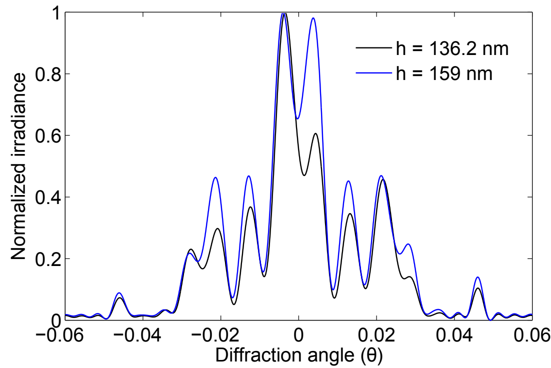


FIGURE 4.10 – *Two irradiance profiles created by an array of four cantilevers that has its outer right cantilever deflected by* 136.2 nm *and* 159 nm. $\Delta I_P = 20.0 \times 10^{-3}$ *for this pair of profiles.*

imately equal the signal strength is increased by a factor of 1.6. The measurements show the effect of the non-linear sensitivity of the technique.

### 4.1.4 Improving the detection signal

For three cantilevers the maximum sensitivity is obtained when the centre cantilever operates around $h = \lambda/8$ deflection with respect to its neighbors. For any other array of cantilevers that can be in any other configuration state, it is not immediately clear when maximum sensitivity is obtained. One possible implementation of this observation is the addition of an offset layer of thickness $\phi$ on top of every second cantilever in an array, see Figure 4.11. Note that the figure is a schematic representation, which is not to scale. In a practical situation, with $t$ the cantilever thickness, $t \gg \phi \gg s$.

In order to verify the increase in sensitivity, we employ Equation (4.6) and calculate $\Delta I_P$ for all configurations, both with and without the offset layer. In the process of simulation we have optimized $\phi$ for very small deflections of $h = 1$ nm. The most beneficial value is $\phi = \lambda/7.1$. This number depends on the ratio $\lambda/h$ and on $N$. The dependency on $N$ is not very strong and we can thus use a constant $\phi = \lambda/7.1$ for all simulations. The array of nine cantilevers shown in Figure 4.11 gives an average increase in $\Delta I_P$ for all configurations of 7.7.

In Figure 4.12 $\Delta I_P$ is calculated for all pairs of configurations of an array of five cantilevers. The black dots represent the values without the use of an offset layer. The unfilled circles represent the calculations with an offset of $\phi = \lambda/7.1$ on every second cantilever and show a clear increase in signal. The mean $M$ is increased from $0.5 \times 10^{-3}$ to $1.3 \times 10^{-3}$. Moreover, the worst-case configuration pairs have

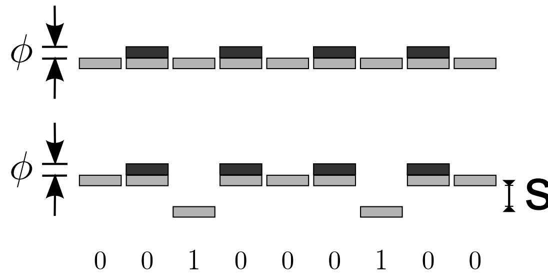


FIGURE 4.11 – *Frontview of two arrays of nine cantilevers with an offset layer of thickness $\phi$ on every second cantilever to improve the sensitivity of the readout method for small deflections s.*

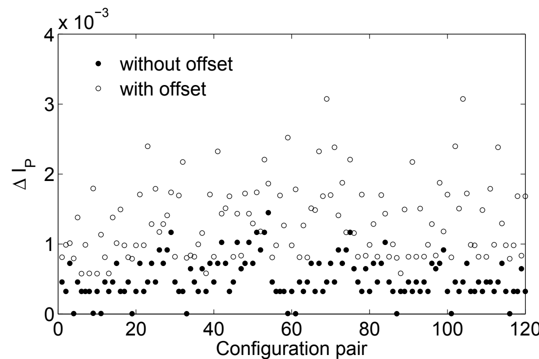


FIGURE 4.12 – *$\Delta I_P$ is calculated for all configuration pairs of an array of five cantilevers. The deflection h is set to* 1 nm. *The filled circles are the values when no offset layer is present. A clear increase in signal is seen when an offset of $\phi = \lambda/7.1$* nm *is added (open circles).*

gained signal far above average. Each of them gives over 13 times more signal and on average 20 times more, making these pairs no longer difficult to detect.

Figure 4.13 shows the effect of the offset as a function of the number $N$ of cantilevers in an array. The mean $M$ of all $\Delta I_P$ is calculated for each $N$, with and without offset. As an extra measure to increase the signal the wavelength is changed from 640 nm to 405 nm. The deflection $h$ is set to 2 nm. It is evident that the mean signal decreases with increasing $N$; however, the decrease can be countered by the addition of the offset layers.

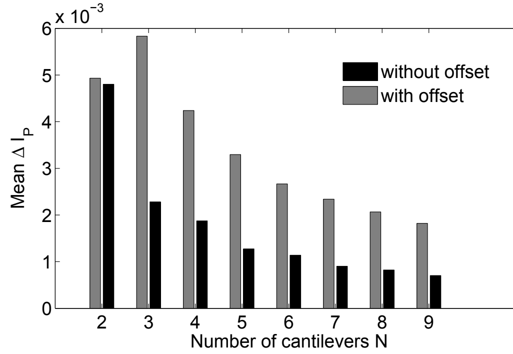


FIGURE 4.13 – *Mean $\Delta I_P$ as a function of the number of cantilevers in an array. Offset layers of $\phi = \lambda/7.1$ on every second cantilever increase the signal significantly.*

### 4.1.5 Discussion

With the help of the measurement in Figure 4.6 a simple estimation can be made of patterns that are detectable with our current setup. The size of signal $\Delta I_P = 1.8 \times 10^{-3}$ that represents the mismatch with the theoretical curve is used as a minimum of detectability. Using an offset layer on every second cantilever and a wavelength of 405 nm we estimate that we can detect all configurations of cantilevers in an array of seven, with a deflection $h = 6$ nm corresponding to tip deflections of $s = 12$ nm. The measurement bandwidth is 111 Hz. Larger arrays and smaller deflections require a better measurement setup. The setup has not been optimized and we expect that the signal can be dramatically improved. The thermal cantilever noise is not large because the tip end is supported. Shot noise is expected to be the major noise source, provided that the optical power is sufficiently large. The prime setup improvement is to replace the CCD camera by a customized array of photodiodes, which should dramatically increase the performance of the detection both in sensitivity as well as in bandwidth. Currently, the frame rate is limited to 8 fps due to the slow CCD camera and limited data rate to the computer. Photodiodes can be both very fast and very sensitive. The second cylindrical lens causes a deviation to the irradiance profile and could be omitted if the size of the array of photodetectors is chosen well. The spot size of the laser on the cantilevers can be decreased and shifted further towards the tip end of the cantilever. In this way the deflection $h$ at the centre of the laser spot approximates the deflection $s$ at the tip.

The occurrence of equal irradiance profiles limits the number of available configurations. This does not have to pose a problem in probe storage. Suitable coding strategies can prevent the use of the equal profiles. Another solution is to add an extra cantilever to the array that does not have a tip. Such a cantilever breaks the symmetry and makes all configurations accessible.

### 4.1.6 Conclusion

Parallel optical readout of a probe array operating in static mode can be achieved by recording the diffraction pattern that the array, which acts as a grating, creates. The diffraction pattern is shown to obey one-dimensional Fraunhofer theory. The developed technique is straightforward applicable when two discrete levels are permitted in cantilever bending. There exist cantilever configurations that give rise to optical fields producing equal irradiance profiles at the array of photodiodes. These equivalent configurations can be prevented by appropriate coding of the data. Based on our current measurements we estimate that all configurations of an array of seven cantilevers can be detected in our setup when the size of deflection is 10 nm.

The proposed technique is very well suited for probe-based data storage. A number of distinct worst-case pairs is present, but coding can be adapted to accommodate for differences in pattern distinguishability. Calculations have shown that it is possible to increase the signal that very small deflections create, by the addition of an offset layer to every second cantilever in the array. The average factor of improvement in signal is 7.7 for an array of nine cantilevers, a deflection of 1 nm and a wavelength of the laser light of 640 nm. The sensitivity can be improved further by reducing the wavelength of the laser light. Moreover, the offset dramatically improves the signal of the set of worst-case pairs. We found that for an array of five cantilevers the detectability of each of the worst-case pairs is increased by at least a factor of 13.

### Acknowledgments

The work presented in this section is a culmination of cooperation with many people that are all gratefully acknowledged for a very pleasant cooperation. The author gratefully acknowledges Maarten Flink for exploratory work on the optical detection technique and, Martin Siekman and Henk van Wolferen for experimental support. Léon Woldering is acknowledged for useful discussions.

## 4.2 Fabrication of probe arrays*

Cantilever arrays are tremendously benefited by a high uniformity in tip-sample distance. In probe-based data storage and imaging applications the tip-sample spacing is usually not controllable per cantilever. When trying to utilize such an array one has to apply a higher load force in order to make all cantilever tips touch the sample underneath. This means that non-uniformity in tip-sample spacing will directly translate into different load forces on the tips. Increased load force greatly increases tip wear and makes application of force modulation schemes to prevent wear more cumbersome.

The optical readout scheme using diffraction patterns presented in §4.1.1 assumes the cantilever surfaces within in an array to be in one plane. Small deviations in respective height will give large changes in the diffraction patterns and could lead to difficulties trying to implement signal improvement schemes via extra layers on the cantilevers.

In this section, we describe a fabrication process for arrays of silicon cantilevers with integrated tips. The focus is on achieving an array that gives rise to a highly uniform tip-sample distance. In order to accomplish this we make use of a silicon-on-insulator (SOI) wafer and define the tips by a highly uniform wet chemical etch. The fabrication process features only one lithographic step for the definition of both the tips and cantilevers. The fabrication process is presented in §4.2.1. The uniformity of the fabricated arrays is measured in §4.2.2. Finally, a conclusion is given.

### 4.2.1 Fabrication

#### Process

The cantilever arrays are fabricated using ⟨100⟩ silicon-on-insulator wafers with a device layer thickness of 10 μm. Figure 4.14 shows the main steps in the process flow schematically. Refer to Appendix C for a detailed list of the complete process flow.

The first step in the process is deposition of a layer stack on the front side of the wafer, which is needed to create a hard-mask for the first front side etch. Using low pressure chemical vapor deposition (LPCVD), 25 nm silicon-rich-nitride (SiRN), 100 nm silicon oxide and 20 nm SiRN are deposited successively.

First, the top SiRN layer is patterned using standard photolithography and a reactive ion etch (RIE) with $CHF_3$ and $O_2$ gases, see Figure 4.14(b). This pattern is transferred into the silicon oxide layer using a buffered hydrofluoric acid (BHF) etch as shown in Figure 4.14(c). A deliberate undercut under the top SiRN layer sharpens the corner that will accommodate the tip, effectively increasing the resolution of our lithography process. §4.2.1 describes this corner sharpening step in more detail.

Using a hot (180 °C) phosphoric acid ($H_3PO_4$) etch, both the top SiRN and the exposed part of the bottom SiRN are removed (Figure 4.14(d)). The cantilevers are

*The fabrication process of these probe arrays is based on a manuscript in preparation.

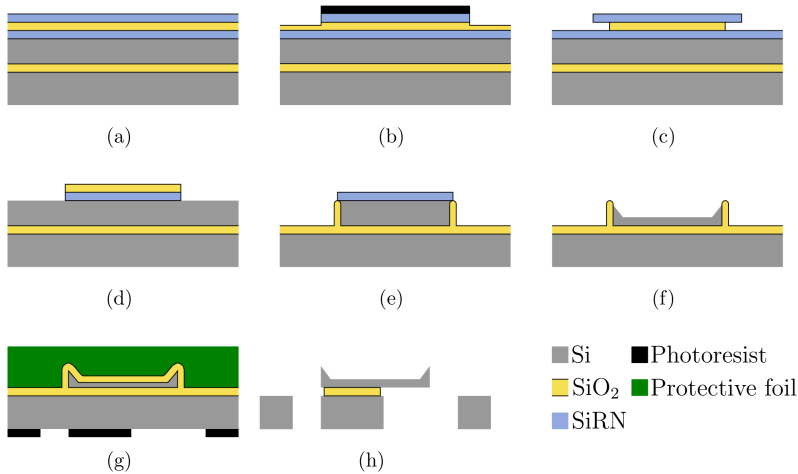


FIGURE 4.14 – *Process flow for fabricating cantilevers with self-aligned tips. (a) SOI wafer with SiRN, $SiO_2$ and again SiRN deposited on top. (b) Pattern top SiRN using standard photolithography (c) Undercut $SiO_2$ in BHF (d) Strip exposed SiRN in hot $H_3PO_4$ etch (e) Transfer pattern into Si using RIE, strip $SiO_2$ and oxidize thermally (f) Strip SiRN in hot $H_3PO_4$ and etch uncovered Si in KOH to create tips (g) Strip $SiO_2$, re-oxidize thermally to sharpen tips, fit protective foil to front side and pattern back side (h) Etch back side, remove foil from front side and strip $SiO_2$*

now etched out of the device layer using a cryogenic RIE with the silicon oxide pattern as mask. This etch method is specifically selected to acquire an optimal pattern transfer. Undercut right underneath the silicon oxide mask influences the shape of the tip and can even reduce its height. By careful optimization we have obtained a straight etch profile with no undercut, so that the tip height is not affected. The RIE is performed with an Adixen AMS100 SE at a temperature of $-100\,°C$, a pressure of $1.3 \times 10^{-2}$ mbar, an $SF_6$ flow of 100 sccm and an $O_2$ flow of 12 sccm.

After removal of the silicon oxide in 1% hydrogen fluoride (HF), the vertical sidewalls of the cantilevers are thermally oxidized, see Figure 4.14(e). The SiRN prevents oxidation of the underlying silicon. After removal of the SiRN in hot $H_3PO_4$, an anisotropic etch using aqueous potassium hydroxide (KOH) (25 wt %, 75 °C) reduces the thickness of the cantilevers and creates the tips, as displayed in Figure 4.14(f). We have chosen a KOH etch because it provides a high uniformity in etch speed (approximately 4% on wafer scale). The thickness of the cantilevers can be precisely controlled by the duration of this etch. Because the cantilevers are aligned with the $\langle 110 \rangle$ direction and have a triangular shaped free end, the slow etching $\{111\}$ planes result in semi-tetrahedral silicon tips on the free end and silicon ridges on the sides of the cantilevers. In §4.2.1 we take a closer look at these

ridges and show how their formation can be successfully prevented.

By stripping the silicon oxide followed by thermal oxidation, the tips are both sharpened and mechanically protected. A polymer film (DuPont MX5000, 20 µm in thickness) is applied onto the front side by lamination. Photoresist is spun on the back side of the wafer and subsequently patterned, again using standard lithography, see Figure 4.14(g). Next, a wafer-through deep reactive ion etch (DRIE) lithographically patterns the chips. A pulsed process is used with $SF_6$ (400 sccm, 4 s) and $C_4F_8$ (25 sccm, 0.5 s). Both the polymer film and the photoresist are removed in an $O_2$ plasma. Finally, the cantilevers are released by etching away both the protective oxide layer and the exposed parts of the buried oxide layer using 1% HF, see Figure 4.14(h).

### Corner sharpening step

The resolution of our lithographical process is limited to 1 µm. The corner at the cantilever tip end will therefore be rounded in the top SiRN mask. It is important in our fabrication process that this corner is well-defined and has a small radius of curvature, because this corner is transferred into the silicon device layer. A rounded corner in the silicon device layer can cause a line shaped tip. The rounded corner in the mask is illustrated in the optical microscope image in Figure 4.15(a). We introduce a so-called corner sharpening step by performing an isotropic etch, that undercuts the top SiRN layer. In work by Kobayashi et al. (2004) it is shown that such an etch preserves the sharpness of the corner. We have used the isotropic etch to sharpen the corner by making the undercut larger than the corner radius. Because the etch speed is the same in all directions, the corner sharpens inherently. Figure 4.15(b) shows the result of such an etch. In this case the radius is reduced from approximately 2 µm to smaller than the resolution limit of our optical microscope. A circle with a radius of 0.2 µm is inserted into Figure 4.15(b) for comparison. The implementation of this corner sharpening step ensures a consistent tip shape with a small radius while reducing variation in cantilever shape.

### Ridge formation and prevention

Due to the anisotropic KOH etch, silicon ridges are created along the length direction at both sides of the cantilevers. The ridges are caused by slow etching $\{111\}$ planes similar to the slow etching $\{111\}$ plane that helps in tip formation. The edges can pose a problem during scanning, when the tip is in contact with the surface. Topographic features on the sample surface potentially touch the ridge instead of the tip, because the ridge is as high as the tip. We can influence the height of these ridges by introducing an angle $\theta$ between cantilever side and the $\langle 110 \rangle$ crystalline direction, see Figure 4.16(a). This angle will cause a misalignment with the $\{111\}$ planes and the KOH can attack the planes from the side. A larger angle leads to a larger misalignment. Figure 4.16(b) shows the sidewall to tip-height ratio as function of angle $\theta$. In case $\theta$ is 10° or larger, the ridge is completely suppressed. The cantilever depicted in Figure 4.16(c) has an angle $\theta$ of 8°. The height $h_T$ of the

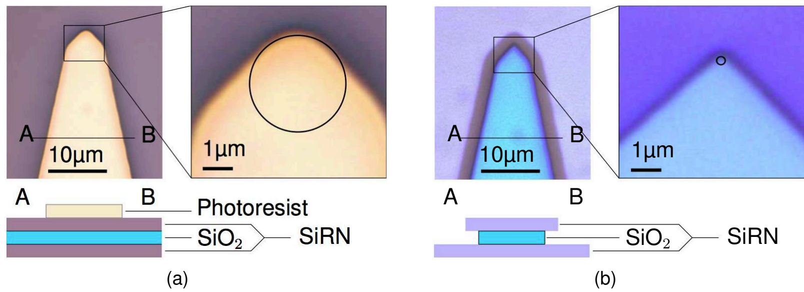


FIGURE 4.15 – *Optical microscope image of mask layers. An intentional isotropic undercut sharpens the corner that will house the tip. The colors in the cross-sections are analog to those in the microscope images (a) Pattern in photoresist before sharpening (b) Pattern in $SiO_2$ after sharpening. The reduction in corner radius is illustrated with two black circles. Color available in digital version.*

tip is significantly larger than the height $h_R$ of the ridge, demonstrating the efficacy of our approach.

### 4.2.2 Measurement results

#### Procedure

We have investigated the variation in tip-sample distance of the fabricated cantilever arrays. Measurements were performed with a commercially available AFM (Nanoscope Dimension 3100). After aligning the laser spot on one of the cantilevers, the complete array is moved towards the sample (a silicon wafer). The moment the tip touches the sample surface, a deflection is detected. This procedure provides the tip-sample distance for one tip. To obtain the variation in tip-sample distance, this measurement is performed for every cantilever in the array. In between the measurements the laser spot is moved from one cantilever to the next. Each measurement is performed shortly after the other to minimize drift. For the resonance frequency measurements we have used the AutoTune option of the AFM.

#### Uniformity measurements

Figure 4.17 shows the measurement results of a 190 µm wide array with 400 µm long cantilevers. Figure 4.17(a) shows a linear increase in $d_{TS}$ as a function of tip position $x$. This increase is caused by a misalignment between array and sample, schematically indicated in Figure 4.17(b). By subtracting the linear fit (indicated by the black line in Figure 4.17), the misalignment is corrected. Figure 4.17(c) shows the variation in tip-sample distance corrected for this linear slope. This correction procedure is analogous to perfectly aligning an array with the sample, as is schematically illustrated in Figure 4.17. By correcting the slope in this manner,

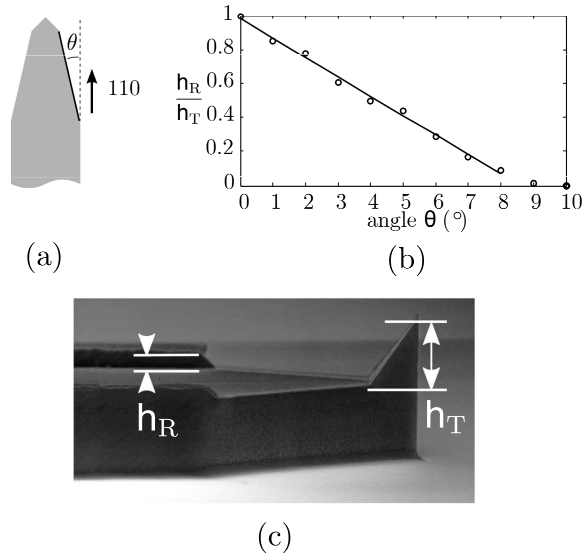


FIGURE 4.16 – *The anisotropic KOH etch causes the formation of silicon ridges on the sides of the cantilever. (a) These ridges can be suppressed by introducing an angle $\theta$ between the cantilever side and the ⟨110⟩ direction. (b) Sidewall to tip-height ratio as function of angle $\theta$. An angle of 10° is sufficient to completely prevent the ridge. (c) A SEM image of a cantilever with $\theta$ =8°. The height $h_T$ of the tip is significantly larger than the height $h_R$ of the ridge.*

we find the tip-sample uniformity without the introduction of errors due to array-sample misalignment.

Five different arrays have been characterized and the results are listed in Table 4.2. It can be seen that the 190 µm wide array of Figure 4.17 has a range in tip-sample distance of only 46 nm with a standard error of the tip-sample distance of 9 nm. The standard error of the tip-sample distance is consistently around 10 nm. These measurement results confirm that our fabrication process creates cantilever arrays with small variations in tip-sample distance.

**Resonance frequency measurements**

The standard error of the resonance frequency of two arrays is included in Table 4.2. No standard error of resonance frequency is shown for the other arrays because they are designed to have cantilevers with different resonance frequencies; these are designed to be used in combination with the readout technique presented in Chapter 3. The measured standard errors of 147 Hz and 33 Hz correspond to a standard error in cantilever length of respectively 0.19 µm and 0.12 µm. These values translate in turn into a standard error in tip-sample distance of 34 nm and 21 nm,

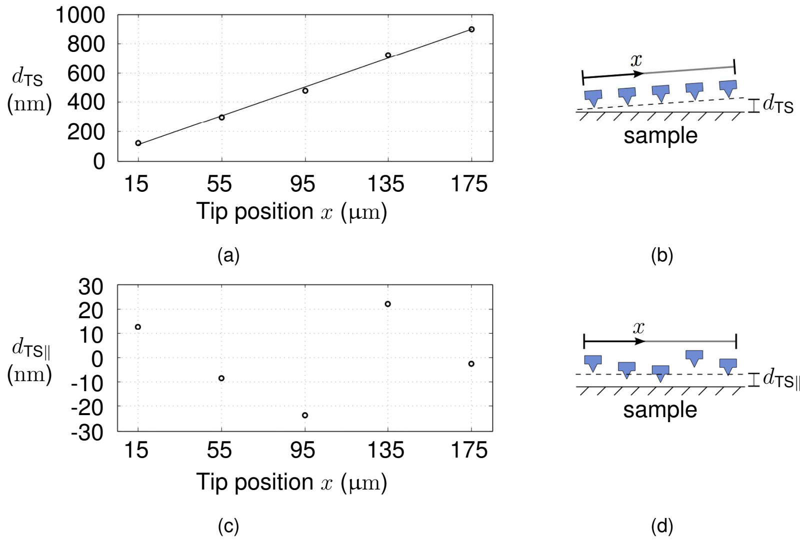


Figure 4.17 – *(a) Tip-sample distance as function of position on array. Measurements performed on a chip with* 400 µm *long cantilevers and an array width of* 190 µm. *The line is a linear fit. (b) Schematic representation of sample and array with tips. (c) Tip-sample distance as function of the position on the array, after subtraction of the linear fit. (d) Schematic representation of the sample and array with tips after subtraction of linear fit.*

| $w$ (µm) | $L$ (µm) | $n$ | $R_d$ (nm) | $SE_{\bar{d}}$ (nm) | $SE_{\bar{f}}$ (Hz) |
|---|---|---|---|---|---|
| 150 | 300 | 4 | 35 | 8 | 147 |
| 190 | 225 | 5 | 61 | 11 | - |
| 190 | 400 | 5 | 46 | 9 | - |
| 240 | 400 | 10 | 116 | 12 | - |
| 430 | 400 | 10 | 94 | 11 | 33 |

Table 4.2 – *Characterization results of five cantilever arrays. $w$ = array width, $L$ = cantilever length, $n$ = number of cantilevers, $R_d$ = range in tip-sample distance, $SE_{\bar{d}}$ = standard error of tip-sample distance and $SE_{\bar{f}}$ = standard error of resonance frequency*

respectively. Because the measured standard error in tip-sample distance is much lower, we conclude that the differences in resonance frequencies can not only be caused by a difference in cantilever length. We speculate that the main reason of the difference in resonance frequencies is a variation in the connection of the cantilever to the chip base due to inaccuracy of the back-side etching process.

### 4.2.3 Conclusion

In conclusion, we have fabricated probe arrays with tips that have a high uniformity in tip-sample distance. For an array of 10 cantilevers spanning 430 μm, a standard error of 11 nm has been measured. Furthermore, we have shown that it is possible to fabricate both cantilevers and tips using a single mask. The tips are self-aligned at the very end of the cantilevers by a KOH etching step. A second mask is required to perform a back-side etch. A critical feature in the process is the sharpness of the corner that houses the tip. We have shown that by means of an isotropic under etch the resolution of our lithography tool can be effectively increased. This results in a corner radii well below 500 nm, instead of approximately 2 μm. An unwanted side-effect of the KOH etch is the occurrence of silicon ridges that remain standing at the sides of the cantilevers. The height of these ridges is fully adjustable controlling the angle between cantilever edge and ⟨110⟩ crystalline direction. No ridge remains when this angle is greater than 10°.

### Acknowledgments

The authors gratefully acknowledge Meint de Boer, Erwin Berenschot, Kees Ma and Hammad Nazeer for their valuable input and help with the fabrication process. Martin Siekman is acknowledged for experimental support on the AFM measurements.

# Chapter 5

# Force modulation for conductive probes

## 5.1 Introduction

Conductive scanning probes are powerful tools to investigate and manipulate electrical properties of surfaces and thin films at the nanoscale. Application areas include, semiconductor metrology (Oliver, 2008), probe-based data storage (Jo et al., 2009; Tanaka et al., 2008b; Tayebi et al., 2010b; Wright et al., 2006; Wuttig and Yamada, 2007) and investigation of nanoscale electrical transport in materials (Kügeler et al., 2008; Sebastian et al., 2011). Conductive probes can also be used to emulate nanoscale electrical contacts such as those occurring in nano-electro-mechanical (NEM) switches for low-power electronic applications (Chen et al., 2008; Lee et al., 2010). For the wide-spread applicability of conductive probes, however, several challenges need to be overcome. Major challenges are related to sustaining a high-quality electrical contact between the tip and sample while not losing spatial resolution over a prolonged tip lifetime. The fast degradation of the tip apex due to wear, and high current densities pose significant challenges to conductive-mode scanning probe microscopy (SPM). The abrasion of the tip apex is accelerated by the significantly high normal load force on the tip required to obtain a good electrical contact with the sample.

There is considerable effort to overcome these issues by carefully selecting the tip apex material. Coatings such as gold and platinum are reported (John and Kulkarni, 2005). These coatings increase the contact area between tip and sample and are often troubled by wear and delamination of the metal film (Bussmann and Williams, 2004). More elaborate and also more expensive solutions such as doped diamond coatings and all-diamond tips harden the tip (Oliver, 2008). A different approach is to employ all-metal tips such that wear of the tip apex does not result

This chapter is based on W. W. Koelmans, A. Sebastian, L. Abelmann, M. Despont and H. Pozidis, "Force modulation for enhanced nanoscale electrical sensing", manuscript accepted for publication in *Nanotechnology*.

in loss of conduction, but it does result in loss of resolution. Recently, silicidation of the tip apex after application of a platinum coating was shown (Bhaskaran et al., 2009*b*), which led to superior wear resistance and higher admissible tip currents as compared to silicon tips. The wear of such a platinum silicide (PtSi) tip apex, however, is still too high for the requirements posed by industrial applications such as electrical probe-based data storage and semiconductor metrology. PtSi tips have been shown to outperform many other types in terms of contact resistance, wear characteristics and the admissibility of high current densities (Bhaskaran et al., 2009*a*). The required load force for PtSi tips is typically between 40 nN and 300 nN (Bhaskaran et al., 2009*b*). Reducing the load force causes further increase in contact resistance (Brezna and Smoliner, 2008) or a loss of tip-sample contact.

The value of the load force at which electrical contact is sufficiently well established depends on several factors. First, it depends on the tip and sample materials and their susceptibility to oxidation. Second, the values of the resistances under investigation determine the allowed tip-sample contact resistance. The contact resistance should be significantly lower than the relevant series resistances of the experiment. Third, the conditions in which the experiment takes place. An ambient environment allows oxidation of many materials, supplies contaminants to tip and sample surface and adds a fluid layer (Moreland et al., 1997). In the search for suitable materials for NEM switches, significant increases in contact resistance are reported due to the buildup of contamination on the contact Chen et al. (2007).

For a tip to establish contact with the sample, fluid contamination layers have to be pushed away and thin oxide layers need to be pierced. Even for a tip and sample made of an inert and highly conductive metal like gold, a minimum load force of 5 nN is reported for tunnelling to be established (Meepagala et al., 1991). The presence of a native oxide layer on either tip or sample can increase the required load force to 20 μN. All these factors result in an unreliable electrical contact and the need for a robust method to contact a sample surface arises. The conventional approach to accomplish a good contact is to increment the load force while scanning and in this manner abrading any layers prohibiting contact; however, this approach is detrimental to tip sharpness.

In this work we present a complementary strategy, a normal force modulation technique, to increase the reliability of nanoscale electrical contact and to reduce tip wear in conductive-mode SPM. The essential idea behind the proposed force modulation technique is to modulate the normal load force while the tip is in contact with the sample. This modulation is achieved by actuating the cantilever at specific mechanical resonant frequencies which correspond to the normal modes of vibration. Unlike the tapping-mode where the tip traverses a wide range of the interaction potential, during the proposed force modulation technique, the tip motion is assumed to be less than a nanometre and the tip is exploring only a fraction of the interaction potential. The idea is inspired by the successful demonstration of force modulation techniques for the reduction and elimination of wear in non-conducting SPM applications (Knoll et al., 2010; Lantz et al., 2009; Radmacher et al., 1992). In this chapter, we show that the modulation of the normal force not only reduces wear, it also effectively enhances the electrical contact between the tip and

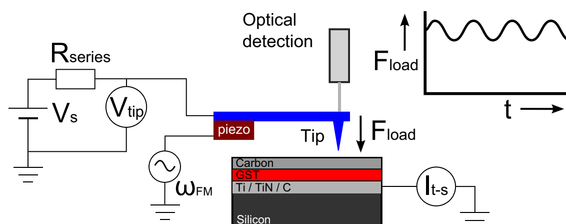


FIGURE 5.1 – *Schematic of the measurement setup: a piezo electric element underneath the cantilever base is employed to add a sinusoidal forcing on top of the load force. The sinusoidal forcing frequencies are chosen to be equal to specific mechanical resonant frequencies corresponding to the normal modes of vibration. Electrical circuitry is present to monitor the tip voltage ($V_{tip}$) and tip-sample current ($I_{t\text{-}s}$).*

sample. This surprising result will be investigated in great detail using a variety of experiments.

A possible implementation of the proposed force modulation technique is illustrated in Figure 5.1. Once the cantilever is brought into contact with the sample, a sinusoidal force is added on top of the load force that acts on the tip. This forcing is usually achieved by means of a dither piezo underneath the cantilever base. Alternative means of actuation such as electrostatic and magnetic can also be employed.

The experimental details are presented in §5.2, followed by the experimental results in §5.3. A discussion on the possible mechanism is presented in §5.4, followed by the conclusions in §5.5.

## 5.2 Experimental details

The experimental setup consists of a home-built SPM with both optical deflection-sensing and conductive-mode operation capability. It is designed such that the micro-cantilevers can be mounted almost parallel to the sample (see Figure 5.1). The sample is mounted on a commercial piezo scanning stage (Physical Instruments P517.3CL) with $xyz$-motion capability. The deflection of the cantilever is monitored using an optical beam deflection system equipped with a four-quadrant photodetector. A feedback loop is in place to adjust the sample height in order to ensure a constant load force. All experiments described are performed in ambient conditions. During conductive-mode operation, a positive voltage is applied to the tip using voltage source $V_s$ and the actual voltage over the tip ($V_{tip}$) is constantly measured. In regular operation the applied and measured voltages are almost identical because the value of series resistance ($R_{series}$ = 20 kΩ) is small compared to the variable sample resistance, which is on the order of 1 MΩ. A second electrical cir-

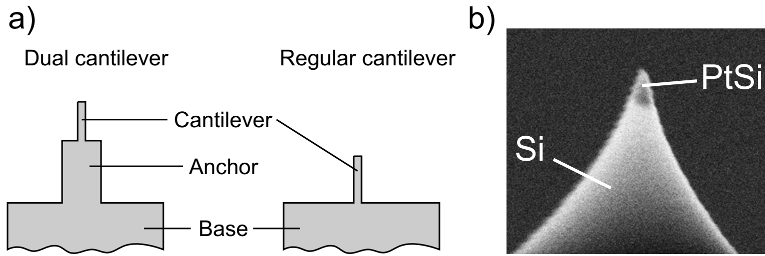


FIGURE 5.2 – *(a) Schematic drawings of the cantilevers used in this study and (b) a SEM image of a PtSi tip.*

cuit is present to actuate the piezo electric element, underneath the cantilever base, at the desired amplitude and frequency ($\omega_{FM}$) for the force modulation.

We have made use of two types of cantilevers, both equipped with PtSi tips with a typical apex radius of 15 nm, see Figure 5.2(b) for an example of a PtSi tip. Type 1 is a regular cantilever design with a fundamental resonant frequency of 67 kHz and a spring constant of 2.8 N m$^{-1}$. Type 2 is a cantilever with an anchor that fixes the cantilever to the chip base, see Figure 5.2(a). Type 2 can be thought of as two cantilevers, the anchor and the protruding cantilever, in line and it will from now on be referred to as the dual cantilever. The fabrication process of the PtSi tip and the dual cantilever is reported in Bhaskaran et al. (2009*b*). The fundamental mode of the dual cantilever as a whole is around 70 kHz and of only the cantilever is around 100 kHz. The spring constant of the dual cantilever is 0.4 N m$^{-1}$, which is predominantly determined by the spring constant of the protruding cantilever.

Most of the experiments are performed on a phase-change layer stack deposited on a silicon substrate shown in Figure 5.1. This sample is chosen for its relevance to probe-based data storage. One type of electrical probe storage employs phase-change materials such as germanium antimony telluride (GST) to store information by locally transforming its phase using a conductive probe. Phase-change materials are also very relevant for non-volatile memory applications (Wetnic and Wuttig, 2008). The fabrication process is similar to that described in Bhaskaran et al. (2009*c*). The stack we use consists of a bottom electrode of titanium (5 nm), titanium nitride (20 nm) and a nitrogen-doped carbon layer (100 nm), followed by the $Ge_8Sb_2Te_{11}$ active phase-change layer (12 nm) and finally a nitrogen-doped amorphous carbon top layer (6 nm).

## 5.3 Experimental results

### 5.3.1 Formation of electrical contact

In the first set of experiments we investigate the influence of force modulation on the formation of nanoscale electrical contact. The objective of the experiments is to monitor the onset of electrical conduction. Tip-sample approach curves are performed whereby the PtSi tip is made to come into contact with the sample and then retract. The cantilever used is of type 1 and the sample is the phase-change stack.

The measurement is performed by ramping up the voltage on the $z$ piezo of the scanning stage to bring the sample into contact with the tip. After the tip comes into contact with the surface the scanning stage is programmed to rise another 200 nm. Figure 5.3 shows the mean conductance of 100 sequentially obtained approach curves along with error bars indicating the standard error. After obtaining each approach curve a 5 nm sample move is performed in order to average out sample irregularity. The experiment has been performed three times with the same tip and sample; a reference measurement without any modulation, and two measurements with force modulation, one at contact resonance (267 kHz, 0.25 V amplitude) and one at 150 kHz, 0.5 V amplitude, in both cases for a tip voltage of 1.0 V. The resulting modulation of the load force is estimated to be smaller than 10 nN, as explained in more detail in §5.3.5. The data clearly show a much steeper evolution of the conductance at the moment the tip comes into contact with the sample surface when force modulation is applied. Moreover, with force modulation the conductance, after the

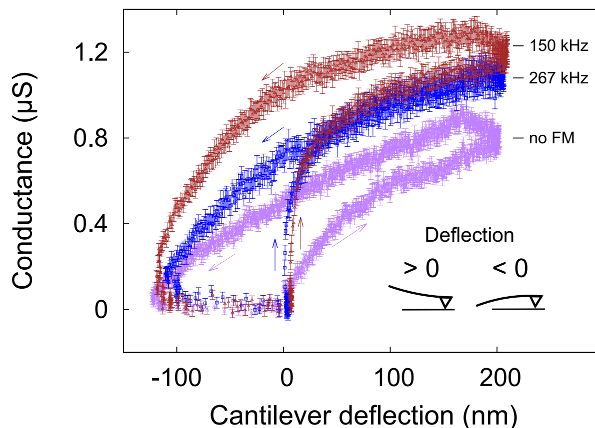


FIGURE 5.3 – *Conductance curves in normal mode (no FM) and with force modulation at 150 kHz and at 267 kHz. Each curve is the mean of 100 consecutive experiments with standard error as error bar. With force modulation the electrical contact is significantly better at the moment the tip reaches the sample.*

first steep increase, is more constant with respect to applied load. This means that the measured tip-sample current and the corresponding sample resistance are less dependent on the applied load.

All three conductance curves show a large amount of hysteresis at cantilever deflections smaller than zero due to the adhesive force between tip and sample. Remarkably, the curve without force modulation shows additional hysteresis at cantilever deflections greater than zero: the conductance in the forward regions is lower than the conductance in the backward region. The curve with force modulation at 150 kHz shows less hysteresis at cantilever deflections greater than zero. When using force modulation at 267 kHz the phenomenon has disappeared. This observation of increasing conductance while the load force is being reduced has been reported before (Mate et al., 1989; Morita et al., 1989). It is ascribed to a continued breakdown of an insulating fluid contaminant layer under the repulsive forces that continue to be exerted while the sample is retracting. The decrease, and even absence of the hysteresis at cantilever deflections greater than zero when force modulation is applied, suggests that this mitigation of insulating surface layers is also achieved by a small dithering motion of the tip.

This observation has significant ramifications for nanoscale electrical contact studies as in the case of NEM switches which are being investigated for ultra-low power applications. It suggests the potential of the force modulation technique to enhance the electrical contact quality between electrodes having nanoscale contact area.

### 5.3.2 Conductive-mode imaging

One of the most important applications of conductive-mode SPM is to resistively map surfaces. This is essential for application areas such as semiconductor metrology and electrical probe-storage. The influence of the force modulation technique in resistance mapping is investigated here in great detail.

We performed a series of imaging experiments in which the strength of the force modulation is varied. This is done by changing the amplitude of the oscillation voltage on the dither piezo. The experiments comprise 50 line scans (trace and retrace) each 2 µm long and are performed on the phase-change stack with a set of cantilevers of type 1. After each scan the mean of the current is calculated, and friction data are extracted from the torsional motion of the cantilever, which is recorded during the scan. The experiment was repeated for several modulation frequencies; the fundamental resonance (67 kHz), the fundamental contact resonance (267 kHz) and two arbitrary frequencies in between. The data are obtained at a scan speed of 62.5 $\mu m\,s^{-1}$ and an average load force of 28 nN. The data at the 67 kHz modulation frequency are obtained at a scan speed of 10 $\mu m\,s^{-1}$ and at an increased average load force of 112 nN. During all measurements feedback on the vertical sample position is used to ensure a constant average load force. The tip voltage is set to 1 V. The mean values of current and friction are displayed in Figure 5.4 and Figure 5.5.

The shape of the curves differs with frequency, because the shape is governed by the tip motion. The tip motion, in turn, is determined by a frequency dependent cantilever response. Moreover, there is an inevitable variation in the sharpness

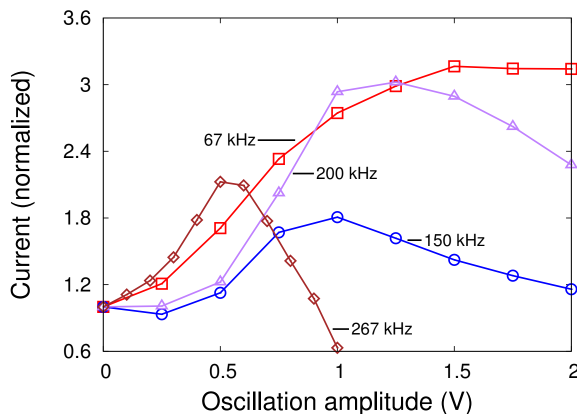


FIGURE 5.4 – *The mean of the tip-sample current during 50 line scans is plotted versus the amplitude of the piezo voltage. Four different frequencies of modulation are chosen; the fundamental resonance (*67 kHz*), the fundamental contact resonance (*267 kHz*) and two arbitrary frequencies in between.*

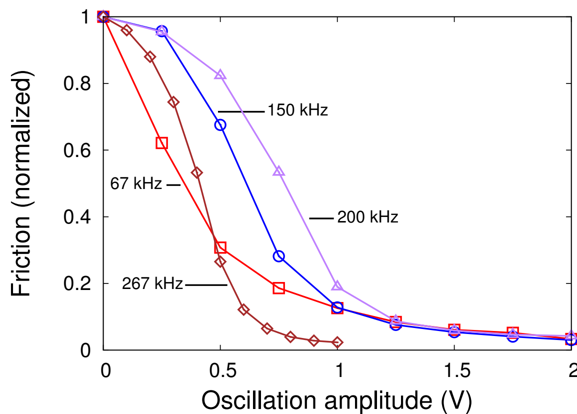


FIGURE 5.5 – *The mean of the friction during 50 line scans is plotted versus the amplitude of the piezo voltage. Four different frequencies of modulation are chosen; the fundamental resonance (*67 kHz*), the fundamental contact resonance (*267 kHz*) and two arbitrary frequencies in between.*

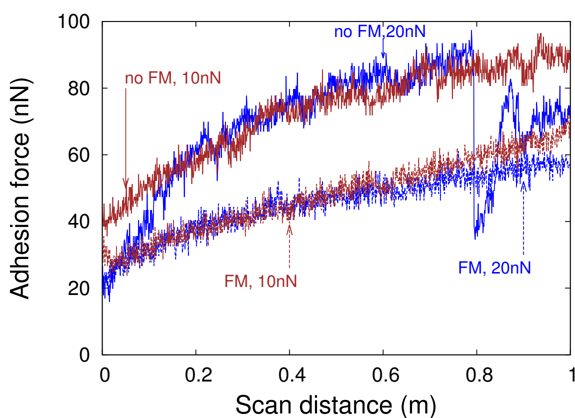


Figure 5.6 – *Tip wear during the long-term imaging experiment. The solid lines are without force modulation and the dotted lines with force modulation.*

of the tips between the experiments, which influences the cantilever frequency response through the tip-sample interaction. Therefore, care has to be taken in comparing the curves at different modulation frequencies. It is, nonetheless, very clear that the trend of all the curves is similar. Specifically, for all frequencies of operation, starting at zero amplitude, a clear decrease in friction is observed. The lower friction is thought to be due to the periodic reduction in the normal force acting on the tip. This reduction reduces the barrier to lateral motion, allowing the tip to move without building up elastic strain. This analysis is in line with previous observations (Lantz et al., 2009). What is more surprising is the increase in average current with increasing forcing amplitude. The current is increased, in some cases, to more than three times the value at zero amplitude. An even further increase of the amplitude leads to a reduction in the average current. This reduction is attributed to too high a vertical tip motion, causing a partial loss of electrical contact. Therefore, at contact resonance a lower oscillation amplitude is used because the current peaks at an amplitude around 0.5 V. The decrease in contact resistance and friction also appears at other frequencies (150 kHz and 200 kHz) than those associated with the normal mechanical resonances (67 kHz and 267 kHz). Because the estimated tip motion that enhances the electrical contact is small, there is potential for the technique to work at a large range of frequencies that induce small tip motion normal to the sample surface.

### 5.3.3 Long-term imaging

To investigate whether the reduced friction indeed translates to reduced tip wear and whether the improved contact quality is sustained over extended periods of time, long-term imaging experiments are performed. In one of the experiments,

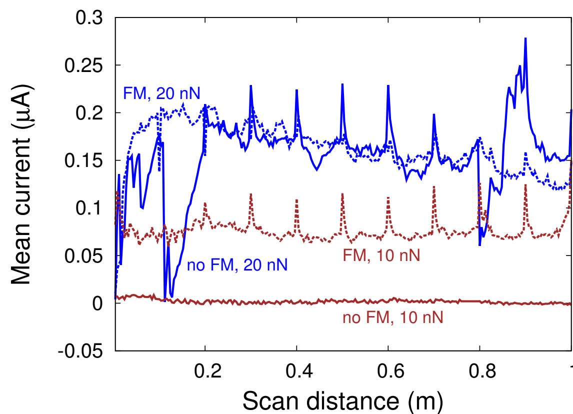


FIGURE 5.7 – *Conduction during the long-term imaging experiment. The data shows a nine-fold increased average current with force modulation at* 10 nN *load force. The solid lines are without force modulation and the dotted lines with force modulation.*

the PtSi tip raster scans the phase-change stack for 1 metre of tip travel. During the long-term wear experiment, continuous feedback using the $z$-scan axis is applied to ensure a constant load force. A total of 1250 raster scans of 0.8 mm of tip travel is performed. Each scan yields topography and conduction images, of which every fifth is stored so that it can be checked for irregularities. After every raster scan, the adhesive force between tip and sample ($F_{adh}$) is measured from a tip-sample approach-and-retract curve. The adhesion force is a very good measure of the tip-sample contact area and thus an excellent means of in situ quantification of tip wear. Because the tip initially wears fast, a tip shape similar to that of a truncated cone is created. For this geometry the adhesion force is approximately proportional to the radius of the flat end $a$ that is in contact with the sample (Gotsmann and Lantz, 2008):

$$F_{adh} = a\, k_{adh}$$

where $k_{adh}$ is a constant of proportionality. $F_{adh}$ is thus a measure of tip wear. The wear experiments are performed at load forces of 10 nN and 20 nN, both with and without force modulation. A set of dual cantilevers is used and the force modulation is performed at the fundamental cantilever resonance frequency, i.e. approximately 100 kHz and at 0.5 V force modulation amplitude.

Figure 5.6 shows the results of the long-term experiments and clearly illustrates that with force modulation, there is a substantial reduction in tip-wear. The wear volume is estimated by SEM imaging of the tips before and after the experiment. At 20 nN load, force modulation reduces the wear by a factor of three (from $2.2 \times 10^5$ nm$^3$ to $7.4 \times 10^4$ nm$^3$). Moreover, wear curves with force modulation are evolving smoothly. These observations are consistent with the atom-by-atom wear

model proposed in Gotsmann and Lantz (2008), in which the wear mechanism is thought to be a thermally activated bond-breaking process described by Arrhenius kinetics, where the barrier to remove an atom from the tip is lowered by the frictional shear stress acting on the tip. Hence, the reduced friction also translates to a reduction of tip wear. It is also important to note that without force modulation, especially at the higher load force of 20 nN, the sharp decreases and subsequent increases in $F_{adh}$ suggest that small parts of the tip break off. These breaking events temporarily sharpen the tip and lead to less predictable wear behaviour.

The mean current through the tip during each raster scan is plotted as a function of total tip travel in Figure 5.7. The figure shows that, especially at 10 nN load force, the conducted current is considerably higher when force modulation is applied. In particular the average current over the full 1 m sliding distance is nine times higher for the 10 nN load force and 8% higher at 20 nN. From Figure 5.7, it can also be seen that the relative variation in the mean current is appreciably smaller with force modulation. Note that for the experiment with 10 nN load force this is difficult to recognize because of the scale of the graph. Also note that the period of the regularly spaced peaks that are visible in two of the curves, exactly match the interval between two consecutive visits of the tip to the same sample area. These experiments clearly illustrate the improved electrical contact quality over extended periods of time and across very long scan distances achieved by adopting force modulation.

### 5.3.4 Imaging of heterogeneous samples

Imaging experiments on heterogeneous samples are performed next to further illustrate the improved conduction with the force modulation technique and to assess its superior ability to differentiate between regions of variable electrical resistivity. Towards this end, a sample was prepared with small platinum pads on top of a phase change material stack. The pads are approximately 300 nm in diameter and approximately 20 nm thick and were fabricated by evaporating platinum through a silicon nitride shadow mask. The presence of carbon, which is the capping layer on the phase change stack, and platinum on the same sample surface enables us to assess the force modulation technique on two entirely different materials.

A dual cantilever with a fundamental cantilever resonance frequency of 99.3 kHz is used in the experiments. The images displayed in Figure 5.8 show resistance maps at different load forces. The images on the left side show the result in conventional contact-mode conductive SPM and the images on the right side show the result when applying force modulation (99.3 kHz, 1.5 V amplitude). Again, a marked improvement in electrical contact between tip and sample is visible when force modulation is applied. Line profiles of the electrical current reveal that the difference in visibility of the pads in the resistance maps is caused by the capability of the tip to sustain the contact with the platinum surface. Although platinum is a material that is prone to contamination (Chen et al., 2007), the tip is able to pierce the contamination layer at exceptionally low load forces when force modulation is employed. At 80 nN load force with force modulation the contact with the surface

is excellent. The small variation in current of approximately 100 nA, on the carbon layer is caused by the surface roughness of the sample.

For a series of load forces varying between 10 nN and 120 nN, the imaging of the sample is repeated and in Figure 5.9 the ratio between the mean current over the entire surface with and without force modulation is plotted as a function of load

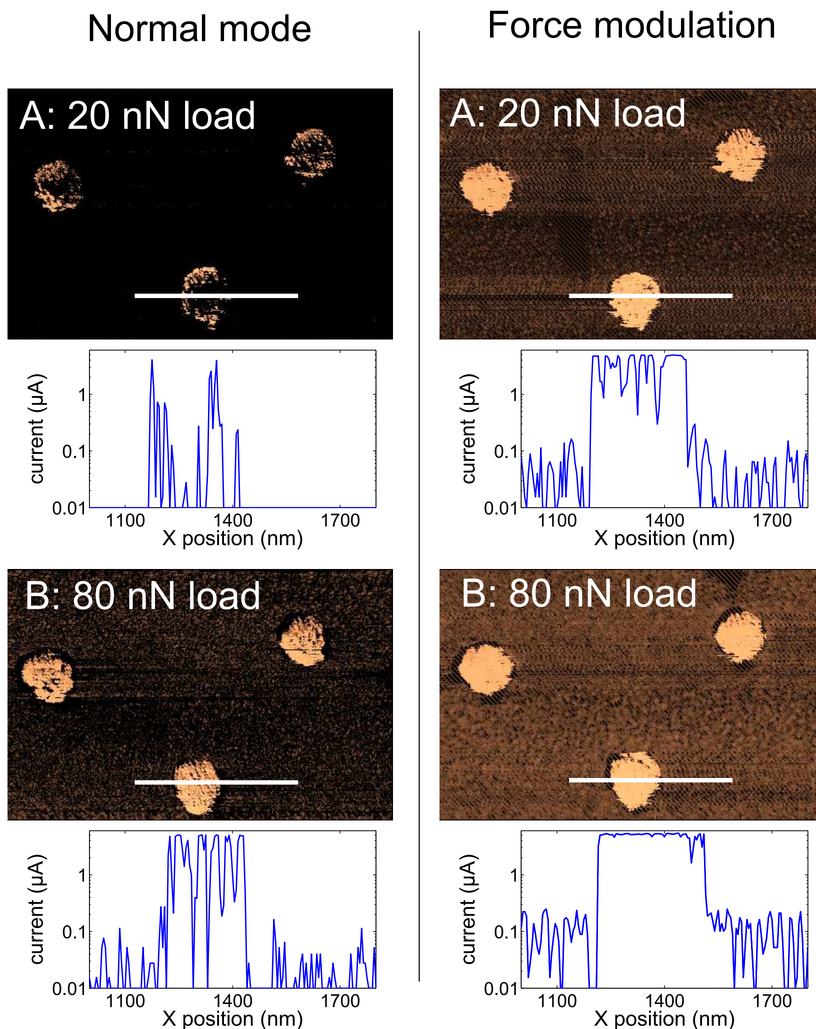


FIGURE 5.8 – *Resistance maps of platinum pads on a carbon background. The graphs show the current along a cross-section indicated by the white lines in the images. The images and cross-sections in normal mode show much more loss of contact than with force modulation. Note that all data are presented on a logarithmic scale.*

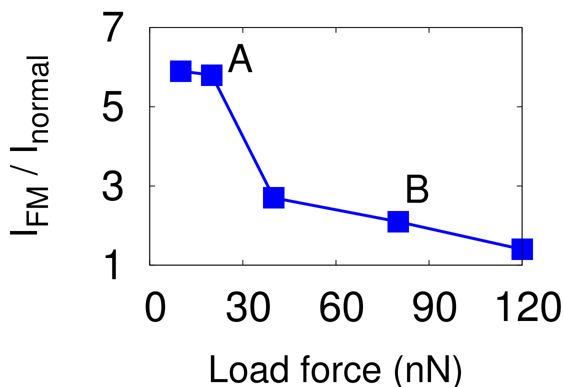


FIGURE 5.9 – *The mean current over the complete image is calculated and the ratio between the current with ($I_{FM}$) and without force modulation ($I_{normal}$) is plotted in the graph. The letters A and B refer to the measurements in Figure 5.8.*

force. It can be seen that at low load forces six times more current is conducted on average, whereas with increasing load force this ratio steadily drops towards unity. The marked data points A and B correspond to the images in Figure 5.8. It is evident from these measurements that lower load forces and the absence of force modulation lead to an increasing chance of contact loss.

In the above experiments, it is essential to confirm that the apparent reduction in contact resistance is not due to some AC component of current created by the cantilever forcing and subsequent modulation of the tip-sample separation. In order to clarify this point, we performed a series of experiments where the signals are monitored at high bandwidth. Because our SPM is normally equipped with a low-pass anti-aliasing filter adjusted to the sample rate of 10 to 50 kS $s^{-1}$, the dynamics of the current signal at the timescale of one cycle of oscillation (approximately 10 µs) are not detected. The imaging experiments were repeated at 80 nN load force and a portion of the data were captured at a sample rate of 2.5 MS $s^{-1}$, while scanning at 10 µm $s^{-1}$. In Figure 5.10 the forcing signal for the dither piezo together with the measured tip-sample current are shown. For comparison, the experiment is repeated without force modulation and superimposed on to the same graph. The data shown in Figure 5.10 are taken from a low resistance area on a platinum pad. No clear, large peaks are observed in the current at the part of each oscillation where the load force is maximum. The DC part of the current is slightly higher in the presence of force modulation. This is a clear indication of a true reduction in the contact resistance. It is also seen that the reduction of the contact resistance is not the only cause of the increment in total conducted current; with force modulation the variation in conducted current is also less, in agreement with the data in Figure 5.8.

### 5.3.5 Tip motion during imaging

It is beneficial to quantify the tip motion during the application of force modulation as it aids the basic understanding of this mode of operation. Unfortunately, such experimental measurements are hindered by the nature of the optical beam deflection system. This difficulty is because beam deflection monitors the angle of the cantilever rather than the vertical position of the tip. Off-contact, in fundamental resonance mode, there is a direct relation between the position of the tip and the angle of the cantilever; however, in-contact, when exciting the base of the cantilever, the cantilever will undergo additional bending because the applied moment is counteracted by the normal sample force. The applied moment results in a rotation of the tip on the sample and thus causes an increased bending of the cantilever beam. Consequently, the measured deflection of the optical beam, approximately 6 nm peak-to-peak motion, overestimates the vertical motion of the tip. In order to obtain a first order estimate of the true vertical tip motion we have employed a mechanical lumped element model with piecewise linear cantilever-sample interaction force which was presented in Sebastian et al. (2001). The model was adjusted to fit our experimental conditions using the dual cantilever. Based on calculations with this model, we estimate the tip oscillation amplitude to be approximately 0.4 nm for 1 V force modulation amplitude at 100 kHz. Here we use a cantilever stiffness of 0.4 $\mathrm{N\,m^{-1}}$ and assume a contact stiffness of 20 $\mathrm{N\,m^{-1}}$. The resulting force modulation therefore has a peak-to-peak value of 9 nN.

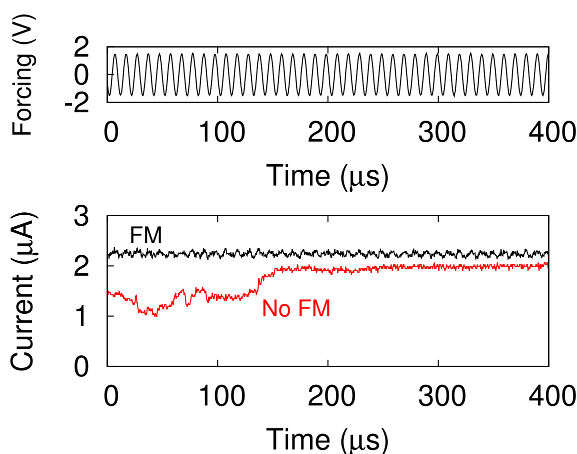


FIGURE 5.10 – *The tip-sample current measured at high bandwidth where the tip is on top of a platinum pad, with (top graph) the forcing signal, and (bottom graph) the current, measured both with and without the force modulation (FM). A true reduction in contact resistance is seen, as well as a more stable current.*

## 5.4 Discussion

We have carried out a series of experiments which clearly demonstrate the ability of the force modulation technique to enhance the contact quality while forming a nanoscale electrical contact. This enhancement comes in addition to significantly lowered friction and reduced tip wear achieved by force modulation. It is hypothesized that the reduction in the contact resistance observed with the force modulation is due to the mitigation of any insulating barrier that is unavoidably present in ambient conditions. The periodic increment in load force causes the tip to reach the conductive sample surface despite contaminants; however, no large peaks in conduction during each oscillation period were found. The absence of such peaks indicates that the tip is consistently making good contact with the sample and the dithering motion of the tip aids to establish and maintain this contact. We speculate that the dithering motion causes a breakdown of the layer of contaminants covering the sample surface by expulsion or penetration of the insulating material. When the load force is reduced at every cycle of oscillation, this layer is not restored and the improved conductance is retained. This explanation is in agreement with previous work (Mamin et al., 1986; Mate et al., 1989; Morita et al., 1989), in which the authors suggest a continuous expulsion or penetration of material during an approach-retract curve, even during the initial part of retraction of the tip. This increase in conductance is less apparent when force modulation is used and even disappears at certain modulation frequencies. This absence indicates that force modulation has a similar effect as many consecutive approach-retract curves, performed at high speed. If this speed is high enough, compared to the speed of scanning, the increase in conduction is effectively instantaneous. If the tip motion is too high, the resulting reduced tip-sample interaction leads to an increasing contact resistance. This increasing resistance agrees with the observation in Figure 5.4 that too high an amplitude reduces the conductance. The relation between the frequency of modulation and tip amplitude is, however, not straight-forward.

To summarize, the normal force modulation technique has been shown to improve the electrical contact quality in addition to reducing friction and wear at multiple frequencies. We see no reason to assume that other frequencies, in between the fundamental free resonance and the contact resonance frequencies, do not lead to similar results. Also, a range of amplitudes is available for which force modulation positively affects friction and conduction.

## 5.5 Conclusion

A novel force modulation technique is presented for conductive-mode SPM, whereby the tip-sample normal load force is modulated at specific frequencies during electrical sensing. These frequencies correspond to mechanical resonances associated with the normal modes of vibration. Using a a mechanical lumped element model the resulting tip motion is estimated to be less than a nanometre. Experimental results using PtSi conductive probes and phase-change material stacks clearly demon-

strate the efficacy of this technique. The force modulation technique has a significant influence on the formation of nanoscale electrical contacts. In conventional contact-mode operation the conductance increases with applied load force, whereas with force modulation the formation of a high-conductance electrical contact is almost instantaneous, as evidenced from conductive-mode approach curve experiments. Conductive-mode imaging experiments clearly illustrate the increased electrical contact quality in addition to reduced friction and wear. Imaging experiments spanning a metre of tip travel demonstrate the long-term reliability of this technique. Due to force modulation a wear reduction of more than three times for PtSi tips is demonstrated and the experiments show no signs of breaking of the tip apex. During long-term imaging a nine-fold increase of the average current was measured. The mechanism behind the wear reduction is shown to be a decrease in friction between tip and sample due to the periodic reduction in load force, which prevents the build-up of lateral forces on the tip. The increased electrical contact quality is hypothesized to be due to the improved piercing of a layer of contaminants covering the sample surface. The periodic increase of the load force aids the normal forces to push the tip into the repulsive regime, where good electrical contact quality can be maintained. Imaging experiments were also performed on specially prepared heterogeneous samples consisting of evaporated platinum marks on an amorphous carbon background. The force modulation scheme proves to be especially beneficial at lower load forces. An almost six-fold increase of mean conducted current was measured at a load force of 10 nN. Low load forces are of great interest because they exert a much lower wear rate. Force modulation is beneficial over a wide operation range, can be performed at multiple frequencies and is tunable to a sweet spot with low friction and enhanced electrical contact. This technique could have a significant impact on nanoscale electrical sensing using conductive-mode SPM.

## Acknowledgments

The authors gratefully acknowledge Andrew Pauza for the GST samples, Laurent Dellmann for the platinum samples, Ute Drechsler and Walter Haeberle for experimental support and Harish Bhaskaran and Niels Tas for helpful discussion. This work is supported by the European Research Council within the FP6 project 'Probe-based Terabit Memory'.

# Chapter 6

# Summary and conclusions

The prime goal of the work presented in this thesis is to propose and conceptually demonstrate strategies for data readout in archival storage using probes. The concepts for probe readout that have been developed are certainly not limited to use in probe storage, other application areas in which arrays of probes or conductive probes are used can benefit. A main topic is the development of three different optical readout techniques for probe arrays to enable remote readout, which is an important step towards the use of a drive concept in probe archival storage. The techniques each have their specific strengths and application areas as will be discussed. A second main topic is the development of a force modulation technique for conductive probes. Conductive probes are employed in phase-change storage to readout data. The first part of this chapter summarizes and discusses the work presented in this thesis. The second part contains a short-list of the main conclusions and, finally, an outlook is given towards future work.

## 6.1 Summary

### 6.1.1 Probe storage

The most mature probe storage technologies have been discussed based on literature, and no clear winner can be appointed. Thermomechanical storage is by far the most mature. Phase-change storage shows promising data rates per probe, but rewriteability remains an issue. Ferroelectric storage is primarily investigated as potential successor of magnetic storage in hard disk drives. Probes are mainly used for research purpose.

Currently, no commercial product using probe storage is available. It is very well possible that probe storage gains new attention in the future, when mechanically addressed storage reaches atomic densities. Atomic scale recording has already been demonstrated, albeit under laboratory conditions and maturing atomic density probe recording for commercialization remains daunting.

### 6.1.2 Optical readout

In many probe arrays sensing of the deflection of the cantilevers is integrated in the cantilever design. Optical readout of probe arrays offers a modular system design and reduces the design constraints and complexity of the cantilever. Optical sensors can operate at very high speeds in contrast to many integrated sensors, e.g. the thermal sensor used for thermomechanical storage is are limited to a speed of about 250 kHz. Solutions for optical readout reported in literature use time-multiplexing, which decreases speed, or use one photodetector for each cantilever, thereby considerably increasing cost and complexity of the optical detection system.

In this thesis solutions are pursued that do not compromise the speed and add little to no extra hardware to the system. In optical readout the alignment of the laser spot with respect to the array and the detectors can be challenging, depending on the geometries and number of cantilevers in the array. This is especially important in applications where cantilever arrays have to be replaced. Probe storage is not one of them, but e.g. biological sensing and surface imaging are. When the number of cantilevers per detector increases, so does thermal noise and the signal strength will decrease (at constant total laser power). Signal strength can be maintained by increasing the amount of laser power per cantilever. In that case case an increase in dynamic range of the photodetector and amplification circuitry is required.

### 6.1.3 Optical readout of probe arrays in dynamic mode

Two optical readout techniques have been developed for the parallel readout of probe arrays in dynamic mode. The well-known optical beam deflection technique has been extended to arrays without any modification to the detection hardware while maintaining the high throughput. Addressing each cantilever at its own resonance frequency is the key in distinguishing the response of each individual cantilever in the received signal from the split photodiode. A second method using interferometric detection functions likewise; however, it requires only a single photodiode instead of a split photodiode by exploiting the inherent destructive interference effects occurring when light is reflected from closely spaced cantilevers. Using one photodiode alleviates the alignment difficulties of the laser spot on the detector. Both techniques have been demonstrated showing accurate measurements of a single cantilever within the array that changes its resonance frequency. Mechanical coupling effects were not observed within the measurement precision (<10 mHz). Moreover, the technique limits the thermal cantilever noise to a minimum by filtering out any contribution outside the frequency spectrum of interest. Conveniently, the largest part of thermal noise of non-interrogated cantilevers is outside this frequency spectrum due to the differences in natural resonance frequencies.

Most of the cantilever-based sensing techniques use resonating cantilevers that shift their natural resonance frequency due to mass-loading or spring stiffening. The two optical readout techniques suggested in this work are very well suited to be used in such applications. A careful design of the spacing between the reson-

ance peaks is needed. Important parameters are the quality factor, the resonance frequency itself and the number of cantilevers per photodetector.

### 6.1.4 Optical readout of probe arrays in static mode

Parallel optical readout of a probe array operating in static mode can be achieved by recording the diffraction pattern that the array creates. The cantilevers form an optical grating and the state of deflection of each cantilever within the array determines the diffraction pattern, which is captured by a 1-dimensional array of photodiodes. Each cantilever can be regarded as a slit in a traditional multiple slit diffraction experiment. In our situation the phase of the reflected light is a function of the amount of deflection of the cantilever, in contrast to a slit diffraction experiment, where the slits are assumed to contain light sources with equal phase. The diffraction pattern is shown to obey one-dimensional Fraunhofer theory. The developed technique is straightforward applicable when two discrete levels are permitted in cantilever bending.

There exist cantilever configurations that give rise to optical fields producing equal irradiance profiles at the array of photodiodes. These equivalent configurations can be prevented by appropriate coding of the data. Based on our current measurements we estimate that all configurations of an array of seven cantilevers can be detected in our setup when the size of deflection is 10 nm. A number of distinct worst-case pairs is present, but coding can be adapted to accommodate for differences in pattern distinguishability. Calculations have shown that it is possible to increase the signal that very small deflections create, by the addition of an offset layer to every second cantilever in the array. The average factor of improvement in signal is 7.7 for an array of nine cantilevers, a deflection of 1 nm and a wavelength of the laser light of 640 nm. The sensitivity can be improved further by reducing the wavelength of the laser light. Moreover, the offset dramatically improves the signal of the set of worst-case pairs. We found that for an array of five cantilevers the detectability of each of the worst-case pairs is increased by at least a factor of 13.

The proposed technique is very well suited for probe-based data storage. Another potential application area is imaging of surfaces that have two levels of depth, e.g. in quality control of lithographical processes.

### 6.1.5 Fabrication of probe arrays

A probe array fabrication process has been developed that results in silicon cantilevers with integrated tips. The focus is on achieving an array that gives rise to a highly uniform tip-medium distance. In order to accomplish this we make use of a silicon-on-insulator (SOI) wafer and define the tips by a highly uniform wet chemical etch. The fabricated micro-cantilever arrays are characterized and shown to have a high uniformity. For an array of 10 cantilevers spanning 430 μm a standard error of 11 nm has been measured. Furthermore, we have shown that it is possible to fabricate both cantilevers and tips using a single mask. The tips are self-aligned at the end of the cantilevers by a KOH etching step. A critical feature in the process

is the sharpness of the corner that houses the tip. We have shown that by means of an isotropic undercut resolution of our lithography tool can be effectively increased. This results in a corner radii of well below 500 nm instead of the ~2 μm of our lithography line. An unwanted side-effect of the KOH etch is the occurrence of silicon ridges that remain standing at the sides of the cantilevers. The height of these ridges is fully adjustable by controlling the angle between cantilever edge and ⟨110⟩ crystalline direction. No ridge remains when the angle is greater than 10°.

### 6.1.6 Force modulation for conductive probes

Conductive-mode SPM is a powerful technique for the investigation and modification of electrical properties at the nanoscale. It has application in areas such as semiconductor metrology and materials research and is a candidate for data readout in probe-based storage on phase-change media. Conductive probes can also be used to emulate nanoscale electrical contacts. However, improvement in tip durability and the maintenance of reliable nanoscale electrical contact are essential requirements for the wide-spread applicability of conductive-mode SPM. To obtain a low resistance electrical contact between tip and sample a significant load force has to be exerted on the tip. The abrasion of the tip apex is accelerated by this large normal load force on the tip.

In this work it is shown that force modulation, originally used used for non-conductive probes, can be very beneficial for conductive probes: force modulation improves the performance of conductive probes regarding wear and conduction. A wear reduction of more than three times for platinum silicide tips is demonstrated and no break up of the tip apex is found. The mechanism behind the wear reduction is a decrease in friction between tip and sample due to the periodic reduction in load force, which prevents the build-up of lateral forces on the tip. A higher conducted current between tip and sample due to force modulation is shown on both carbon and metal samples. The current is more stable, reliable and less dependent on load force than without additional actuation of the tip. The periodic increase of the load force aids the normal forces to push the tip into the repulsive regime. The increased electrical contact quality is hypothesized to be due to the improved piercing of the layer of contaminants covering the sample surface. The periodic increase of the load force aids the normal forces to push the tip into the repulsive regime, where good electrical contact quality can be maintained. Both, a lower contact resistance, as well as larger tolerance for irregularities is found, where the latter leads to less events of contact loss during operation. The force modulation scheme is especially beneficial at lower load forces. An almost six-fold increase of mean conducted current has been measured at a load force of 10 nN. During long-term measurements a nine-fold increase has been measured. Low load forces are of great interest since they provide a much lower wear rate. Force modulation is beneficial over a wide operation range, can be performed at multiple frequencies and is tunable to a sweet spot with low friction and enhanced electrical contact. This technique could have a significant impact on nanoscale electrical sensing using conductive-mode SPM.

## 6.2 Conclusions

- Multi-frequency addressing enables application of optical beam deflection to arrays of cantilevers, because multi-frequency addressing reduces the required hardware to do optical beam deflection on arrays of cantilevers down to only one laser and one split photodiode.
- By leveraging interference effects between light, reflected from closely spaced cantilevers, the split photodiode can be replaced by a single photodiode in case the cantilever amplitudes of oscillation are small compared to the wavelength of the light ($\lambda/8$).
- Operation in dynamic mode of one cantilever in an array of cantilevers of different length has not given rise to detectable mechanical coupling. The detection limit of the setup is below 10 mHz.
- Diffraction patterns that are created by illumination of an array of cantilevers contain the deflection state of every cantilever. In case the cantilevers deflections have two discrete levels, each diffraction pattern can accurately be related to the deflections of the cantilevers in the array.
- Calculations have shown that it is possible to increase the signal that very small deflections create, by adding an offset layer to every second cantilever. The average factor of improvement is 7.7 at a deflection of 1 nm, where an array of 9 cantilevers and a wave length of the laser light of 640 nm is used.
- Force modulation is very beneficial for conductive probes:
  - (i) modulating the normal load force of the tip improves the tip durability by a factor of three during one metre of tip travel, and
  - (ii) enhances the formation of nanoscale electrical contact. At a load force of 10 nN, it leads to an almost six-fold increase of mean conducted current and during long-term measurements a nine-fold increase has been measured.

## 6.3 Future work

The multi-frequency addressing technique has been demonstrated using magnetic cantilevers and an externally applied magnetic field. This experimental approach is very well suited to characterize the readout technique and allowed us to measure very small frequency shifts. The technique might be used for the development of miniature magnetic field sensors with high linearity and dynamic range. The experiment is similar to mass-loading of the cantilevers for sensing applications.

For application in data storage each probe has to operate at approximately the same distance from the storage medium. Arrays of high uniformity in tip-medium distance are presented in Chapter 4, but variations of tens of nanometres are still

present. These variations rule out the use of non-contact atomic force microscopy to detect topography variations. Other non-contact methods such as magnetic force microscopy or electric force microscopy may already be within reach for small arrays. The variation in tip-medium distance will, however, lead to loss in signal.

The fabrication of extremely uniform cantilever arrays is of paramount importance for probe storage. Uniform cantilever arrays lead to less wear and make implementation of force modulation or dithering schemes much simpler. Future work should therefore be directed towards reducing the tip-medium distance variation. As shown in this thesis, SOI wafers and the use of the wafer surface as reference plane are a good starting point.

In probe storage on magnetic dots or on phase-change material the detection limits at relevant bandwidths will have to be determined. Also, it seems inevitable that open-loop methods have to be used, which do not require the added complexity of individual height regulation for each cantilever. Non-contact operation without individual height regulation poses more stringent demands on the array and the positioning system. To increase the bandwidth of the readout technique the cantilever resonance frequencies should increase. In case a stiff cantilever is undesirable, e.g. because of increased tip wear and sample damage, one could use higher modes of vibration of the cantilevers. Other modes of operation, such as intermittent-contact mode, could also work in conjunction with multi-frequency addressing.

Optical readout of arrays operating in static mode is demonstrated with the help of diffraction patterns. Two important aspects need to be considered in future work. The detection of the diffraction patterns has to be optimized by choosing or fabricating suitable arrays of photodiodes. Special attention has to be paid to the position of the diodes with respect to the pattern. Secondly, non-uniformity in arrays affects, also for this readout technique, the readout signal. This non-uniformity might, however, be exploited, because addition of specific offsets has been shown to increase the signal. Ultimately, a read demonstration of indentations at high density is targeted.

The force modulation technique for conductive probes is shown to lead to improved electrical contact and this surprising result is hypothesized to be due to piercing or expulsion of insulating material between tip and sample. This hypothesis could be addressed by a number of experiments. All contamination from tip and sample should be removed, for this removal operation in a vacuum is required. Also, the nature of the contamination has to be taken into account. Next, dependency of the effect of force modulation on humidity and also on different tip materials can be studied. The range of frequencies for force modulation can be extended to higher modes of vibration. Friction measurements in combination with long-term wear studies could identify frequencies that possibly lead to higher reductions in wear. It might be necessary to experiment on very well-defined sample surfaces to obtain more reproducible results. We have seen signs that not only tip wear is reduced, also medium wear. This should be studied in more detail and in a systematic way on different media.

# Appendices

# Appendix A

# Noise of cantilever arrays

## A.1 Introduction

In this appendix the noise of a cantilever array is derived when optical readout is used. The analysis is partly based on the analysis of a single cantilever in Sarid (1991) and is extended to be applicable to an array of cantilevers. The main noise sources are:

- Thermal noise of the cantilevers
- Shot noise at the photodetectors
- Laser intensity noise
- Electronics noise

The contribution of the electronics and laser intensity noise are the smallest of the four noise sources (Sarid, 1991). Thermal noise and shot noise will rise with increasing number of cantilevers; however, electronics noise does not depend on the amount of cantilevers in an array. Laser intensity noise does rise when the laser power rises proportionally with the number of cantilevers. In that case, intensity noise is still smaller. In the remainder of this study electronics and laser intensity noise are neglected and thermal and shot noise are analyzed in detail.

## A.2 Thermal noise

The atoms present in the cantilever system undergo Brownian motion and exert pressure on the cantilever that is zero when averaged over time, but does not need to be zero at each instant of time. As a result the cantilever will vibrate, even when it is in vacuum and not excited externally.

In thermal equilibrium, every vibration mode of the cantilever has a mean thermal energy of $k_B T$, where $k_B$ is the Boltzmann constant and $T$ is the temperature. That is, for both potential, as well as kinetic energy $\frac{1}{2}k_B T$ (Butt and Jaschke,

1995). This stems from the equipartition theorem, which states that if a system is in thermal equilibrium every independent quadratic term in the systems total energy (position $z$ and momentum $p$) has a mean value equal to $\frac{1}{2}k_B T$ (Butt and Jaschke, 1995). Since, for each vibration mode, the total thermal energy consists of the sum of the potential and kinetic energy, each vibration mode contributes $k_B T$. We are interested in the noise on the position for the tip end of the cantilever, because this part is monitored by the optical readout system. Now, the equipartition theorem states for the potential energy term of the tip motion, $\frac{1}{2}k\left\langle z^2\right\rangle = \frac{1}{2}k_B T$, where $\left\langle z^2\right\rangle$ is the mean square deflection of the cantilever tip end.

The root means square (RMS) of the thermal noise of one cantilever as a function of frequency (Sarid, 1991), under the condition that the change in noise spectral density is small over bandwidth $B$ that has a centre frequency $\omega$, is given by

$$\sqrt{\langle \delta z^2(\omega) \rangle} = \sqrt{\frac{4k_B TB}{k\omega_0}} \frac{\sqrt{Q}}{\sqrt{Q^2\left(1+\omega^2/\omega_0^2\right)^2 + \omega^2/\omega_0^2}}, \tag{A.1}$$

where:

$$\begin{aligned} k_B &= 1.38 \times 10^{-23}\,\mathrm{J\,K^{-1}}, \\ T &= \text{temperature (K)}, \\ k &= \text{spring constant (N m}^{-1}\text{)}, \\ \omega_0 &= \text{natural resonance frequency (rad s}^{-1}\text{)}, \\ Q &= \text{quality factor}(-). \end{aligned}$$

Equation (A.1) evaluated at $\omega = \omega_0$ gives

$$\sqrt{\langle \delta z^2(\omega = \omega_0) \rangle} = \sqrt{\frac{4k_B TBQ}{k\omega_0}}. \tag{A.2}$$

Equation (A.1) evaluated at $\omega$ is much smaller than $\omega_0$ gives

$$\sqrt{\langle \delta z^2(\omega < \omega_0) \rangle} \approx \sqrt{\frac{4k_B TB}{Qk\omega_0}}. \tag{A.3}$$

If $\omega$ is larger than $\omega_0$, than $\frac{\omega}{\omega_0} > 1$ and Equation (A.1) can be approximated by

$$\sqrt{\langle \delta z^2(\omega > \omega_0) \rangle} \approx \sqrt{\frac{4k_B TB}{Qk\omega_0 \frac{\omega^3}{\omega_0^3}}} < \sqrt{\frac{4k_B TB}{Qk\omega_0}}. \tag{A.4}$$

Let us assume $Q$ to be larger than 100. The highest noise occurs at resonance, see Equation (A.2). Choosing an $\omega$ below resonance gives a factor of $Q$ less noise, see Equation (A.3). An $\omega$ above fundamental resonance, and still below the first vibration mode, reduces the noise further, see Equation (A.4). Therefore, we can neglect

Table A.1 – *Specification of the parameters used for calculation.*

| | | |
|---|---|---|
| $k$ | = | $1\,\mathrm{N\,m^{-1}}$ |
| $\omega_0$ | = | 100 kHz |
| $T$ | = | 300 K |
| $B$ | = | 100 Hz |
| $Q$ | = | 100 |

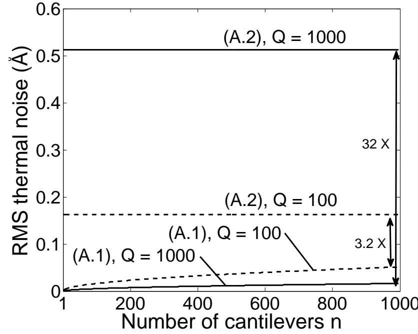


Figure A.1 – *Thermal noise contribution of Equation* (A.5) *and Equation* (A.2) *for* $Q = 100$ *(dotted lines) and* $Q = 1000$ *(solid lines) as a function of the number of cantilevers in an array. Equation* (A.2) *contributes significantly more noise and the discrepancy scales with* $Q$.

the contribution of thermal noise of cantilevers that have resonance frequencies outside the frequency band of interest.

In order to obtain the RMS thermal noise of an array of $n$ cantilevers with different resonance frequencies we can perform squared addition, because thermal noise is independent and random. The RMS thermal noise of an array of $n$ cantilevers with different resonance frequencies, where $\omega_{0,i}$ is the fundamental resonance frequency of the $i$–th cantilever is then given by

$$\sqrt{\langle \delta z^2(\omega) \rangle} = \sqrt{\sum_{i=1}^{n} \frac{4k_\mathrm{B}TB}{k\omega_{0,i}} \frac{Q}{Q^2\left(1+\omega^2/\omega_{0,i}^2\right)^2 + \omega^2/\omega_{0,i}^2}}.$$

The RMS thermal noise of an array of $n$ cantilevers at $\omega$ smaller than the smallest $\omega_{0,i}$ is given by

$$\sqrt{\langle \delta z^2(\omega < \omega_{0,i}) \rangle} = \sqrt{n\frac{4k_\mathrm{B}TB}{Qk\omega_0}}. \tag{A.5}$$

Using the parameters listed in Table A.1 the thermal noise is calculated as a function of the number of cantilevers in an array. The results are plotted in Figure A.1, for a quality factor of 100 and 1000. It is evident from the figure that the contribution (Equation (A.2)) of the cantilever that has its resonance frequency inside the frequency band of interest, $\omega \pm B/2$, is much larger than the contribution (Equation (A.5)) of all other cantilevers. At a quality factor of 100 and for $n = 1000$ cantilevers the difference is more than a factor of three. The discrepancy increases proportional to $Q$.

## A.3 Shot noise

The shot noise on a photo detector due to light reflected by a single cantilever is (Sarid, 1991)

$$\sqrt{\langle \delta i^2 \rangle} = \sqrt{2e\eta BP},$$

where:

$$\begin{aligned} e &= 1.6 \cdot 10^{-19} \text{ (C)} \\ \eta &= \frac{i}{P} \text{ (A/W)} \\ B &= \text{bandwidth (Hz)} \\ P &= \text{light power per cantilever (W)}. \end{aligned}$$

When we assume that the light power is equal for each cantilever the shot noise will go up with the square root of the number of cantilevers. With $n$ the total number of cantilevers in an array the total shot noise is

$$\left\langle \delta i^2 \right\rangle = 2e\eta BnP. \tag{A.6}$$

Optical beam deflection uses a split-photodiode and outputs the difference in light power on the two photodiodes ($A$ and $B$). In case of a laser spot that is perfectly aligned on a split-photodiode the shot noise for each photodiode is

$$\left\langle \delta i_{\mathrm{A}}^2 \right\rangle = 2e\eta Bn\frac{P}{2} \tag{A.7}$$

and

$$\left\langle \delta i_{\mathrm{B}}^2 \right\rangle = 2e\eta Bn\frac{P}{2}. \tag{A.8}$$

Even though two photodiodes are used, the total amount of shot noise in the resulting signal does not change. To calculate the total shot noise equations (A.7) and (A.8) have to be added before the square root operation, because the shot noise is independent and random. Thus, resulting again in (A.6). This holds in general for any number of photodiodes.

## A.4 Noise comparison

To be able to compare the size of the different noise contributions one unit of noise has to be chosen. Transforming current noise into cantilever mechanical noise or vice versa requires knowledge of the complete optical readout system. Optical readout modulates the available laser power and the difference in power is used to determine the cantilever motion. In the case of interferometry, interference changes the intensity per photodiode. In the case of optical beam deflection the total power remains (ideally) constant, however the movement of the laser beam changes the power per photodiode. The optical readout system determines by how much the power measured by each photodiode varies as a function of cantilever deflection. In the case of interferometry this relation is usually not linear.

As an example we use the simple implementation of the optical beam deflection setup given in Sarid (1991). First the size of the laser spot is found based on the far-field diffraction limit. To illuminate a cantilever array a line shaped laser spot is used. This makes the width of the reflective area on the cantilever exactly equal to the width $w$ of the cantilever. When we assume the line thickness of the line shaped laser spot to be equal to width of the cantilever, the reflective area on each cantilever is a square of size $w \times w$, which we define as $2a \times 2a$. The far-field diffraction limited spot size $w$ at distance $z$ is (see (A.9) with derivation in §A.4.1)

$$w(z) = \frac{\lambda}{\pi} \frac{z}{w_0}$$

The relation between the detector output (difference in the photocurrents) and the cantilever deflection (at the tip) is then given by (Sarid, 1991)

$$\delta i(t) = \frac{3\pi a}{\lambda l} \eta P z(t),$$

where

$$\begin{aligned}
\delta i(t) &= i_A - i_B = \text{output current (A)},\\
a &= \text{half of laser spot width and height (m)},\\
\lambda &= \text{wavelenght of laser light (m)},\\
l &= \text{cantilever length (m)},\\
\eta &= \frac{i}{P} \text{ (A/W)},\\
P &= \text{light power per cantilever (W)},\\
z(t) &= \text{tip deflection (m)}.
\end{aligned}$$

The relation between thermal noise and shot noise is now fixed to

$$\sqrt{\delta i^2(t)} = \frac{3\pi a}{\lambda l} \eta P \sqrt{\langle \delta z^2(\omega) \rangle}.$$

This allows us to express the shot noise as a function of cantilever motion:

$$\begin{aligned}\sqrt{\langle \delta z^2 \rangle}_{shot} &= \frac{\lambda l}{3\pi a \eta P}\sqrt{2e\eta BnP} \\ &= \frac{\lambda l}{3\pi a}\sqrt{\frac{2eBn}{P\eta}}.\end{aligned}$$

### A.4.1 Laser spot size

A Gaussian $TEM_{00}$ flat laser-beam wavefront evolves, starting from plane $z = 0$ and a waist diameter $w_0$ to a waist diameter $w$ given by:

$$w(z) = w_0\sqrt{1 + \left(\frac{\lambda z}{\pi w_0^2}\right)^2}$$

The far-field diffraction-limited spot size is given by:

$$w(z) = \frac{\lambda}{\pi}\frac{z}{w_0} \tag{A.9}$$

This approximation is only valid when:

$$\begin{aligned}1 &<< \left(\frac{\lambda z}{\pi w_0^2}\right)^2 \\ \frac{1}{z} &<< \left(\frac{\lambda}{\pi w_0^2}\right) \\ z &>> \pi w_0^2/\lambda.\end{aligned}$$

When we take the flat laser-beam wavefront exactly at the cantilever surface and $z$ sufficiently large, the size of the laser spot at the detector will be equal to the diffraction-limited spot size according to Equation (A.9). The far field approximation is given in Equation (A.9).

## A.5 Total noise

The calculation of the total noise depends on the mode of operation. In case the optical readout technique developed in Chapter 3 is used, the cantilever array operates in dynamic mode. Each cantilever has a different natural resonance frequency, at which it vibrates and the thermal cantilever noise has to be calculated according to (A.2). Since the detection will take place using band-pass filtering the thermal noise in the signal is in good approximation originating from only one cantilever. This assumption is valid if the measurement bandwidth is smaller than the distance between the natural resonance frequencies and the quality factor is ≥ 100. Refer to

TABLE A.2 – *Specification of the parameters used for calculation.*

| | | |
|---|---|---|
| $n$ | = | 100 (cantilevers) |
| $k$ | = | $1\,\mathrm{N\,m^{-1}}$ |
| $\omega_0$ | = | 500 kHz |
| $T$ | = | 300 K |
| $B$ | = | 100 Hz |
| $Q$ | = | 100 |

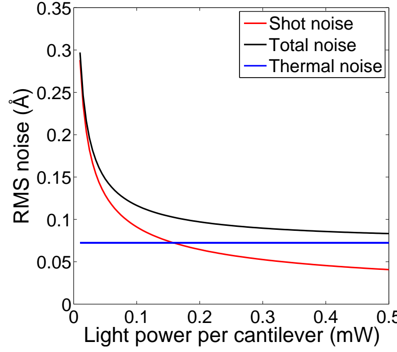


FIGURE A.2 – *Calculated equivalent RMS tip noise as a function of light power per cantilever when operating in dynamic mode. The contributions of thermal and shot noise are shown in separate curves.*

Chapter 3 for an experimental implementation meeting these requirements. The total noise can now be calculated:

$$\sqrt{\langle \delta z^2 \rangle_{\mathrm{total}}} = \sqrt{\langle \delta z^2 \rangle_{\mathrm{thermal}} + \langle \delta z^2 \rangle_{\mathrm{shot}}} = \sqrt{B \frac{4 k_{\mathrm{B}} T Q}{k \omega_0} + n B \frac{\lambda^2 l^2}{9 \pi^2 a^2} \frac{2e}{P \eta}}.$$

We consider a second mode of operation in which all cantilevers operate far below resonance and no band-pass filtering is applied. This situation occurs when the cantilever array is operating in static mode. The total noise is now given by

$$\sqrt{\langle \delta z^2 \rangle_{\mathrm{total}}} = \sqrt{\langle \delta z^2 \rangle_{\mathrm{thermal}} + \langle \delta z^2 \rangle_{\mathrm{shot}}} = \sqrt{n B \frac{4 k_{\mathrm{B}} T}{Q k \omega_0} + n B \frac{\lambda^2 l^2}{9 \pi^2 a^2} \frac{2e}{P \eta}}.$$

Figure A.2 shows the calculated total noise for operation in dynamic mode using the parameters from Table A.2. The total noise is an equivalent noise at the

cantilever tip end. Shot noise dominates when a low light power per cantilever is used, thermal noise dominates at higher light power. In this example the break even point is 150 μW per cantilever.

# Appendix B

# Tortoise – a multi-probe SPM

The multi-probe SPM nicknamed 'Tortoise' has been built to serve as a test system for optical readout techniques. The system is also used to explore other aspects of an architecture for archival data storage using probes. One of these aspects is a large storage area, which requires long-range positioning of the probe arrays. The system is discussed, including the optical readout and a demonstration of the long-range positioning capabilities of the system is given, using thermomechanical probes from IBM.

## B.1 Tortoise system

The Tortoise system is a multi-probe SPM that can operate under a controlled environment. A measurement chamber houses the core of the SPM. The chamber is supported by two steel girders which rest on a table made of wood, see the photograph in Figure B.1. Wood is selected because it damps vibrations. The table rests on four damper legs that use pneumatic isolation (I2000, Newport). Underneath the measurement chamber a cross piece with six 8" (CF) flanges is connected. On one side of the cross piece a turbo pump is mounted via a manual valve. The turbo pump has an appropriate roughing pump connected to it. A second manual valve is fixed to the bottom flange of the cross piece. The valve is connected to an ion pump (Varian plus 300). The vacuum system is capable of reaching UHV pressures, since all connections have copper gaskets. The top of measurement chamber, however, can be removed and for this purpose a rubber ring is used in between the top and bottom of the measurement chamber. Even with the presence of the rubber ring a pressure of $1 \times 10^{-6}$ mbar can be reached.

Multi-TB capacity, even at ultra-high densities of 5-10 Tb inch$^{-2}$, requires a storage areas of several tens of square centimetres. A critical issue of large scale storage area is the positioning of probes with respect to the medium over centimetre distance. The Tortoise system is equipped with a long-range positioning stage in one dimension (Physik Instrumente M-510), which is capable of moving a 10 cm distance, see Figure B.2. On top of the long-range positioning stage a conventional

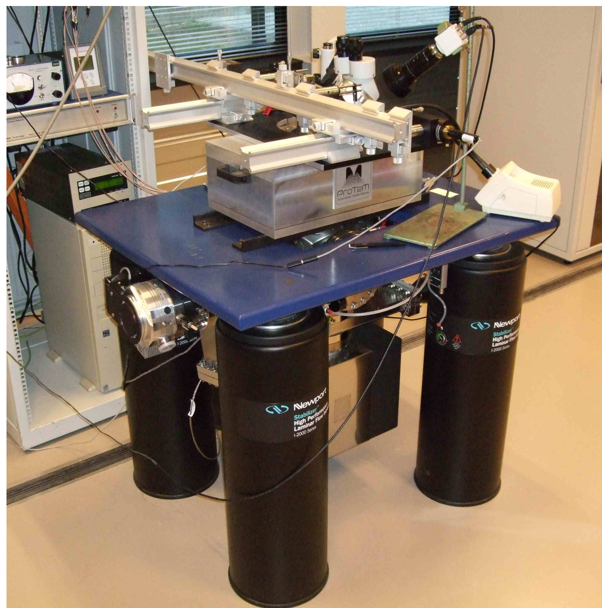

Figure B.1 – *Photograph of the Tortoise setup. The four damper legs support a wooden table. The setup rests on two steel girders that are spanning across a rectangular hole in the centre of the table. The measurement chamber with the optical path is above the table, the vacuum system including feedthroughs for electrical signals is below the table.*

$xyz$ scantable (Physik Instrumente P-527.3CL) is placed. The probe array is mounted on a printed circuit board, which in turn is mounted on a small tower at the side of the scan table. The small tower incorporates two slip-stick motors to adjust the height of the probe array (Attocube $ANP_z100$) and the roll angle (Attocube $ANG_t100$). The height regulation is used for coarse approach of the array to the medium surface. The roll angle motor makes accurate alignment of the probes with the medium possible, such that each probe touches the medium at the same time.

The Tortoise system uses an RHK V-scan box with a digital signal processor to control the scan table and data acquisition. The necessary analog-digital and digital-analog converters are also in the V-scan box. A user interface is written in LabVIEW. The SPM has electronic circuitry enclosed in a protective box to drive the IBM thermomechanical cantilevers. This analog front end electronics detects changes in the thermal sensor resistance by sensing the current through the sensor. The circuitry is implemented twice, such that two probes can be monitored simultaneously. This also facilitates alignment of the array with respect to medium by comparison of the signal from two different probes.

The optical path that is installed on top of the measurement chamber of the

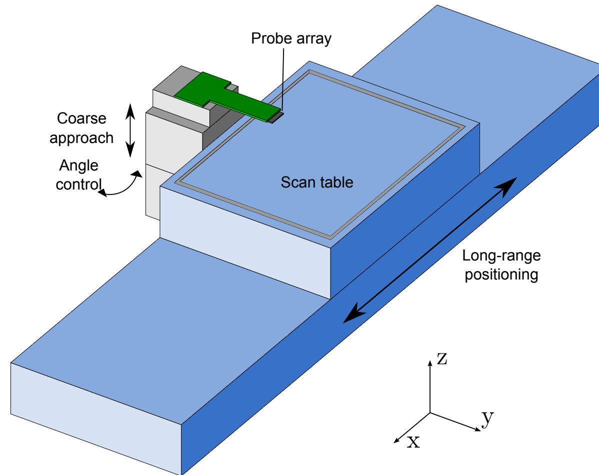


Figure B.2 – *Schematic depiction of the positioning system. The scan table is mounted on a long-range positioning stage capable of moving* 10 cm.

Tortoise is explained in detail in §4.1.2. Here we suffice with displaying an illustrated photograph of the optical path, see Figure B.3. The laser is not within the range of the picture, it is situated more to the left.

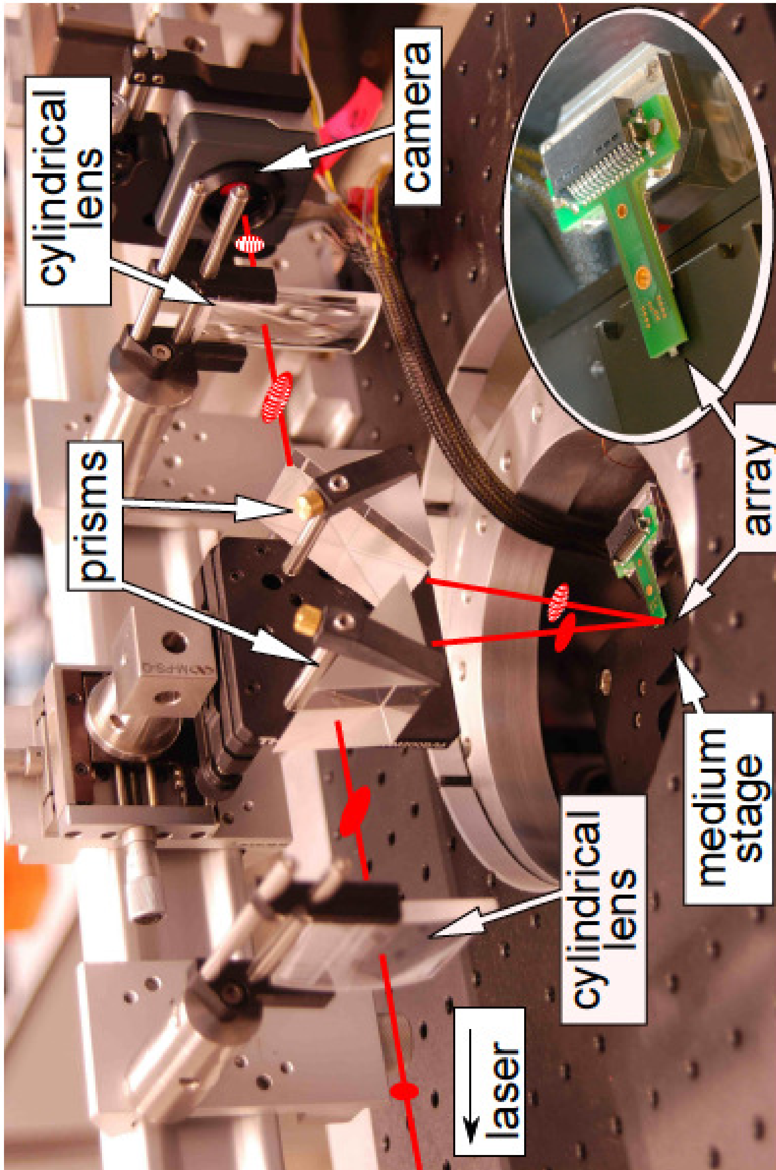


FIGURE B.3 – *An illustrated photograph of the optical readout path that is installed on top of the measurement chamber. The laser is not within the range of the picture, it is situated more to the left.*

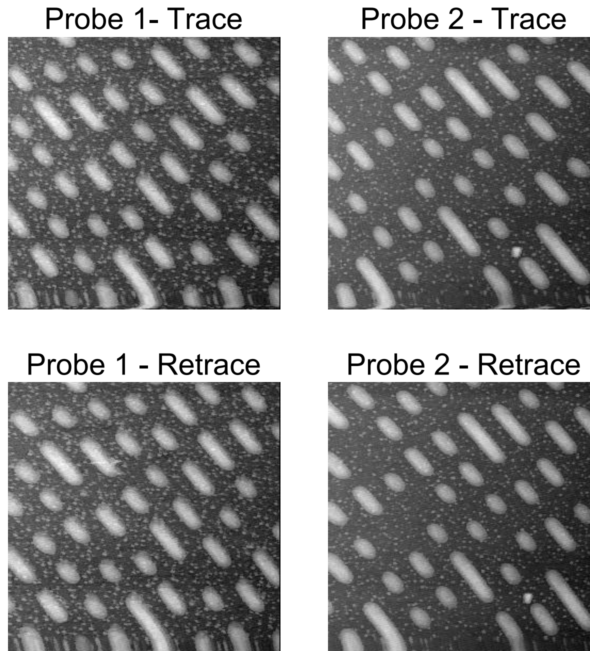


FIGURE B.4 – *Parallel imaging of a CD master with thermomechanical levers. The trace and retrace images of both probes are very similar. The distortion at the bottom of the images is caused by a slight change in the sample position.*

## B.2 Parallel imaging with thermomechanical probes

Parallel imaging of a CD master has been performed using an array of 8 A-levers from IBM. The imaging is performed by first aligning the array with the medium and consequently scanning the medium with respect to the probes. The read resistances of two out of the eight scanning probes are monitored. The images are displayed in Figure B.4 and all have 256 pixels × 256 pixels. The fast scan axis is from left to right, the slow scan axis from bottom to top. The bottom scan lines are slightly distorted due to motion of the sample. Fixing the sample to the scan table proved to solve the problem. We use double-sided tape and wait for a few hours to get rid of drift.

## B.3 Long-range positioning

To demonstrate the long-range positioning capability of the setup an experiment containing a long-range move is performed. Our test sample is a laser interference lithography (LIL) patterned medium (Engelen et al., 2010) with dots of approxim-

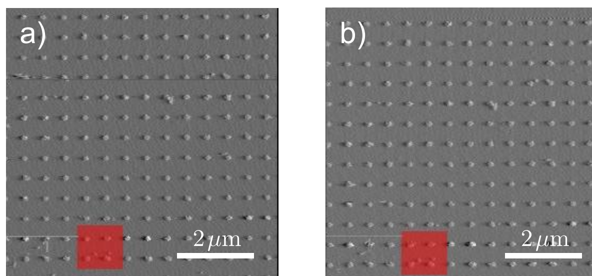


FIGURE B.5 – *Images of a LIL sample by a thermomechanical cantilever in the Tortoise, showing the long-range returnability accuracy, which is for this pair of images* 120 nm *in the long-range move direction (horizontal). With a) the image before the long-range move is performed and b) the image after the long-range move is performed.*

ately 185 nm in diameter with a period of approximately 550 nm in two dimensions. First a read operation of a 7 μm × 7 μm area is done, followed by a second read operation at a different location several centimetres away. After the second read operation the long-range stage moves back to the position of the first read operation and another read operation is performed. Every read operation consists of 256 pixels × 256 pixels and a line time of 0.51 s. Figure B.5 shows the scan before the long-range move and after the long-range move, which should ideally give twice the same image. From the figure it can be seen that there is a slight translation between the two images in the direction of the long-range move. The translation is estimated to be 120 nm, by means of correlation of part of the scan. Note that the sample is properly fixed to the scan table and the distortion of the first scan lines does not occur anymore. The offset can therefore be solely attributed to the returnability precision of the coarse positioning system.

# Appendix C

# Cantilever array process flow

Cantilever arrays with and without tips have been fabricated. In this appendix the process flow of the cantilever arrays with tips is given. The arrays without tips are fabricated much along the lines of this process, with exclusion of the steps concerning the tip fabrication.

Table C.1: Process steps

| Step | Process | Comment |
|---|---|---|
| 1a | **Substrate selection – Silicon ⟨100⟩ OSP**<br>Orientation: ⟨100⟩<br>Diameter: 100 mm<br>Thickness: 525 μm ±25 μm<br>Polished: Single side<br>Resistivity: 5-10 Ω cm (p-doped) | 10 wafers<br>(dummies) |
| 1b | **Substrate selection – Silicon ⟨110⟩ DSP**<br>Orientation: ⟨110⟩<br>Diameter: 100 mm<br>Thickness: 380 μm ±10 μm<br>Polished: Double side<br>Resistivity: 5-10 Ω cm (p-doped) | 2 wafers<br>(dummies) |
| 1c | **Substrate selection – SOI ⟨100⟩ DSP**<br>Orientation: ⟨100⟩<br>Diameter: 100 mm<br>Device layer thickness: 10 μm ± 0.5 μm<br>Device layer resistivity: 0.01-0.02 Ω cm (p-doped)<br>Handle wafer thickness: 380 μm ±5 μm<br>Handle wafer resistivity: 1-20 Ω cm (p-doped)<br>BOX thickness: 0.5 μm +/- 5% | 5 wafers<br>(process wafers) |

Table C.1 Process steps (continued)

| Step | Process | Comment |
|---|---|---|
| 2 | **Standard cleaning**<br>$HNO_3$ (100%) Selectipur: MERCK<br>$HNO_3$ (69%) VLSI: MERCK<br>• Beaker 1: fumic $HNO_3$ (100%), 5 min<br>• Beaker 2: fumic $HNO_3$ (100%), 5 min<br>• Quick Dump Rinse < 0.1 µS<br>• Beaker 3: 95 °C $HNO_3$ (69%), 10 min<br>• Quick Dump Rinse < 0.1 µS<br>• Spin drying | |
| 3 | **Etching HF (1%) Native Oxide**<br>HF (1%) VLSI: MERCK 112629.500<br>• Etch time: > 1 min<br>• Quick Dump Rinse < 0.1 µS<br>• Spin drying | Just before SiRN deposition |
| 4 | **LPCVD SiRN – uniform thickness**<br>Tempress LPCVD G4<br>Program: LSNit-G4<br>• $SiH_2Cl_2$ flow: 155 sccm<br>• $NH_3$ flow: 45 sccm<br>• temperature: 830/850/873 °C<br>• pressure: 200 mTorr<br>• $N_2$ flow: 150 sccm<br>• deposition rate: ±6 – 7 nm $min^{-1}$ | Thickness:<br>25 nm ±5 nm<br>Time: 2 min 10 s |
| 5 | **Ellipsometer Measurement**<br>Plasmos Ellipsometer | Use dummies |
| 6 | **LPCVD TEOS**<br>Tempress LPCVD B4<br>Bubbler: 40.0 °C<br>Temperature: 700 °C<br>pressure: 400 mTorr<br>• deposition rate: 10.7 nm $min^{-1}$ (25 wafers)<br>• Uniformity per wafer: 3% | Thickness =<br>100 nm ± 10 nm<br>Time = 10 min |
| 7 | **Ellipsometer Measurement**<br>Plasmos Ellipsometer | Use dummies |

Table C.1 Process steps (continued)

| Step | Process | Comment |
| --- | --- | --- |
| 8 | **LPCVD SiRN – uniform thickness**<br>Tempress LPCVD G4<br>• $SiH_2Cl_2$ flow: 155 sccm<br>• $NH_3$ flow: 45 sccm<br>• temperature: 830/850/873 °C<br>• pressure: 200 mTorr<br>• $N_2$ flow: 150 sccm<br>• deposition rate: ± 6-7 nm $min^{-1}$ | Thickness =<br>20 nm ± 5 nm<br>Time = 100 s |
| 9 | **Ellipsometer Measurement**<br>Plasmos Ellipsometer | Use dummies |
| 10 | **Standard cleaning**<br>$HNO_3$ (100%) Selectipur: MERCK<br>$HNO_3$ (69%) VLSI: MERCK<br>• Beaker 1: fumic $HNO_3$ (100%), 5 min<br>• Beaker 2: fumic $HNO_3$ (100%), 5 min<br>• Quick Dump Rinse < 0.1 µS<br>• Beaker 3: 95 °C $HNO_3$ (69%), 10 min<br>• Quick Dump Rinse < 0.1 µS<br>• Spin drying | |
| 11 | **Lithography – Olin 907-17**<br>Suss Micro Tech Spinner (Delta 20)<br>• Dehydration bake (120 °C): 5 min<br>HexaMethylDiSilazane (HMDS):<br>• Spin program: 4 (4000 rpm, 20 s)<br>Olin 907-17:<br>• Spin program: 4 (4000 rpm, 20 s)<br>• Prebake (95 °C): 90 s<br>Electronic Vision Group 620 Mask Aligner:<br>• Hg-lamp: 12 mW $cm^{-2}$<br>• Exposure Time: 4 s<br>Developer OPD4262:<br>• Time: 30 s in Beaker 1<br>• Time: 15-30 s in Beaker 2<br>• Quick Dump Rinse <0.1 µS<br>• Spin drying | Front side mask,<br>hard contact. |
| 12 | **Optical microscopic inspection**<br>Nikon Microscope | Inspection of<br>lithography |

Table C.1 Process steps (continued)

| Step | Process | Comment |
|---|---|---|
| 13 | **Plasma etching – chamber cleaning**<br>Elektrotech PF310/340<br>• Electrode temp.: 10 °C or 25 °C<br>• $O_2$ flow: 20 sccm<br>• pressure: 50 mTorr<br>• power: 150 W<br>• DC-Bias: 780 V | |
| 14 | **Plasma etching SiN**<br>Elektrotech PF310/340<br>Styros + Quartz electrode<br>• Electrode temp.: 10 °C<br>• $CHF_3$ flow: 25 sccm<br>• $O_2$ flow: 5 sccm<br>• pressure: 10 mTorr<br>• power: 75 W<br>Etchrate Olin resist = 95 nm $min^{-1}$ | Etch through top nitride layer (30 s), stop in TEOS $SiO_2$ layer<br>Total time: 60 s |
| 15 | **Optical microscopic inspection**<br>Olympus Microscope | |
| 16 | **Stripping of Olin PR - $HNO_3$ standard**<br>$HNO_3$ (100%) Selectipur: MERCK 100453<br>• Time: 40 min<br>• Quick Dump Rinse <0.1 µS<br>• Spin drying | |
| 17 | **Strip PR by oxygen plasma Tepla 300**<br>Barrel Etcher (2.45 GHz)<br>Ultra clean system only (no metals except Al)<br>• $O_2$ flow: 200 sccm (50%)<br>• Power: up to 1000 W<br>• Pressure: 1 mbar | 10 min |
| 18 | **Optical microscopic inspection**<br>Nikon Microscope | Inspection of PR-residue |
| 19 | **Etching BHF (1:7) $SiO_2$**<br>$HF/NH_4F$(1:7) VLSI: BASF<br>• Quick Dump Rinse <0.1 µS<br>• Spin drying | Time: 12 min 30 s |
| 20 | **SEM Inspection**<br>JEOL 5610 | inspect underetch |

Table C.1 Process steps (continued)

| Step | Process | Comment |
|---|---|---|
| 21 | **Standard cleaning**<br>$HNO_3$ (100%) Selectipur: MERCK<br>$HNO_3$ (69%) VLSI: MERCK<br>• Beaker 1: fumic $HNO_3$ (100%), 5 min<br>• Beaker 2: fumic $HNO_3$ (100%), 5 min<br>• Quick Dump Rinse < 0.1 µS<br>• Beaker 3: 95 °C $HNO_3$ (69%), 10 min<br>• Quick Dump Rinse < 0.1 µS<br>• Spin drying | |
| 22 | **Etching HF (1%) Native Oxide**<br>HF (1%) VLSI: MERCK 112629.500<br>• Etch time: > 1 min<br>• Quick Dump Rinse < 0.1 µS<br>• Spin drying | |
| 23 | **Etching of SiN (Hot $H_3PO_4$)**<br>$H_3PO_4$ 85% Merck VLSI 1.00568.2500<br>• Temp.: 180 °C<br>• Quick Dump Rinse < 0.1 µS<br>• Spin drying<br>Etchrate SiRN: 3.5 nm min$^{-1}$<br>High selectivity for $SiO_2$ layers | Etch rate<br>by dummy<br>Time: 8 min 50 s |

| Temperature (°C) | etch rate $Si_xN_y$ (nm/min) | etch rate $SiO_2$ (nm/min) |
|---|---|---|
| 180 | 4.1 | 0.48 |
| 160 | 1.4 | 0.16 |
| 140 | 0.5 | 0.05 |

| Step | Process | Comment |
|---|---|---|
| 24 | **SEM Inspection**<br>JEOL 5610 | Inspect bottom<br>nitride profile |
| 25 | **Surface profile measurement**<br>Veeco Dektak 8 | Thickness bottom<br>nitride + TEOS |

Table C.1 Process steps (continued)

| Step | Process | Comment |
|---|---|---|
| 26 | **Plasma etching of Si – chamber cleaning**<br>Adixen SE | |
| 27 | **Plasma etching of Si: C-Cryo-$SF_6$**<br>Adixen SE<br>Application: Etching of deep trenches<br>**Note:** The gas flow is optimised for the mask | Etch depth 10 µm (device layer)<br>Time: 4 min 35 s |
| 28 | **Surface profile measurement**<br>Veeco Dektak 8 | |
| 29 | **Etching HF (1%) Native Oxide**<br>HF (1%) VLSI: MERCK 112629.500<br>• Quick Dump Rinse < 0.1 µS<br>• Spin drying | Time: 5 min |

Step 26 parameters:

| Parameters | Etch |
|---|---|
| Gas | $O_2$ |
| Flow (sccm) | 200 |
| Time (min) | 10 |
| Priority | nvt |
| APC (%) | 100 |
| ICP (Watt) | 2000 |
| CCP (Watt [LF]) | 0 |
| Pulsed - LF (msec) | off |
| He (mBar) | 10 |
| SH (mm) | 110 |
| Electrode temp. (°C) | −100 °C |

Step 27 parameters:

| Parameters | Etch |
|---|---|
| Gas $SF_6$ (sccm) | 100 |
| Gas $O_2$ (sccm) | 12 |
| ICP (Watt) | 500 |
| CCP (Watt [pulsed LF]) | 20 |
| on/off (msec) | 20/80 |
| SH (mm) | 200 |
| APC (%) | 100 |
| He (mBar) | 10 |
| Electrode temp. (°C) | -100 |

Table C.1 Process steps (continued)

| Step | Process | Comment |
|---|---|---|
| 30 | **Standard cleaning**<br>$HNO_3$ (100%) Selectipur: MERCK<br>$HNO_3$ (69%) VLSI: MERCK<br>• Beaker 1: fumic $HNO_3$ (100%), 5 min<br>• Beaker 2: fumic $HNO_3$ (100%), 5 min<br>• Quick Dump Rinse < 0.1 µS<br>• Beaker 3: 95 °C $HNO_3$ (69%), 10 min<br>• Quick Dump Rinse < 0.1 µS<br>• Spin drying | |
| 31 | **Dry Oxidation of Silicon**<br>Standby temp.: 700 °C<br>• Temp.: 950 °C<br>• Gas: $O_2$ | Time: 5 hr |
| 32 | **Ellipsometer Measurement**<br>Plasmos Ellipsometer | Use dummies |
| 33 | **Standard cleaning**<br>$HNO_3$ (100%) Selectipur: MERCK<br>$HNO_3$ (69%) VLSI: MERCK<br>• Beaker 1: fumic $HNO_3$ (100%), 5 min<br>• Beaker 2: fumic $HNO_3$ (100%), 5 min<br>• Quick Dump Rinse < 0.1 µS<br>• Beaker 3: 95 °C $HNO_3$ (69%), 10 min<br>• Quick Dump Rinse < 0.1 µS<br>• Spin drying | |
| 34 | **Etching HF (1%) Native Oxide**<br>HF (1%) VLSI: MERCK 112629.500<br>• Etch time: > 1 min<br>• Quick Dump Rinse < 0.1 µS<br>• Spin drying | |
| 35 | **Etching of SiN (Hot $H_3PO_4$)**<br>$H_3PO_4$ 85% Merck VLSI 1.00568.2500<br>• Temp.: 180 °C<br>• Quick Dump Rinse < 0.1 µS<br>• Spin drying<br>Etchrate SiRN: 3.5 nm $min^{-1}$ | Time: 12 min 30 s |
| 36 | **Optical microscopic inspection**<br>Olympus Microscope | |

Table C.1 Process steps (continued)

| Step | Process | Comment |
|---|---|---|
| 37 | **Standard cleaning**<br>$HNO_3$ (100%) Selectipur: MERCK<br>$HNO_3$ (69%) VLSI: MERCK<br>• Beaker 1: fumic $HNO_3$ (100%), 5 min<br>• Beaker 2: fumic $HNO_3$ (100%), 5 min<br>• Quick Dump Rinse < 0.1 µS<br>• Beaker 3: 95 °C $HNO_3$ (69%), 10 min<br>• Quick Dump Rinse < 0.1 µS<br>• Spin drying | |
| 38 | **Etching HF (1%) Native Oxide**<br>HF (1%) VLSI: MERCK 112629.500<br>• Etch time: > 1 min<br>• Quick Dump Rinse < 0.1 µS<br>• Spin drying | |
| 39 | **Etching of Silicon by KOH – standard**<br>KOH: MERCK 105019.500<br>KOH:DI = (1:3)<br>25 wt% KOH: 500 g KOH pellets<br>in 1500 ml DI water<br>• Temp.: 75 °C<br>• Stirrer<br>• Quick Dump Rinse <0.1 µS<br>• Spin drying<br>SiRN < 0.6 nm $hr^{-1}$ | 5 min |
| 40 | **Cleaning RCA-2 (HCL/$H_2O_2$/$H_2O$)**<br>HCL (36%) Selectipur, BASF<br>$H_2O_2$ (31%) VLSI, BASF<br>HCL:$H_2O_2$:$H_2O$ (1:1:5) vol%<br>• add HCL to $H_2O$<br>• add $H_2O_2$ when mixture at 70 °C<br>• temperature 70-80 °C<br>• cleaning time 10-15 min<br>• Quick Dump Rinse < 0.1 µS<br>• Spin drying | |
| 41 | **Surface profile measurement**<br>Veeco Dektak 8 | |

Table C.1 Process steps (continued)

| Step | Process | Comment |
|---|---|---|
| 42 | **SEM Inspection**<br>JEOL 5610 | inspect bottom nitride profile |
| 43 | **Etching HF (1%)**<br>HF (1%) VLSI: MERCK 112629.500<br>• Quick Dump Rinse < 0.1 µS<br>• Spin drying | Remove $SiO_2$<br>Time: 30 min |
| 44 | **Standard cleaning**<br>$HNO_3$ (100%) Selectipur: MERCK<br>$HNO_3$ (69%) VLSI: MERCK<br>• Beaker 1: fumic $HNO_3$ (100%), 5 min<br>• Beaker 2: fumic $HNO_3$ (100%), 5 min<br>• Quick Dump Rinse < 0.1 µS<br>• Beaker 3: 95 °C $HNO_3$ (69%), 10 min<br>• Quick Dump Rinse < 0.1 µS<br>• Spin drying | |
| 45 | **Dry Oxidation of Silicon**<br>Standby temperature: 700 °C<br>Temperature: 950 °C<br>Gas: $O_2$ | Sharpening + protection<br>Time: 5 hrs |
| 46 | **Lithography – Olin 908-35**<br>Suss Micro Tech Spinner (Delta 20)<br>Hotplate 120 °C:<br>• Dehydration bake (120 °C): 5 min<br>HexaMethylDiSilazane (HMDS):<br>• Spin program: 4 (4000 rpm, 20 s)<br>Olin 908-35:<br>• Spin program: 4 (4000 rpm, 20 s)<br>• Prebake (95 °C): 120 s<br>Electronic Vision Group 620 Mask Aligner:<br>• Hg-lamp: 12 mW $cm^{-2}$<br>• Exposure Time: 9 s<br>• After Exposure Bake (120 °C): 60 s<br>Developer OPD4262:<br>• Time: 30 s in Beaker 1<br>• Time: 15-30 s in Beaker 2<br>• Quick Dump Rinse <0.1 µS<br>• Spin drying | Back side mask hard contact |

Table C.1 Process steps (continued)

| Step | Process | Comment |
|---|---|---|
| 47 | **Lithography – Postbake**<br>Hotplate 120 °C<br>• Time: 60 min | |
| 48 | **Front side protection**<br>DuPont MX5000 20 µm thick<br>Laminator settings:<br>Temperature: 90 °C<br>Speed: 2 | |
| 49 | **Plasma etching of Si – chamber cleaning**<br>Adixen SE | |
| 50 | **Plasma etching of Si: Twin-3 BOX**<br>Adixen SE | etch oxide (500 nm)<br>Time: 2 min 30 s |

Step 49:

| Parameters | Etch |
|---|---|
| Gas | O2 |
| Flow (sccm) | 200 |
| Time (min) | 10 |
| Priority | nvt |
| APC (%) | 100 |
| ICP (Watt) | 2000 |
| CCP (Watt [LF]) | 0 |
| Pulsed - LF (msec) | off |
| He (mBar) | 10 |
| SH (mm) | 110 |
| Electrode temp. (°C) | −40 °C |

Step 50:

| Parameters | Value |
|---|---|
| Flow $CHF_3$ (sccm) | 100 |
| Flow Ar (sccm) | 100 |
| $V_{DC}$ (V) | 560 |
| APC (%) | 100 |
| ICP (Watt) | 1200 |
| CCP (Watt) | 150 |
| Electrode temp. | −40 °C |
| He (mbar) | 10 |
| SH (mm) | 200 |

Table C.1 Process steps (continued)

| Step | Process | Comment |
|---|---|---|
| 51 | **Plasma etching of Si: A-pulsed-$C_4F_8$**<br>Adixen SE<br><table><tr><th>Parameters</th><th>Etch</th><th>Deposition (pulsed)</th></tr><tr><td>Gas</td><td>$SF_6$</td><td>$C_4F_8$</td></tr><tr><td>Flow (sccm)</td><td>400</td><td>25</td></tr><tr><td>Time (sec)</td><td>4</td><td>0.5</td></tr><tr><td>Priority</td><td>2</td><td>1</td></tr><tr><td>APC (%)</td><td>15</td><td>15</td></tr><tr><td>ICP (Watt)</td><td>2500</td><td>2500</td></tr><tr><td>CCP (Watt)</td><td>nvt</td><td>20</td></tr><tr><td>Pulsed (msec)</td><td>nvt</td><td>20 on/180 off</td></tr><tr><td>SH (mm)</td><td>110</td><td>110</td></tr><tr><td>Electrode temp.</td><td>−40 °C</td><td>−40 °C</td></tr><tr><td>He (mbar)</td><td>10</td><td>10</td></tr></table> | Etch 380 μm<br>Time: 32 min |
| 52 | **Strip PR by oxygen plasma Tepla 300**<br>Barrel Etcher (2.45 GHz)<br>Ultra clean system only (no metals except Al)<br>• $O_2$ flow: 200 sccm (50%)<br>• Power: up to 1000 W<br>• Pressure: 1 mbar<br>• Time: see recipes on the wall | Time: 60 min |
| 53 | **Vapor HF etching of $SiO_2$**<br>Idonius Vapor HF Tool<br>• Temperature: 25 °C | Time: 3 min |

# Bibliography


Abelmann L, Bolhuis T, Hoexum A M, Krijnen G J M, Lodder J C, 2003
"Large capacity probe recording using storage robots"
*IEE Proceedings-Science Measurement and Technology* **150**, pp. 218–221, doi:10.1049/ip-smt:20030693

Albrecht T R, Akamine S, Carver T E, Quate C F, 1990
"Microfabrication of cantilever styli for the atomic force microscope"
*J. Vac. Sci. Technol., A* **8**, pp. 3386–3396

Alexander S, Hellemans L, Marti O, Schneir J, Elings V, Hansma P K, Longmire M, Gurley J, 1989
"An atomic-resolution atomic-force microscope implemented using an optical lever"
*J. Appl. Phys.* **65**, pp. 164–167, doi:10.1063/1.342563

Alvarez M, Tamayo J, 2005
"Optical sequential readout of microcantilever arrays for biological detection"
*Sens. Actuators B* **106**, pp. 687–690, doi:10.1016/j.snb.2004.09.016

Aziz M M, Wright C D, 2005
"A slope-theory approach to electrical probe recording on phase-change media"
*J. Appl. Phys.* **97**, p. 103537, doi:10.1063/1.1904156

Baller M K, Lang H P, Fritz J, Gerber Ch, Gimzewski J K, Drechsler U, Rothuizen H, Despont M, Vettiger P, Battiston F M, Ramseyer J P, Fornaro P, Meyer E, Guntherodt H J, 2000
"A cantilever array-based artificial nose"
*Ultramicroscopy* **82**, pp. 1–9, doi:10.1016/S0304-3991(99)00123-0

Bao H, Li X, 2008
"A heater-integrated scanning probe microscopy probe array with different tip radii for study of micro-nanosize effects on silicon-tip/polymer-film friction"
*Rev. Sci. Instrum.* **79**, p. 033701, doi:10.1063/1.2885682

Bauschlicher Jr C W, So C R, 2001
"Using hydrogen and chlorine on Si(111) to store data"
*Chem. Phys. Lett.* **333**, pp. 1–5, doi:10.1016/S0009-2614(00)01340-3

Bennewitz R, Crain J N, Kirakosian A, Lin J L, McChesney J L, Petrovykh D Y, Himpsel F J, 2002
"Atomic scale memory at a silicon surface"
*Nanotechnol.* **13**, pp. 499–502, doi:10.1088/0957-4484/13/4/312

Bhaskaran H, Sebastian A, Despont M, 2009*a*
"Nanoscale PtSi tips for conducting probe technologies"
*IEEE Trans. Nanotechnol.* **8**, pp. 128–131, doi:10.1109/TNANO.2008.2005199

Bhaskaran H, Sebastian A, Drechsler U, Despont M, 2009*b*
"Encapsulated tips for reliable nanoscale conduction in scanning probe technologies"
*Nanotechnol.* **20**, p. 105701, doi:10.1088/0957-4484/20/10/105701

Bhaskaran H, Sebastian A, Pauza A, Pozidis H, Despont M, 2009*c*
"Nanoscale phase transformation in $Ge_2Sb_2Te_5$ using encapsulated scanning probes and retraction force microscopy"
*Rev. Sci. Instrum.* **80**, p. 083701, doi:10.1063/1.3204449

Bhaskaran H, Sebastian A, Pauza A, Wang L, Wright C D, Despont M, Pozidis H, Eleftheriou E, 2009*d*
"Recent advances in conduction mode scanning probes for phase change probe storage applications"
In: *E*PCOS2009 Proceedings*,

Bichet O, Wright C D, Samson Y, Gidon S, 2004
"Local characterization and transformation of phase-change media by scanning thermal probes"
*J. Appl. Phys.* **95**, pp. 2360–2364, doi:10.1063/1.1644899

Binnig G, Quate C F, Gerber Ch, 1986
"Atomic force microscope"
*Phys. Rev. Lett.* **56**, pp. 930–933, doi:10.1103/PhysRevLett.56.930

Binnig G, Despont M, Drechsler U, Häberle W, Lutwyche M, Vettiger P, Mamin H J, Chui B W, Kenny T W, 1999
"Ultrahigh-density atomic force microscopy data storage with erase capability"
*Appl. Phys. Lett.* **74**, pp. 1329–1331, doi:10.1063/1.123540

Van den Bos A, Heskamp I, Siekman M, Abelmann L, Lodder J C, 2002
"The canticlever: A dedicated probe for magnetic force microscopy"
*IEEE Trans. Magn.* **38**, pp. 2441–2443, doi:10.1109/TMAG.2002.803585

Brezna W, Smoliner J, 2008
"Investigation of contact-force dependent effects in conductive atomic force microscopy on Si and GaAs"
*J. Appl. Phys.* **104**, p. 044309, doi:10.1063/1.2964107

Brugger J, Buser R A, de Rooij N F, 1992
"Silicon cantilevers and tips for scanning force microscopy"
*Sens. Actuators A* **34**, pp. 193–200

Burr G W, Breitwisch M J, Franceschini M, Garetto D, Gopalakrishnan K, Jackson B, Kurdi B, Lam C, Lastras L A, Padilla A, Rajendran B, Raoux S, Shenoy R S, 2010
"Phase change memory technology"
*J. Vac. Sci. Technol. B* **28**, pp. 223–262, doi:10.1116/1.3301579

Bussmann E, Williams C C, 2004
"Sub-10 nm lateral spatial resolution in scanning capacitance microscopy achieved with solid platinum probes"
*Rev. Sci. Instrum.* **75**, pp. 422–425, doi:10.1063/1.1641161

Butt H J, Jaschke M, 1995
"Calculation of thermal noise in atomic force microscopy"
*Nanotechnol.* **6**, pp. 1–7, doi:10.1088/0957-4484/6/1/001

Cannara R J, Gotsmann B, Knoll A, Dürig U, 2008
"Thermo-mechanical probe storage at Mbps single-probe data rates and Tbit $\text{in}^{-2}$ densities"
*Nanotechnol.* **19**, p. 395305, doi:10.1088/0957-4484/19/39/395305

Chen F, Kam H, Markovic D, Liu T J K, Stojanovic V, Alon E, 2008
"Integrated circuit design with NEM relays"
In: *Int. Conf. on Computer-Aided Design (ICCAD)*, pp. 750–757, San Jose, CA, USA, doi:10.1109/ICCAD.2008.4681660

Chen L, Lee H, Guo Z J, McGruer N E, Gilbert K W, Mall S, Leedy K D, Adams G G, 2007
"Contact resistance study of noble metals and alloy films using a scanning probe microscope test station"
*J. Appl. Phys.* **102**, p. 074910, doi:10.1063/1.2785951

Cho Y, Fujimoto K, Hiranaga Y, Wagatsuma Y, Onoe A, Terabe K, Kitamura K, 2002
"Tbit/inch$^2$ ferroelectric data storage based on scanning nonlinear dielectric microscopy"
*Appl. Phys. Lett.* **81**, pp. 4401–4403, doi:10.1063/1.1526916

Cho Y, Fujimoto K, Hiranaga Y, Wagatsuma Y, Onoe A, Terabe K, Kitamura K, 2003*a*
"Tbit/inch$^2$ data storage using scanning nonlinear dielectric microscopy"
*Ferroelectrics* **292**, pp. 51–58, doi:10.1080/00150190390222817

Cho Y, Fujimoto K, Hiranaga Y, Wagatsuma Y, Onoe A, Terabe K, Kitamura K, 2003*b*
"Terabit inch$^{-2}$ ferroelectric data storage using scanning nonlinear dielectric microscopy nanodomain engineering system"
*Nanotechnol.* **14**, pp. 637–642, doi:10.1088/0957-4484/14/6/314

Cho Y, Hiranaga Y, Fujimoto K, Wagatsuma Y, Onoe A, 2004
"Fundamental study on ferroelectric data storage with the density above 1 Tbit/inch$^2$ using congruent lithium tantalate"
*Integrated Ferroelectrics* **61**, pp. 77–81, doi:10.1080/10584580490458810

Cho Y, Hashimoto S, Odagawa N, Tanaka K, Hiranaga Y, 2005
"Realization of 10 Tbit/in$^2$ memory density and subnanosecond domain switching time in ferroelectric data storage"
*Appl. Phys. Lett.* **87**, pp. 232907–1, doi:10.1063/1.2140894

Cho Y, Hashimoto S, Odagawa N, Tanaka K, Hiranaga Y, 2006
"Nanodomain manipulation for ultrahigh density ferroelectric data storage"
*Nanotechnol.* **17**, pp. S137–S141, doi:10.1088/0957-4484/17/7/S06

Chong N B, Yang J, Mou J, Guo G, 2005
"Thermo-mechanical data bit formation of small-sized microcantilever probe tip array"
In: *Proc. SPIE*, volume 5852 part I, pp. 270–275, Singapore, Singapore, doi:10.1117/12.621530

Cuberes M T, Schlittler R R, Gimzewski J K, 1996
"Room-temperature repositioning of individual $C_{60}$ molecules at Cu steps: operation of a molecular counting device"
*Appl. Phys. Lett.* **69**, pp. 3016–3018, doi:10.1063/1.116824

Despont M, Brugger J, Drechsler U, Durig U, Haberle W, Lutwyche M, Rothuizen H, Stutz R, Widmer R, Binnig G, Rohrer H, Vettiger P, 2000
"VLSI-NEMS chip for parallel AFM data storage"
*Sens. Actuators A* **80**, pp. 100–107, doi:10.1016/S0924-4247(99)00254-X

Despont M, Drechsler U, Yu R, Pogge H B, Vettiger P, 2004
"Wafer-scale microdevice transfer/interconnect: Its application in an AFM-based data-storage system"
*J. Microelectromech. Syst.* **13**, pp. 895–901, doi:10.1109/JMEMS.2004.835769

Drechsler U, Burer N, Despont M, Dürig U, Gotsmann B, Robin F, Vettiger P, 2003
"Cantilevers with nano-heaters for thermomechanical storage application"
*Microelectron. Eng.* **67-68**, pp. 397–404, doi:10.1016/S0167-9317(03)00095-9

Dürig U, 2005
"Fundamentals of micromechanical thermoelectric sensors"
*J. Appl. Phys.* **98**, p. 044906, doi:10.1063/1.2006968

Dürig U, Cross G, Despont M, Drechsler U, Häberle W, Lutwyche M I, Rothuizen H, Stutz R, Widmer R, Vettiger P, Binnig G K, King W P, Goodson K E, 2000
""Millipede" - an AFM data storage system at the frontier of nanotribology"
*Tribology Letters* **9**, pp. 25–32, doi:10.1023/A:1018844124754

Eigler D M, Schweizer E K, 1990
"Positioning single atoms with a scanning tunnelling microscope"
*Nature* **344**, pp. 524–526, doi:10.1038/344524a0

Engelen J B C, Delalande M, le Fèbre A J, Bolhuis T, Shimatsu T, Kikuchi N, Abelmann L, Lodder J C, 2010
"Thermally induced switching field distribution of a single CoPt dot in a large array"
*Nanotechnol.* **21**, p. 035703, doi:10.1088/0957-4484/21/3/035703

Favre M, Polesel-Maris J, Overstolz T, Niedermann P, Dasen S, Gruener G, Ischer R, Vettiger P, Liley M, Heinzelmann H, Meister A, 2011
"Parallel afm imaging and force spectroscopy using two-dimensional probe arrays for applications in cell biology"
*J. Mol. Recognit.* **24**, pp. 446–452, doi:10.1002/jmr.1119

Forrester M G, Ahner J W, Bedillion M D, Bedoya C, Bolten D G, Chang K C, De Gersem G, Hu S, Johns E C, Nassirou M, Palmer J, Roelofs A, Siegert M, Tamaru S, Vaithyanathan V, Zavaliche F, Zhao T, Zhao Y, 2009
"Charge-based scanning probe readback of nanometer-scale ferroelectric domain patterns at megahertz rates"
*Nanotechnol.* **20**, p. 225501, doi:10.1088/0957-4484/20/22/225501

Franke K, Besold J, Haessler W, Seegebarth C, 1994
"Modification and detection of domains on ferroelectric PZT films by scanning force microscopy"
*Surf. Sci.* **302**, pp. L283–L288, doi:10.1016/0039-6028(94)91089-8

Gemelli M, Abelmann L, Engelen J B C, Khatib M G, Koelmans W W, Zaboronski O, 2011
*Memory Mass Storage*, chapter Probe storage, pp. 99–168,
Springer-Verlag
ISBN 978-3-642-14751-7

Ghatnekar-Nilsson S, Graham J, Hull R, Montelius L, 2006
"Multi-frequency response from a designed array of micromechanical cantilevers fabricated using a focused ion beam"
*Nanotechnol.* **17**, pp. 5233–5237, doi:10.1088/0957-4484/17/20/031

Gidon S, Lemonnier O, Rolland B, Bichet O, Dressler C, Samson Y, 2004
"Electrical probe storage using joule heating in phase change media"
*Appl. Phys. Lett.* **85**, pp. 6392–6394, doi:10.1063/1.1834718

Gotoh T, Sugawara K, Tanaka K, 2004
"Minimal phase-change marks produced in amorphous $Ge_2Sb_2Te_5$ films"
*Jpn. J. Appl. Phys.* **43**, pp. L818–L821, doi:10.1143/JJAP.43.L818

Gotsmann B, Lantz M A, 2008
"Atomistic wear in a single asperity sliding contact"
*Phys. Rev. Lett.* **101**, p. 125501, doi:10.1103/PhysRevLett.101.125501

Gotsmann B, Duerig U, Frommer J, Hawker C J, 2006*a*
"Exploiting chemical switching in a diels-alder polymer for nanoscale probe lithography and data storage"
*Adv. Funct. Mater.* **16**, pp. 1499–1505, doi:10.1002/adfm.200500724

Gotsmann B, Duerig U T, Sills S, Frommer J, Hawker C J, 2006*b*
"Controlling nanowear in a polymer by confining segmental relaxation"
*Nano Lett.* **6**, pp. 296–300, doi:10.1021/nl0520563

Hamann H F, O'Boyle M, Martin Y C, Rooks M, Wickramasinghe H K, 2006
"Ultra-high-density phase-change storage and memory"
*Nat. Mater.* **5**, pp. 383–387, doi:10.1038/nmat1627

Hecht E, 2002
*Optics*,
Addison-Wesley

Hidaka T, Maruyama T, Saitoh M, Mikoshiba N, Shimizu M, Shiosaki T, Wills L A, Hiskes R, Dicarolis S A, Amano J, 1996
"Formation and observation of 50 nm polarized domains in pbzr$_{1-x}$ti$_x$o3 thin film using scanning probe microscope"
*Appl. Phys. Lett.* **68**, pp. 2358–2359, doi:10.1063/1.115857

Hilbert M, López P, February 2011
"The world's technological capacity to store, communicate, and compute information"
*Science* doi:10.1126/science.1200970

Hiranaga Y, Fujimoto K, Cho Y, Wagatsuma Y, Onoe A, Terabe K, Kitamura K, 2002
"Nano-sized inverted domain formation in stoichiometric litao3 single crystal using scanning nonlinear dielectric microscopy"
*Integrated Ferroelectrics* **49**, pp. 203–209, doi:10.1080/10584580215489

Hiranaga Y, Cho Y, Fujimoto K, Wagatsuma Y, Onoe A, 2003
"Ultrahigh-density ferroelectric data storage using scanning nonlinear dielectric microscopy"
*Jpn. J. Appl. Phys., Part 1* **42**, pp. 6050–6054, doi:10.1143/JJAP.42.6050

Hiranaga Y, Fujimoto K, Tanaka K, Wagatsuma Y, Cho Y, 2007
"Study on SNDM ferroelectric probe memory"
*Record of Electrical and Communication Engineering Conversazione Tohoku University* **75**, pp. 107–110

Hiranaga Y, Uda T, Kurihashi Y, Tochishita H, Kadota M, Cho Y, 2009
"Nanodomain formation on ferroelectrics and development of hard-disk-drive-type ferroelectric data storage devices"
*Jpn. J. Appl. Phys.* **48**, pp. 09KA18–1–5, doi:10.1143/JJAP.48.09KA18

Hoffmann M, Bezzaoui H, Voges E, 1994
"Micromechanical cantilever resonators with integrated optical interrogation"
*Sens. Actuators A* **44**, pp. 71–75, doi:10.1016/0924-4247(94)00776-4

Ilic B, Czaplewski D, Craighead H G, Neuzil P, Campagnolo C, Batt C, 2000
"Mechanical resonant immunospecific biological detector"
*Appl. Phys. Lett.* **77**, pp. 450–452

Iwamura S, Nishida Y, Hashimoto K, 1981
"Rotating mnos disk memory device"
*IEEE Trans. Electron Devices* **28**, pp. 854–860

Jo A, Joo W, Jin W H, Nam H, Kim J, 2009
"Ultrahigh-density phase-change data storage without the use of heating"
*Nat. Nanotechnol.* **4**, pp. 727–731, doi:10.1038/nnano.2009.260

John N S, Kulkarni G U, 2005
"Gold-coated conducting-atomic force microscopy probes"
*J. Nanosci. Nanotechnol.* **5**, pp. 587–591, doi:10.1166/jnn.2005.066

Kado H, Tohda T, 1997
"Nanometer-scale erasable recording using atomic force microscope on phase change media"
*Jpn. J. Appl. Phys., Part 1* **36**, pp. 523–525

Kim B H, Maute M, Prins F E, Kern D P, Croitoru M, Raible S, Weimar U, Göpel W, 2000
"Parallel frequency readout of an array of mass-sensitive transducers for sensor applications"
*Microelectron. Eng.* **53**, pp. 229–232, doi:10.1016/S0167-9317(00)00303-8

Kim B H, Mader O, Weimar U, Brock R, Kern D P, 2003
"Detection of antibody peptide interaction using microcantilevers as surface stress sensors"
*J. Vac. Sci. Technol. B* **21**, pp. 1472–1475

Kim B M, Adams D E, Tran Q, Ma Q, Rao V, 2009
"Scanning probe charge reading of ferroelectric domains"
*Appl. Phys. Lett.* **94**, p. 063105, doi:10.1063/1.3081020

Kim Y, Cho Y, Hong S, Buhlmann S, Park H, Min D K, Kim S H, No K, 2006*a*
"Correlation between grain size and domain size distributions in ferroelectric media for probe storage applications"
*Appl. Phys. Lett.* **89**, p. 162907, doi:10.1063/1.2363942

Kim Y S, Sunyong Lee C, Jin W H, Jang S, Nam H J, Bu J U, 2005
"100×100 thermo-piezoelectric cantilever array for SPM nano-data-storage application"
*Sensors and Materials* **17**, pp. 57–63

Kim Y S, Nam H J, Jang S, Lee C S, Jin W H, Cho I J, Bu J U, Chang S I, Yoon E, 2006*b*
"Wafer-level transfer of thermo-piezoelectric $Si_3N_4$ cantilever array on a CMOS circuit for high density probe-based data storage"
In: *19th Int. Conf. on Micro Electro Mechanical Systems (MEMS 2006)*, pp. 922–925, Istanbul, Turkey, doi:10.1109/MEMSYS.2006.1627951

Kim Y S, Jang S, Lee C, Jin W H, Cho I J, Ha M H, Nam H J, Bu J U, Chang S I, Yoon E, 2007
"Thermo-piezoelectric $Si_3N_4$ cantilever array on CMOS circuit for high density probe-based data storage"
*Sens. Actuators A* **135**, pp. 67–72, doi:10.1016/j.sna.2006.10.021

King W P, Kenny T W, Goodson K E, Cross G, Despont M, Durig U, Rothuizen H, Binnig G K, Vettiger P, 2001
"Atomic force microscope cantilevers for combined thermomechanical data writing and reading"
*Appl. Phys. Lett.* **78**, pp. 1300–1302, doi:10.1063/1.1351846

King W P, Kenny T W, Goodson K E, Cross G L W, Despont M, Durig U T, Rothuizen H, Binnig G, Vettiger P, 2002
"Design of atomic force microscope cantilevers for combined thermomechanical writing and thermal reading in array operation"
*J. Microelectromech. Syst.* **11**, pp. 765–774, doi:10.1109/JMEMS.2002.803283

Knoll A, Rothuizen H, Gotsmann B, Duerig U, 2010
"Wear-less floating contact imaging of polymer surfaces"
*Nanotechnol.* **21**, p. 185701, doi:10.1088/0957-4484/21/18/185701

Kobayashi D, Mita Y, Shibata T, Bourouina T, Fujita H, 2004
"Batch bulk-micromachined high-precision metal-on-insulator microspires and their application to scanning tunneling microscopy"
*J. Micromech. Microeng.* **14**, pp. S76–S81

Koyama H, Oohira F, Hosogi M, Hashiguchi G, Hamada T, Suga K, 2007
"2D cantilever array SPM using optical interference"
pp. 2413–2416, Lyon, doi:10.1109/SENSOR.2007.4300657

Kügeler C, Nauenheim C, Meier M, Rüdiger A, Waser R, 2008
"Fast resistance switching of $TiO_2$ and MSQ thin films for non-volatile memory applications (RRAM)"
In: *9th Annual Non-Volatile Memory Tech. Symp. (NVMTS)*, pp. 1–6, Pacific Grove, CA, USA, doi:10.1109/NVMT.2008.4731195

Lang H P, Berger R, Andreoli C, Brugger J, Despont M, Vettiger P, Gerber Ch, Gimzewski J K, Ramseyer J P, Meyer E, Güntherodt H J, 1998
"Sequential position readout from arrays of micromechanical cantilever sensors"
*Appl. Phys. Lett.* **72**, pp. 383–385, doi:10.1063/1.120749

Lang H P, Baller M K, Berger R, Gerber C, Gimzewski J K, Battiston F M, Fornaro P, Ramseyer J P, Meyer E, Güntherodt H J, 1999
"An artificial nose based on a micromechanical cantilever array"
*Anal. Chim. Acta* **393**, pp. 59–65, doi:10.1016/S0003-2670(99)00283-4

Lang H P, Hegner M, Gerber Ch, 2005
"Cantilever array sensors"
*Mater. Today* **8**, pp. 30–36, doi:10.1016/S1369-7021(05)00792-3

Lang H P, Ramseyer J P, Grange W, Braun T, Schmid D, Hunziker P, Jung C, Hegner M, Gerber Ch, 2007
"An artificial nose based on microcantilever array sensors"
*J. Phys. Conf. Ser.* **61**, pp. 663–667, doi:10.1088/1742-6596/61/1/133

Lantz M A, Gotsmann B, Dürig U T, Vettiger P, Nakayama Y, Shimizu T, Tokumoto H, 2003
"Carbon nanotube tips for thermomechanical data storage"
*Appl. Phys. Lett.* **83**, pp. 1266–1268, doi:10.1063/1.1600835

Lantz M A, Wiesmann D, Gotsmann B, 2009
"Dynamic superlubricity and the elimination of wear on the nanoscale"
*Nat. Nanotechnol.* **4**, pp. 586–591, doi:10.1038/nnano.2009.199

Lee C S, Nam H J, Kim Y S, Jin W H, Cho S M, uk Bu J, 2003
"Microcantilevers integrated with heaters and piezoelectric detectors for nano data-storage application"
*Appl. Phys. Lett.* **83**, pp. 4839–4841, doi:10.1063/1.1633009

Lee D W, Ono T, Esashi M, 2002
"Electrical and thermal recording techniques using a heater integrated microprobe"
*J. Micromech. Microeng.* **12**, pp. 841–848, doi:10.1088/0960-1317/12/6/315

Lee T H, Bhunia S, Mehregany M, 2010
"Electromechanical computing at 500°c with silicon carbide"
*Science* **329**, pp. 1316–1318, doi:10.1126/science.1192511

Loth S, Etzkorn M, Lutz C P, Eigler D M, Heinrich A J, 2010
"Measurement of fast electron spin relaxation times with atomic resolution"
*Science* **329**, pp. 1628–1630, doi:10.1126/science.1191688

Lutwyche M, Andreoli C, Binnig G, Brugger J, Drechsler U, Haberle W, Rohrer H, Rothuizen H, Vettiger P, Yaralioglu G, Quate C, 1999
"5×5 2D AFM cantilever arrays a first step towards a terabit storage device"
*Sens. Actuators A* **73**, pp. 89–94, doi:10.1016/S0924-4247(98)00259-3

Lutwyche M I, Despont M, Drechsler U, Dürig U, Häberle W, Rothuizen H, Stutz R, Widmer R, Binnig G K, Vettiger P, 2000
"Highly parallel data storage system based on scanning probe arrays"
*Appl. Phys. Lett.* **77**, pp. 3299–3301, doi:10.1063/1.1326486

Mamin H J, Rugar D, 1992
"Thermomechanical writing with an atomic force microscope tip"
*Appl. Phys. Lett.* **61**, pp. 1003–1005, doi:10.1063/1.108460

Mamin H J, Ganz E, Abraham D W, Thomson R E, Clarke J, 1986
"Contamination-mediated deformation of graphite by the scanning tunneling microscope"
*Phys. Rev. B* **34**, pp. 9015–9018, doi:10.1103/PhysRevB.34.9015

Mamin H J, Terris B D, Fan L S, Hoen S, Barrett R C, Rugar D, 1995
"High-density data storage using proximal probe techniques"
*IBM J. Res. Dev.* **39**, pp. 681–699, doi:10.1147/rd.396.0681

Mamin H J, Ried R P, Terris B D, Rugar D, 1999
"High-density data storage based on the atomic force microscope"
*Proc. IEEE* **87**, pp. 1014–1027, doi:10.1109/5.763314

Manalis S R, Minne S C, Atalar A, Quate C F, 1996
"Interdigital cantilevers for atomic force microscopy"
*Appl. Phys. Lett.* **69**, pp. 3944–3946

Maruyama T, Saitoh M, Sakai I, Hidaka T, Yano Y, Noguchi T, 1998
"Growth and characterization of 10-nm-thick c-axis oriented epitaxial $PbZr_{0.25}Ti_{0.75}O3$ thin films on (100)Si substrate"
*Appl. Phys. Lett.* **73**, pp. 3524–3526, doi:10.1063/1.122824

Mate C M, Erlandsson R, McClelland G M, Chiang S, 1989
"Direct measurement of forces during scanning tunneling microscope imaging of graphite"
*Surf. Sci.* **208**, pp. 473–486

Maute M, Raible S, Prins F E, Kern D P, Weimar U, Göpel W, 1999
"Fabrication and application of polymer coated cantilevers as gas sensors"
*Microelectron. Eng.* **46**, pp. 439–442, doi:10.1016/S0167-9317(99)00128-8

Meepagala S C, Real F, Reyes C B, 1991
"Tip-sample interaction forces in scanning tunneling microscopy - effects of contaminants"
*J. Vac. Sci. Technol. B* **9**, pp. 1340–1342

Mertens J, Alvarez M, Tamayo J, 2005
"Real-time profile of microcantilevers for sensing applications"
*Appl. Phys. Lett.* **87**, p. 234102

Meyer G, Amer N M, 1988*a*
"Erratum: Novel optical approach to atomic force microscopy [appl. phys. lett. 53, 1045 (1988)]"
*Appl. Phys. Lett.* **53**, pp. 2400–2402, doi:10.1063/1.100425

Meyer G, Amer N M, 1988*b*
"Novel optical approach to atomic force microscopy"
*Appl. Phys. Lett.* **53**, pp. 1045–1047, doi:10.1063/1.100061

Millipede, 2005
"'Millipede' small scale MEMS prototype shown at CeBIT"
URL `http://www.physorg.com/news3361.html`
(accessed 3 Mar. 2011)

Moreland J, Russek S E, Hopkins P F, 1997
"Surface potential imaging for magnetoresistive head development"
*IEEE Trans. Magn.* **33**, pp. 4068–4070

Morita S, Ishizaka T, Sugawara Y, Okada T, Mishima S, Imai S, Mikoshiba N, 1989
"Surface conductance of metal surfaces in air studied with a force microscope"
*Jpn. J. Appl. Phys., Part 1* **28**, pp. 1634–1636

Naberhuis S, 2002
"Probe-based recording technology"
*J. Magn. Magn. Mater.* **249**, pp. 447–451, doi:10.1016/S0304-8853(02)00459-6

Nam H J, Kim Y S, Lee C S, Jin W H, Jang S S, Cho I J, Bu J U, Choi W B, Choi S W, 2007
"Silicon nitride cantilever array integrated with silicon heaters and piezoelectric detectors for probe-based data storage"
*Sens. Actuators A* **134**, pp. 329–333, doi:10.1016/j.sna.2006.05.030

Nicolau D V, 2004
"Simulation of the chemical storage of data via metal-ligand chelation"
*Current Applied Physics* **4**, pp. 312–315

Nishimura T, Iyoki M, Sadayama S, 2002
"Observation of recording pits on phase-change film using a scanning probe microscope"
*Ultramicroscopy* **91**, pp. 119–126, doi:10.1016/S0304-3991(02)00090-6

Oliver R A, 2008
"Advances in AFM for the electrical characterization of semiconductors"
*Rep. Prog. Phys.* **71**, p. 076501, doi:10.1088/0034-4885/71/7/076501

Pantazi A, Sebastian A, Antonakopoulos T A, Bächtold P, Bonaccio A R, Bonan J, Cherubini G, Despont M, DiPietro R A, Drechsler U, Dürig U, Gotsmann B, Häberle W, Hagleitner C, Hedrick J L, Jubin D, Knoll A, Lantz M A, Pentarakis J, Pozidis H, Pratt R C, Rothuizen H E, Stutz R, Varsamou M, Weismann D, Eleftheriou E, 2008
"Probe-based ultrahigh-density storage technology"
*IBM J. Res. Dev.* **52**, pp. 493–511, doi:10.1147/rd.524.0493

Pertsev N A, Rodriguez Contreras J, Kukhar V G, Hermanns B, Kohlstedt H, Waser R, 2003
"Coercive field of ultrathin $Pb(Zr_{0.52}Ti_{0.48})O_3$ epitaxial films"
*Appl. Phys. Lett.* **83**, pp. 3356–3358, doi:10.1063/1.1621731

Petersen K E, 1982
"Silicon as a mechanical material"
*Proc. IEEE* **70**, pp. 420–457

Pires D, Gotsmann B, Porro F, Wiesmann D, Duerig U, Knoll A, 2009
"Ultraflat templated polymer surfaces"
*Langmuir* **25**, pp. 5141–5145, doi:10.1021/la804191m

Pozidis H, Häberle W, Wiesmann D, Drechsler U, Despont M, Albrecht T R, Eleftheriou E, 2004
"Demonstration of thermomechanical recording at 641 Gbit/in$^2$"
*IEEE Trans. Magn.* **40**, pp. 2531–2536, doi:10.1109/TMAG.2004.830470

Radmacher M, Tillmann R W, Fritz M, Gaub H E, 1992
"From molecules to cells: Imaging soft samples with the atomic force microscope"
*Science* **257**, pp. 1900–1905

Repp J, Meyer G, Olsson F E, Persson M, 2004
"Controlling the charge state of individual gold adatoms"
*Science* **305**, pp. 493–495, doi:10.1126/science.1099557

Rosi M, Bauschlicher Jr C W, 2001
"Using hydrogen and chlorine on Si(1 1 1) to store data, an improved model"
*Chem. Phys. Lett.* **347**, pp. 291–296, doi:10.1016/S0009-2614(01)01060-0

Rothuizen H, Despont M, Drechsler U, Hagleitner C, Sebastian A, Wiesmann D, 2009
"Design of power-optimized thermal cantilevers for scanning probe topography sensing"
In: *22nd IEEE International Conference on Micro Electro Mechanical Systems, MEMS 2009*, pp. 603–606, Sorrento, doi:10.1109/MEMSYS.2009.4805454

Sache L, Kawakatsu H, Emery Y, Bleuler H, 2007
"Massively parallel atomic force microscope with digital holographic readout"
*J. Phys. Conf. Ser.* **61**, pp. 668–672, doi:10.1088/1742-6596/61/1/134

Sahoo D R, Haberle W, Bachtold P, Sebastian A, Pozidis H, Eleftheriou E, 2008
"On intermittent-contact mode sensing using electrostatically-actuated micro-cantilevers with integrated thermal sensors"
In: *2008 American Control Conference, ACC*, pp. 2034–2039, Seattle, WA, doi:10.1109/ACC.2008.4586792

Sarid D, 1991
*Scanning force microscopy*,
Oxford University Press

Satoh H, Sugawara K, Tanaka K, 2006
"Nanoscale phase changes in crystalline $Ge_2Sb_2Te_5$ films using scanning probe microscopes"
*J. Appl. Phys.* **99**, pp. 1–7, doi:10.1063/1.2163010

Saurenbach F, Terris B D, 1990
"Imaging of ferroelectric domain walls by force microscopy"
*Appl. Phys. Lett.* **56**, pp. 1703–1705, doi:10.1063/1.103122

Saurenbach F, Terris B D, 1992
"Electrostatic writing and imaging using a force microscope"
*IEEE Trans. Ind. Appl.* **28**, pp. 256–260, doi:10.1109/28.120239

Sebastian A, Wiesmann D, 2008
"Modeling and experimental identification of silicon microheater dynamics: A systems approach"
*J. Microelectromech. Syst.* **17**, pp. 911–920, doi:10.1109/JMEMS.2008.926980

Sebastian A, Salapaka M V, Chen D J, Cleveland J P, 2001
"Harmonic and power balance tools for tapping-mode atomic force microscope"
*J. Appl. Phys.* **89**, pp. 6473–6480, doi:10.1063/1.1365440

Sebastian A, Pantazi A, Pozidis H, Eleftheriou E, 2008
"Nanopositioning for probe-based data storage [applications of control]"
*IEEE Control Syst. Mag.* **28**, pp. 26–35, doi:10.1109/MCS.2008.924795

Sebastian A, Wiesmann D, Baechtold P, Rothuizen H, Despont M, Drechsler U, 2009
"Feedback enhanced thermo-electric topography sensing"
In: *Proc. 15th Int. Conf. on Solid-State Sensors, Actuators and Microsystems (Transducers '09)*, pp. 1963–1966, Denver, CO, doi:10.1109/SENSOR.2009.5285675

Sebastian A, Pauza A, Rossel C, Shelby R M, Rodriguez A F, Pozidis H, Eleftheriou E, 2011
"Resistance switching at the nanometre scale in amorphous carbon"
*New J. Phys.* **13**, p. 013020

Severi S, Heck J, Chou T K A, Belov N, Park J S, Harrar D, Jain A, Hoof R V, Bois B D, Coster J D, Pedreira O V, Willegems M, Vaes J, Jamieson G, Haspeslagh L, Adams D, Rao V, Decoutere S, Witvrouw A, 2009
"CMOS-integrated poly-SiGe cantilevers with read/write system for probe storage device"
In: *Int. Solid-State Sensors, Actuators and Microsystems Conf. (TRANSDUCERS 2009)*, Denver, CO, USA, doi:10.1109/SENSOR.2009.5285430

Shin H, Lee K M, Moon W K, Jeon J U, Lim G, Pak Y E, Park J H, Yoon K H, 2000
"Application of polarized domains in ferroelectric thin films using scanning probe microscope"
*IEEE Trans. Ultrason. Ferr. Freq. Control* **47**, pp. 801–807, doi:10.1109/58.852061

Stipe B C, Mamin H J, Stowe T D, Kenny T W, Rugar D, 2001
"Magnetic dissipation and fluctuations in individual nanomagnets measured by ultrasensitive cantilever magnetometry"
*Phys. Rev. Lett.* **86**, pp. 2874–2877, doi:10.1103/PhysRevLett.86.2874

Sulchek T, Grow R J, Yaralioglu G G, Minne S C, Quate C F, Manalis S R, Kiraz A, Aydine A, Atalar A, 2001
"Parallel atomic force microscopy with optical interferometric detection"
*Appl. Phys. Lett.* **78**, pp. 1787–1789, doi:10.1063/1.1352697

Takahashi H, Ono T, Cho Y, Esashi M, 2004
"Diamond probe for ultra-high-density ferroelectric data storage based on scanning nonlinear dielectric microscopy"
In: *Proceedings of the IEEE International Conference on Micro Electro Mechanical Systems (MEMS)*, pp. 536–539, Maastricht, Netherlands, doi:10.1109/MEMS.2004.1290640

Takahashi H, Ono T, Onoe A, Cho Y, Esashi M, 2006*a*
"A diamond-tip probe with silicon-based piezoresistive strain gauge for high-density data storage using scanning nonlinear dielectric microscopy"
*J. Micromech. Microeng.* **16**, pp. 1620–1624, doi:10.1088/0960-1317/16/8/025

Takahashi H, Onoe A, Ono T, Cho Y, Esashi M, 2006*b*
"High-density ferroelectric recording using diamond probe by scanning nonlinear dielectric microscopy"
*Jpn. J. Appl. Phys., Part 1* **45**, pp. 1530–1533, doi:10.1143/JJAP.45.1530

Takahashi H, Mimura Y, Mori S, Ishimori M, Onoe A, Ono T, Esashi M, 2007
"Multi-probe with metallic tips for ferroelectric recording probe storage"
In: *Int. Solid-State Sensors, Actuators and Microsystems Conf. (TRANSDUCERS 2007 & EUROSENSORS XXI)*, pp. 2509–2512, Lyon, France, doi:10.1109/SENSOR.2007.4300681

Takahashi H, Mimura Y, Mori S, Ishimori M, Onoe A, Ono T, Esashi M, 2009
"The fabrication of metallic tips with a silicon cantilever for probe-based ferroelectric data storage and their durability experiments"
*Nanotechnol.* **20**, p. 362501, doi:10.1088/0957-4484/20/36/365201

Tanaka K, Cho Y, 2010
"Actual information storage with a recording density of 4 Tbit/in$^2$ in a ferroelectric recording medium"
*Appl. Phys. Lett.* **97**, p. 092901, doi:10.1063/1.3463470

Tanaka K, Hiranaga Y, Cho Y, 2008*a*
"Study of servo tracking technique for ferroelectric data storage system"
*Record of Electrical and Communication Engineering Conversazione Tohoku University* **76**, pp. 384–385

Tanaka K, Kurihashi Y, Uda T, Daimon Y, Odagawa N, Hirose R, Hiranaga Y, Cho Y, 2008*b*
"Scanning nonlinear dielectric microscopy nano-science and technology for next generation high density ferroelectric data storage"
*Jpn. J. Appl. Phys.* **47**, pp. 3311–3325, doi:10.1143/JJAP.47.3311

Tayebi N, Narui Y, Chen R J, Collier C P, Giapis K P, Zhang Y, 2008
"Nanopencil as a wear-tolerant probe for ultrahigh density data storage"
*Appl. Phys. Lett.* **93**, p. 103112, doi:10.1063/1.2981641

Tayebi N, Narui Y, Franklin N, Collier C P, Giapis K P, Nishi Y, Zhang Y, 2010*a*
"Fully inverted single-digit nanometer domains in ferroelectric films"
*Appl Phys Lett* **96**, p. 023103, doi:10.1063/1.3280371

Tayebi N, Zhang Y, Chen R J, Tran Q, Chen R, Nishi Y, Ma Q, Rao V, 2010*b*
"An ultraclean tip-wear reduction scheme for ultrahigh density scanning probe-based data storage"
*ACS Nano* **4**, pp. 5713–5720, doi:10.1021/nn1013512

Thundat T, Finot E, Hu Z, Ritchie R H, Wu G, Majumdar A, 2000
"Chemical sensing in fourier space"
*Appl. Phys. Lett.* **77**, pp. 4061–4063

Tohda T, Kado H, 1995
"Ultra-high density recording on phase change material using an atomic force microscope"
*National Technical Report* **41**, pp. 31–36

Van Honschoten J, De Jong H W, Koelmans W W, Parnell T P, Zaboronski O V, 2011
"Information storage and retrieval for probe storage using optical diffraction patterns"
*Accepted for publication in J. Appl. Phys.* URL `http://arxiv.org/abs/1104.0871`

Vettiger P, Despont M, Drechsler U, Dürig U, Häberle W, Lutwyche M I, Rothuizen H E, Stutz R, Widmer R, Binnig G K, 2000
"'Millipede' - more than one thousand tips for future AFM data storage"
*IBM J. Res. Dev.* **44**, pp. 323–340, doi:10.1147/rd.443.0323

Vettiger P, Cross G, Despont M, Drechsler U, Dürig U, Gotsmann B, Häberle W, Lantz M A, Rothuizen H E, Stutz R, Binnig G K, 2002
"The "Millipede"—Nanotechnology entering data storage"
*IEEE Trans. Nanotechnol.* **1**, pp. 39–54, doi:10.1109/TNANO.2002.1005425

Wetnic W, Wuttig M, 2008
"Reversible switching in phase-change materials"
*Mater. Today* **11**, pp. 20–27, doi:10.1016/S1369-7021(08)70118-4

Wiesmann D, Rawlings C, Vecchione R, Porro F, Gotsmann B, Knoll A, Pires D, Duerig U, 2009
"Multi Tbit/in$^2$ storage densities with thermomechanical probes"
*Nano Lett.* **9**, pp. 3171–3176, doi:10.1021/nl9013666

Wright C D, Armand M, Aziz M M, Senkader S, Yu W, 2003
"Understanding the electro-thermal and phase-transformation processes in phase-change materials for data storage applications"
In: *Materials Research Society Symposium - Proceedings*, volume 803, pp. 61–72, Boston, MA, United States

Wright C D, Armand M, Aziz M M, 2006
"Terabit-per-square-inch data storage using phase-change media and scanning electrical nanoprobes"
*IEEE Trans. Nanotechnol.* **5**, pp. 50–61, doi:10.1109/TNANO.2005.861400

Wright C D, Armand M, Aziz M M, Bhaskaran H, Choo B C, Davies C, Despont M, Gidon S, M K, Lemonnier O, Maisse A, Pauza A, Salinga M, Sebastian A, Wang L, Wuttig M, 2008
"Scanning probe-based phase-change terabyte memories"
In: *Proceedings EPCOS 2008*,

Wright C D, Shah P, Wang L, Aziz M M, Sebastian A, Pozidis H, 2010
"Write strategies for multiterabit per square inch scanned-probe phase-change memories"
*Appl Phys Lett* **97**, p. 173104, doi:10.1063/1.3506584

Wuttig M, Yamada N, 2007
"Phase-change materials for rewriteable data storage"
*Nat. Mater.* **6**, pp. 824–832, doi:10.1038/nmat2009

Yang J P, Mou J Q, Chong N B, Lu Y, Zhu H, Jiang Q, Kim W G, Chen J, Guo G X, Ong E H, 2007
"Probe recording technology using novel MEMS devices"
*Microsyst. Technol.* **13**, pp. 733–740, doi:10.1007/s00542-006-0267-z

Yang Z, Yu Y, Li X, Bao H, 2006
"Nano-mechanical electro-thermal probe array used for high-density storage based on nems technology"
*Microelectronics Reliability* **46**, pp. 805–810, doi:10.1016/j.microrel.2005.07.117

Yaralioglu G G, Atalar A, Manalis S R, Quate C F, 1998
"Analysis and design of an interdigital cantilever as a displacement sensor"
*J. Appl. Phys.* **83**, pp. 7405–7415

Zhao Y, Johns E, Forrester M, 2008
"A MEMS read-write head for ferroelectric probe storage"
In: *Proc. MEMS 2008*, pp. 152 – 5, Tucson, AZ, USA, doi:10.1109/MEMSYS.2008.4443615

Zybill C E, Li B, Koch F, Graf T, 2000
"Substrate influence on the domain structure of (111) PZT $PbTi_{0.75}Zr_{0.25}O_3$ films"
*Physica Status Solidi (A) Applied Research* **177**, pp. 303–309, doi:10.1002/(SICI)1521-396X(200001)177:1<303::AID-PSSA303>3.0.CO;2-G

# Samenvatting

Dit proefschrift beschrijft technieken die zijn ontwikkeld om minuscule naaldjes (probes[*]) uit te lezen. We hebben met name gekeken naar nieuwe technieken om meerdere van deze probes tegelijk uit te lezen. Het hoofdzakelijk beoogde toepassingsgebied is dataopslag met parallelle probes. Het werk draagt ook bij aan andere toepassingsgebieden zoals metrologie, biologische sensoren, materiaalonderzoek en nano-electro-mechanische schakelaars.

Allereerst is een uitvoerige literatuurstudie gedaan die de huidige stand van het onderzoek naar dataopslag met probes beschrijft. Een uitkomst van de literatuurstudie is dat optische uitleestechnieken veel gebruikt worden in toepassingen die probes gebruiken, maar dat de zeer veeleisende applicatie dataopslag daar niet bij is. Het optisch uitlezen van probes biedt betrouwbaarheid, een hoge snelheid, een laag ruisniveau en is eenvoudig te implementeren. Optisch uitlezen moet echter geschikt gemaakt worden voor het uitlezen van meerdere probes tegelijk om succesvolle implementatie in dataopslag mogelijk te maken.

De eerste techniek, die ontwikkeld is in deze thesis, is uitlezing van meerdere probes met behulp van parallelle frequentie uitlezing. Elke probe bestaat uit een kleine bladveer (cantilever[†]). Adressering met meerdere frequenties maakt het mogelijk om de individuele nano-mechanische respons van elke cantilever te onderscheiden binnen het ontvangen signaal met slechts een enkel laser-diode paar. Het adresseren is gedaan door alle cantilevers aan te sturen met de som van de resonantiefrequenties van alle cantilevers. Deze techniek gebruikt aanzienlijk minder apparatuur dan andere technieken die parallel optisch uitlezen. Het uitlezen is gedemonstreerd in laserbundel-verschuivings modus en in interferentie modus. Een groot aantal cantilevers kan parallel worden uitgelezen, gelimiteerd door de kwaliteitsfactor van de oscillator en de beschikbare bandbreedte. De voorgestelde techniek faciliteert parallellisatie in toepassingen op de nanoschaal, inclusief dataopslag en biologische sensoren.

Een tweede techniek om parallelle optische uitlezing van probes te doen, maakt gebruikt van diffractiepatronen die het gevolg zijn van een laserbundel, die invalt op een rij van probes. De cantilevers vormen een optische tralie waarbij het diffractiepatroon bepaald wordt door de stand van de cantilevers. Het diffractiepatroon

[*] Een *probe* is letterlijk vertaald een sonde.

[†] Een *cantilever* is een eenzijdig ingeklemde balk, in dit geval gaat het over een balk op micro-schaal.

wordt door een rij van fotodiodes gemeten. Elke cantilever kan vergeleken worden met een enkele opening worden in een traditioneel tralie experiment, waarin licht wordt gebroken. In tegenstelling tot het tralie experiment, waarbij alle openingen beschouwd worden als lichtbronnen met gelijke fase, is in onze situatie defase verschuiving van het gereflecteerde licht een maat voor de doorbuiging van de cantilever. De ontwikkelde techniek is rechtstreeks toe te passen als twee discrete standen zijn toegestaan voor de cantilevers.

Een nieuwe methode is ontwikkeld om rijen van probes te maken met scherpe tips[‡], die vanzelf uitlijnen op de cantilever. De focus is gelegd op het maken van een rij die leidt tot een gelijke afstand tussen de tips en het oppervlak. Om dit te bereiken maken we gebruik van silicium-op-isolator (SOI) wafers en creëren we de tips met een zeer uniform chemisch etsproces. De gemaakte rijen van cantilevers zijn gekarakteriseerd en daaruit blijkt dat ze erg uniform zijn. Een rij van 10 cantilevers, met een reikwijdte van 430 μm, vertoont een standaard afwijking van slechts 11 nm in afstand tot het oppervlak. Verder laten we zien dat het mogelijk is om zowel de cantilevers als de tips met een enkel fotolithografisch masker te maken.

Het laatste deel van deze scriptie gaat over scanning probe microscopie met geleidende probes. Deze vorm van microscopie is een krachtig instrument om op nanoschaal elektrische eigenschappen te onderzoeken en aan te passen. Het toepassingsgebied omvat halfgeleider metrologie, dataopslag met parallelle probes en materiaalonderzoek. Geleidende probes kunnen ook gebruikt worden om elektrische contacten op de nanoschaal na te bootsen. Onbetrouwbare elektrische contacten en slijtage van de tip vormen echter een ernstige belemmering voor het wijdverbreide gebruik van geleidende probes. In dit werk introduceren we een kracht-modulatie techniek die resulteert in een lagere frictie, verminderde tip slijtage en een verhoogde kwaliteit van het elektrische contact. Experimentele resultaten met *phase change* materiaal en geleidende probes van platinum-silicide laten duidelijk de effectiviteit van deze techniek zien. De experimenten op een speciaal geprepareerd platinum/koolstof oppervlak demonstreren de uitgebreide toepassingsmogelijkheden van deze techniek.

[‡] Een *tip* is het uiteinde van een probe en heeft typische afmetingen van tientallen nanometers.

# Woord van dank

Beter de voltooiing van de dingen dan dat ze beginnen. En bij de voltooiing van dit 'ding' sta ik stil bij de mensen met wie ik opgetrokken heb tijdens mijn promotie. Sommigen waren direct betrokken bij het onderzoekswerk, anderen meer bij mijn persoonlijk leven. Uiteindelijk valt er in het eindresultaat moeilijk een scheiding te maken, omdat het één niet zonder het ander kan. Na een dag van mislukte experimenten is het heerlijk om stoom af te kunnen blazen met een potje voetbal of een 10 km op tempo. Een goed gesprek, een dag met familie of vrienden, een zeil- of bergtocht, en er is weer nieuwe energie om mysteriën op te lossen. Zo heeft alles en iedereen zijn bijdrage. Toch is veel hiervan – gelukkig – niet voorbehouden aan mijn promotietijd en begin ik daarom met woorden over hetgeen wel voorbehouden is aan het leven van een promovendus.

Daarvan is het allerbelangrijkste een begeleider. Een begeleider die ziet wat je kunt, maar daar geen genoegen mee neemt. Een begeleider die weet dat het product niet een proefschrift of een artikel is, maar een jonge doctor. Een begeleider die je continue uitdaagt, maar ook akkoord gaat met een "nee, nu even niet". Een begeleider die je laat worstelen, maar niet verdrinken. Kortom, een begeleider met de intentie om zijn leerling beter te laten worden dan hijzelf is – of dat lukt is een tweede. . . Leon, de reden dat ik op deze promotieplek solliciteerde, was dat jij mijn begeleider werd. Daar heb ik nooit spijt van gekregen. Dank je wel.

Mijn promotor, Miko Elwenspoek, ik heb altijd het gevoel gehad dat je vertrouwen had in een goede afloop van mijn promotie. Of het nu door mezelf kwam of door dat Leon mijn begeleider was, het heeft me geholpen. Je vragen naar de reden achter de dingen inspireren me. Je leert me om nog dieper te graven en naar de grotere verbanden te zoeken. Het '*Mic*ro *Mec*hanische' praatje over *dark energy* zal ik niet snel vergeten!

Ik dank van harte Harold Zandvliet, David Wright, Peter Vettiger, Urs Staufer, Abu Sebastian en Anne-Johan Annema voor de interesse en het zitting nemen in mijn promotiecommissie.

Dit proefschrift bevat veel experimenteel werk. Ik heb vele uren doorgebracht in het probe-lab alwaar ik mijn overdenkingen verwezenlijkte in een opstelling, een experiment, een praktisch resultaat. Martin, zonder jou had het er heel anders uitgezien. Mijn drive voor perfectie werd door jou pragmatische instelling geoefend om eerst eens even een iets simpels te proberen en het vervolgens uit te bouwen.

Jouw ervaring deed het bouwen van een nieuwe multi-probe AFM in een keer slagen. Ik heb de tijden in het lab met jou erg gewaardeerd en mis die eigenlijk nu al door het vele reizen en tikwerk van het afgelopen jaar. Ook op persoonlijk vlak heb ik genoten van ons contact; tijdens ons verblijf in Zürich, het hardlopen, de gesprekken.

Ik dank Joost van Honschoten voor de mooie samenwerking die we hadden. Bedankt voor je inzichten die mijn theoretisch begrip hebben verrijkt. Bedankt voor je lovende woorden, die me hebben gemotiveerd. Bedankt voor de lol die we hebben gehad. Rust nu in vrede, je strijd is gestreden.

En af en toe (eigenlijk best vaak) moest er iets nieuws gemaakt worden om het daarna te kunnen gebruiken in het probe-lab. In de cleanroom werd ik vaak bijgestaan door Johnny. Uren achter de FIB om de eerste *arrays* te maken en na veel proberen lukte het ook nog. De persoonlijke aandacht die je aldoor toont, waardeer ik erg. Bedankt, staf van de cleanroom voor het meedenken en jullie bereidheid te helpen. Ik dank ook de technici Thijs – ICT en LabVIEW –, Henk – optica –, Pino – nooit een saaie lunch – en Kees – dat doe ik wel even – voor jullie nuchtere kijk en hulpvaardigheid. En natuurlijk de *technologen* Erwin en Meint, zonder jullie zouden er heel wat minder staaltjes van techniek uit de cleanroom komen! En hier houdt het nog niet op; door de diversiteit van mijn promotiewerk is de lijst met mensen die mij hebben moeten helpen enorm. Bedankt, Peter voor het ontwerp van de scan-o-matic, Henk voor de electronica, de mannen van de werkplaats voor de mechanica, alsook Jan Talman en George voor de 'vacuumservice'.

En om alles in goede banen te leiden waren daar Karen, Thelma, Satie en Susan. Bedankt! Karen, ik kon altijd bij je terecht en ik bewonder je organisatorische talent! Ik dank ook de wetenschappelijke staf van onze groep, Theo, Henri, Niels, Remco en Hans bedankt voor jullie kritische blik en af en toe een inspirerend gesprek. Gijs, bedankt voor je wijze woorden over het onderzoeksleven, vooral tijdens de lange autorit vanuit Lyon – "ontwerp een experiment". De post-docs, Ozlem en Léon, jullie staan altijd klaar om een pre-doc te helpen, zeker met oefenpraatjes voor een interview! Léon, bedankt voor je grote interesse voor wat ik doe en je bereidwilligheid om me verder te helpen.

Dan kom ik bij de studenten die het aangedurfd hebben om onder mijn begeleiding te werken aan soms bijna niet te realiseren doelen. Harald, een zeer moedige poging, als het iemand het in zo'n korte tijd had kunnen flikken, was jij het. Sebastiaan, Jeroen jullie bedankt voor jullie grote bijdrages aan het beam deflection werk. Tjitte-Jelte, je *arrays* zijn uitstekend, hopelijk komt er binnenkort een mooi paper uit. Olti, je enthousiasme is aanstekelijk. Het is erg leuk om een *M.Sc* student af te moeten remmen in plaats van aan te moedigen. Dan de *B.Sc* studenten Marcel, Hylco, Jasper, Niels en Maarten. Bedankt voor jullie inzet en bijdrages. Alle tien hebben jullie op je eigen manier mijn promotieonderzoek een stuk meer kleur gegeven.

The ProTeM team – David, Purav, Lei, Patricia, Richard, Candice, Marilyn, Enrico, Roberto, Urs, Michel, Haris, Abu, Harish, Matthias, Martin, Oleg, Tom, Hans-Joachim, Hylke – thank you for introducing me in the international world of science. You allowed a young researcher to make mistakes and have taught him a

lot. The group dinners were very nice, Patricia!

Then there is the visit to IBM Zürich. Some five or six months in which I learned a great deal. Abu, you are mainly responsible for that, thanks. Haris, thank you for giving me the opportunity. Harish and Michel, you made me feel welcome. Walther and Urs, thank you for introducing me so quickly in a new environment and new lab. Daniel, Tomas, Urs Frey, Gael, Aggeliki, Evangelos, Nikos, thank you all for a great time!

Op het sportieve vlak waren daar de voetbalteams, BIOS futsal en het IBM Zürich team. Hardlopen en squashen in de lunchpauze. Kees, Edin, Daniël, Egbert, Paul en nog vele anderen, dat jullie het met zo'n fanatiekeling uithouden! Mijn kamergenoten, Johan, Jeroen, Regina en Shahina, bedankt voor de vele gesprekken. Alexander, bedankt voor je adviezen over hoe een promovendus succesvol de eindstreep haalt. Bedankt, allen van SMI, NE en TST die ik nog niet bij naam heb genoemd voor een prachtige tijd.

Johan, een beste herinnering is inderdaad lastig, ik weet nog wel een historisch dieptepunt: het restaurantje op Rigi Scheidegg, dat na uren tot aan onze heupen door de zachte sneeuw geploeterd te hebben – met een Gutschein op zak! – gesloten bleek. Ik heb veel van je geleerd. De reden dat dit proefschrift er fatsoenlijk uit ziet, ben jij!

Mijn paranimfen, Jeroen en Johan, bedankt!

Jasper, Minne and 'the worst best men' Marthijn en Thierry, bedankt voor jullie vriendschap tijdens deze jaren. Marthijn, ik weet nog dat je vijf jaar geleden opschreef "Promoveren?" en daaronder: "W. W. Koelmans".

Heit en mem, altijd daar, een wijze raad, behulpzaam, jullie hebben dit mee mogelijk gemaakt. Amarens, Sjoerd Pieter, Titianne, Patrick, pap en mam bedankt voor jullie diepe betrokkenheid. Martin, erg leuk om met je over het onderzoek te praten en samen een brug te slaan tussen twee velden.

Dan ben ik aangeland bij mijn thuisfront. Als eerste en ook als laatste is daar Ellen. Je hebt mijn mislukkingen en successen, tegenslagen en overwinningen aangehoord. Je steun is enorm belangrijk voor me. Ons avontuur in Zwitserland, de keren dat we niet bij elkaar konden zijn vanwege mijn promotiewerk. Dat jij er helemaal achter staat, maakt dat ik dit kan doen. Samen! Lasse Siem, het schrijven van dit proefschrift is enkel onderbroken door jouw komst. Zo jong als je nog bent, geef je me veel vreugde.

Groot is de Heer, Hem komt alle lof toe.

Psalmen 96:4a

— Wabe, mei 2011 Enschede.

# Publications

## Journal articles


Koelmans W W, Van Honschoten J, De Vries J, Vettiger P, Abelmann L, Elwenspoek M C, 2010
"Parallel optical readout of cantilever arrays in dynamic mode"
*Nanotechnol.* **21**, p. 395503, doi:10.1088/0957-4484/21/39/395503

Koelmans W W, Sebastian A, Abelmann L, Despont M, Pozidis H, 2011
"Force modulation for enhanced nanoscale electrical sensing"
*Nanotechnol.* **22**, p. 355706, doi:10.1088/0957-4484/22/35/355706

Timmer B H, Van Delft K M, Koelmans W W, Olthuis W, Van Den Berg A, 2006
"Selective low concentration ammonia sensing in a microfluidic lab-on-a-chip"
*IEEE Sensors J.* **6**, pp. 829–834, doi:10.1109/JSEN.2006.874020

Van Honschoten J, De Jong H W, Koelmans W W, Parnell T P, Zaboronski O V, 2011
"Information storage and retrieval for probe storage using optical diffraction patterns"
*Accepted for publication in J. Appl. Phys.* URL `http://arxiv.org/abs/1104.0871`


Three more manuscripts are in preparation for publication: an article based on Chapter 2, an article based on §4.1 about readout of cantilever arrays using diffraction patterns and a third article about the fabrication and characterization of cantilever arrays, based on §4.2.

## Book chapters


Gemelli M, Abelmann L, Engelen J B C, Khatib M G, Koelmans W W, Zaboronski O, 2011
*Memory Mass Storage*, chapter Probe storage, pp. 99–168,
Springer-Verlag
ISBN 978-3-642-14751-7


## Conference contributions


Hoexum A M, Koelmans W W, Bolhuis T, Abelmann L, Lodder J C, 18-20 Jun. 2007
"Image charge stepping actuator for data storage purposes"
In: *Innovative Mass Storage Technologies (IMST 2007)*, Enschede, The Netherlands

Koelmans W W, van Honschoten J W, Vettiger P, Abelmann L, Elwenspoek M C, May 20-22 2009
"Parallel optical readout of a cantilever array in dynamic mode"
In: *Proc. of the International Workshop on Nanomechanical cantilever sensors*, p. L.2.3, Jeju, South-Korea

Koelmans W W, Peters T, Abelmann L, Elwenspoek M C, 26-29 Sept. 2010
"Fabrication of cantilever arrays with tips for parallel optical readout"
In: *Proc. Micromechanics and Microsystems Europe*, pp. 277–280, Enschede, The Netherlands

Koelmans W W, Sebastian A, Despont M, Pozidis H, Aug. 17-20 2010
"Force modulation for improved conductive-mode atomic force microscopy"
In: *10th IEEE Conference on Nanotechnology, IEEE NANO 2010*, pp. 875–878, Seoul, South-Korea

Pjetri O, Koelmans W W, Abelmann L, Siekman M H, Elwenspoek M C, 19-22 Jun. 2011
"Using diffraction to detect deflection of the cantilevers in an array"
In: *Proc. Micromechanics and Microsystems Europe*, Toensberg, Norway

Van Honschoten J W, Koelmans W W, Konings S M, Abelmann L, Elwenspoek M C, Sept. 7-10 2008
"Nanotesla torque magnetometry using a microcantilever"
In: *Proc. Eurosensors XXII*, Dresden, Germany

Vera Marun I J, Koelmans W W, Jansen R, Nov. 5-9 2007
"Spin filter STM (SF-STM): Towards imaging a single atomic spin"
In: *Proc. Annual Magnetism and Magnetics Materials Conference*, Tampa, Florida

# About the author

Wabe Koelmans was born in Leeuwarden, the Netherlands on 14 October, 1981. He attended the secondary school Christelijk Gymnasium Beyers Naudé from 1994 to 2000, where he received his VWO diploma. In the same year he started studying Electrical Engineering at the University of Twente in Enschede, the Netherlands. He finished the *B.Sc.* program with an individual research assignment at the Lab-on-a-chip (BIOS) group, led by Albert van den Berg, where he designed a prototype ammonia sensor in glass chips for human breath analysis. During the *M.Sc.* program of his studies he was an intern for four months at the Seagate Research Lab in Pittsburgh, USA. At Seagate Research he worked on the development of a test-stand for next generation recording heads and patterned media. Upon his return in Twente he commenced his *M.Sc.* graduation project in which he successfully fabricated and characterized multi-terminal tips for spin-polarized scanning tunneling microscopy. The work was performed within the Nanoelectronics (NE) group led by Ron Jansen. In 2006 he received the *M.Sc.* degree (*in Dutch: ir.*) in Electrical Engineering.

In 2007 he started his *Ph.D.* research at the Transducers Science and Technology (TST) group led by Miko Elwenspoek. The group is part of the MESA$^+$ Institute for Nanotechnology of the University of Twente. His work was funded in part by the Dutch Technology foundation (STW) through a VIDI grant of his supervisor Leon Abelmann. The other part was funded by the European Research Council through the FP6 project 'Probe-based Terabit Memory' (ProTeM). Within the framework of the ProTeM project he was a visiting researcher in 2009 and 2010 with the IBM Zurich Research Lab in Switzerland. During the visits, with a total duration of five months, he worked on nanoscale electrical contacts.

Electronic mail address: w.w.koelmans@alumnus.utwente.nl

*The term is over: the holidays have begun.*
*The dream is ended: this is the morning.*

— C. S. Lewis

doi:10.3990/1.9789036531924